

THE CHARACTERISATION OF ULTRAFILTRATION MEMBRANES USED IN WATER PURIFICATION

Presented by:

Kevin Dizon^{1,2}

Master of Research

Primary supervisor: Dr Marion Gaborieau^{1,2}

Co-supervisors: Dr Patrice Castignolles¹, Dr James Oliver¹, Dr
Geoffrey Johnston-Hall³, Dr Richard Wuhrer⁴

¹Australian Centre for Research on Separation Science
(ACROSS), School of Science and Health (SSH), Western Sydney
University (WSU), Parramatta, Australia

²Medical Sciences Research Group (MSRG), WSU, Parramatta,
Australia

³Evoqua Water Technologies, Memcor®, South Windsor, NSW,
Australia

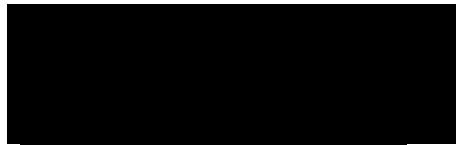
⁴Advanced Materials Characterisation Facility (AMCF), WSU,
Parramatta, Australia

Western Sydney

June 2018

Statement of Authentication

The work presented in this thesis is, to the best of my knowledge and belief, original except as acknowledged in the text. I hereby declare that I have not submitted this material, either in full or in part, for a degree at this or any other institution.

A solid black rectangular box used to redact the signature of the author.

.....

Kevin Dizon

June 2018

ACKNOWLEDGEMENT

Emily Dizon & Ernesto Dizon: Thank you for housing and feeding me for the past two years. I know I have been a handful : however, I am very appreciative of your tolerance towards my goals.

Chloe Dizon and Darren Dizon: It was not my choice to be blood related to both of you; however, I do enjoy the company. Jokes aside, I will be the most successful sibling out of you two.

Hannah Nguyen: You are a large reason I stayed on and a large reason why I will continue to strive towards my goals.

Patrice Castignolles and Marion Gaborieau: The realisation of fulfilling my dreams was made possible through the work and commitment the both of you had shown to moulding me into a researcher. You took me into your care as a student who scraped through GPA requirements for the MRes degree and had previously shown no passion for chemistry. Such commitments inspired me dedicate my mind and soul into this project to ensure that you did not make a bad decision. I am forever grateful and inspire to be an individual that you are proud to have mentored.

Macromolecular Characterisation Team- I extend my gratitude towards the MCT team, for not only the support in a very demanding field but also the camaraderie that was given. I hope we all flourish in our respective careers and I wish you all the best for future endeavours.

I appreciate the time and effort spent by Geoffrey Johnston-Hall and the RnD team at Evoqua for their expertise on teaching me several analytical techniques. I am also appreciative of the grant given by Evoqua.

I would like to thank Ric Wuhrer and the AMCF staff for their help and advice towards the realisation of my project.

I am also thankful towards Adam Hale and the SSH technical team. I would also like to thank Western Sydney University for providing me the MRes scholarship and RTP to develop my project.

I am grateful to the organisers of the NMR of polymers symposium at 255th ACS National Meeting for a student travel award.

RESEARCH OUTPUT

Oral Presentations as Presenter

K.P. Dizon, J.J. Thevarajah, J. D. Oliver, P. Castignolles, M. Gaborieau, End group characterisation of poly(N-vinyl pyrrolidone) through capillary electrophoresis, 2017 Honours and Masters-by-Research Student Presentation, Parramatta (Australia), November 2017

K.P. Dizon, J.J Thevarajah, P. Castignolles, M. Gaborieau, Molecular Characterisation of Amphiphilic Polymer Blends used in water purification through Solid-State NMR Spectroscopy. 2016 Research and Development Topics Conference, Parramatta (Australia), December 2016.

K.P. Dizon, J.J Thevarajah, P. Castignolles, M. Gaborieau, Molecular Characterisation of Amphiphilic Polymer Blends through Solid-State NMR Spectroscopy, 2016 Honours and Masters-by-Research Student Presentation Evening, Kensington (Australia), November 2016.

Poster Presentation as Presenter

K.P. Dizon, J.D. Oliver, P. Castignolles, G. Johnston-Hall, R Wuhrer, M Gaborieau, Miscibility analysis of polymer based ultrafiltration membranes through two dimensional WIdeline SEparation solid state NMR spectroscopy, 255th American Chemical Society National Meeting and Exposition, New Orleans (United States of America), March 2018

K.P. Dizon, J.D. Oliver, P. Castignolles, M. Gaborieau, Miscibility analysis of polymer based ultrafiltration membranes used as water filtration devices, HDR showcase, NSW, Parramatta (Australia), November 2017

K.P. Dizon, J.D. Oliver, P. Castignolles, M. Gaborieau, Miscibility analysis of polymer based ultrafiltration membranes used as water filtration devices, HDR showcase, NSW, Parramatta (Australia), November 2017

K.P. Dizon, T. Henin, J.D. Oliver, P. Castignoles, M. Gaborieau, Molecular Characterisation of amphiphilic polymer blends used as water filtration devices through solid-state 2-Dimensional Wideline SEparation (2D WISE) NMR spectroscopy, Surfaces and Soft Stuff Meeting (SASSY), NSW, Kensington (Australia), June 2017

TABLE OF CONTENTS

Acknowledgement	ii
Research Output	iv
Oral Presentations as Presenter	iv
Poster Presentation as Presenter	iv
Table of Contents	vi
List of Figures	x
List of Tables	xv
Table of Abbreviations	xvii
Abstract	xx
1 Background	1
1.1 The Need for Water Purification	2
1.2 Conventional Methods of Water Purification	3
1.2.1 Coagulation, Flocculation, Sedimentation and Sand Filtration	3
1.2.2 Conventional Water Filtration Processes	4
1.3 Advanced Methods of Water Purification- Membrane Based Filtration	5
1.4 Structure Variance in Polymers upon Membrane Synthesis	8
1.5 Characterisation of Polymer Blends	11
1.6 Relationship between Structure and Physical Properties	13
1.7 Characterisation Methods	14
1.7.1 Capillary Electrophoresis	15
1.7.1.1 Expressing Migration Time as Electrophoretic Mobility	16
1.7.1.2 Correcting for the Analyte Velocity through the Detector	16
1.7.1.3 Capillary Electrophoresis in the Critical Conditions	17
1.7.2 Nuclear Magnetic Resonance Spectroscopy	18
1.7.2.1 Introduction to NMR theory	19
1.7.2.2 Introduction to Solid-State NMR Spectroscopy	21
1.7.2.3 Line Shapes and Line Widths	22
1.7.2.4 Pulse Programs: Solution and Solid-state NMR Spectroscopy ..	23

1.7.2.4.1 Single Pulse Excitation.....	23
1.7.2.4.2 Longitudinal Relaxation	25
1.7.2.4.3 Determining Longitudinal Relaxation through the Inversion Recovery Sequence	26
1.7.2.5 Pulse Programs: Applied Only in Solid-State NMR	28
1.7.2.5.1 ¹³ C Cross Polarization.....	28
1.7.2.5.2 Two-Dimensional Wideline Separation	29
1.7.3 Scanning Electron Microscopy	31
1.8 Aims and Objectives	32
1.9 Chapters and Potential Publications Overview	33
1.9.1.1 Characterisation of Poly(N-vinyl pyrrolidone) End Groups through Capillary Electrophoresis (chapter 2).	33
1.9.1.2 Molecular Characterisation of Ultrafiltration Membranes (chapter 3).....	33
1.9.1.3 Relation of Surface Composition to Functionality (chapter 4)...	34
2 Characterisation of poly(N-vinyl pyrrolidone) end groups through capillary electrophoresis	35
2.1 Introduction	36
2.1.1 Means of Characterisation.....	37
2.1.2 Pressure Mobilisation	38
2.2 Materials and Methods.....	39
2.2.1 Chemicals	39
2.2.2 Dissolution of PVP.....	39
2.2.3 Sample and Buffer Preparation.....	39
2.2.4 Capillary Electrophoresis Analysis	40
2.2.5 Pressure Mobilisation Analysis	40
2.3 Results and Discussion.....	41
2.3.1 Qualitative Observations of PVP Dissolution	41
2.3.2 Selection of an Appropriate Mobility Marker	42
2.3.3 Determination of the Distribution of Electrophoretic Mobilities of Different PVP Samples	44
2.3.4 Adsorption and Solubility of PVP	45
2.3.5 Characterisation of PVP End Groups.....	48
2.4 Conclusion.....	49

3 Molecular characterisation of Ultrafiltration membranes.....	50
3.1 Introduction	51
3.1.1 Optimising Functionality through Miscibility	51
3.1.2 Characterisation of Polymer Blends through NMR Spectroscopy	52
3.2 Materials and Methods.....	54
3.2.1 Chemicals	54
3.2.2 NMR Analysis.....	55
3.3 Results and Discussion.....	55
3.3.1 Molecular Structure Identification	55
3.3.2 Semi Quantitative Analysis of Precursor Content.....	59
3.3.3 Miscibility Determinations through 2D WISE NMR Spectroscopy ..	
.....	68
3.4 Conclusion.....	74
4 The relation of surface composition to functionality	76
4.1 Introduction	77
4.1.1 Surface Structure Composition.....	77
4.1.2 Functional Properties.....	77
4.2 Materials and Method	78
4.2.1 Chemicals	78
4.2.2 Scanning Electron Microscopy	78
4.2.3 NMR Spectroscopy	79
4.2.4 Tensiometry Tests	79
4.2.5 Tensile Strength Tests	79
4.3 Results and Discussion.....	80
4.3.1 Membrane Surface Analysis	80
4.3.2 Physical Features and Element Identification	80
4.3.3 Determination of Surface Composition through ¹ H Static NMR Spectroscopy	84
4.3.4 Functionality Measurements.....	89
4.3.4.1 Contact Angle Determinations through Tensiometry Tests ..	89
4.3.4.2 Tensile Strength Determinations	90
4.4 Conclusion.....	92
5 Conclusion and Future Research Opportunities	94

5.1 Interpretations and Comparisons of UF Membranes	95
5.2 Methods to Characterise Membranes	96
5.2.1 Developing Relationships between Surface Composition and Pore-size 97	
5.2.2 Identifying Different Phases within the Membranes	98
5.3 Potential Application of 2D WISE NMR Spectroscopy to Other Complex Systems	99
6 References	101
7 Appendix	111

LIST OF FIGURES

Figure 1-1 Rainfall records during the peak of the millennial drought ³	2
Figure 1-2 Pressure (black arrows) applied to the feed water on the porous membrane (grey). Permeation occurs for particles smaller than the pores (blue) and particles larger (orange) than the pores adhere to the membrane.	6
Figure 1-3 Different types of filtration process (orange circles). Length measurements given are the maximum value of the filtrates size (blue lines).	7
Figure 1-4: Different types of polymers composed of monomer unit 1 (green) and monomer unit 2 (blue). Compositions show a (A) Homopolymer, repeating sub units of an individual monomer unit, (B) Statistical copolymer, Monomer unit 1 and 2 exhibit a statistical ratio composition, (C) Block copolymer monomers form 'block' compositions respective to a monomer unit.	9
Figure 1-5 A schematic diagram showing that polymers are characterised by different types of distributions: molar mass, branching, chain ends and monomeric unit arrangement ¹⁴	10
Figure 1-6 Schematic diagram of the outcomes of blending two polymers. Formation of localised regions can be seen in a partially miscible blend. ...	12
Figure 1-7 Migration of ions in CE. Vector of the ions are represented by arrows; the length of the arrow represents the magnitude of the vector.	15
Figure 1-8 General trend of electrophoretic mobility in respect to the number of monomer units in a polyelectrolyte ³⁰	18
Figure 1-9 Precession of a single nucleus affected by a static magnetic field B_0 . B_0 is directed along the z-axis and the nucleus motion is represented as a vector moving in a pattern similar to the surface of a cone.	20

Figure 1-10 Bulk magnetisation of the sample in a pulsed NMR experiment; (a) and (e) at equilibrium, (b) at the time of acquisition, (c) and (d) during the relaxation delay.	21
Figure 1-11 Magic angle spinning (MAS) of a solid-state NMR sample. taken from ⁴⁰	23
Figure 1-12 ¹ H single pulse excitation pulse scheme. Adapted from ⁴⁰	23
Figure 1-13 Pulse scheme of a ¹³ C SPE experiment. Adapted from ⁴⁰	24
Figure 1-14 Longitudinal relaxation dictated by the time constant (τ/T_1) and magnetisation approaching thermal equilibrium. Longitudinal relaxation is considered complete at a period of $5T_1$. Image taken from ³⁶	26
Figure 1-15 Pulse scheme of a ¹³ C inversion recovery experiment.....	27
Figure 1-16 Pulse scheme of a ¹³ C cross polarisation experiment. Adapted from ⁴⁰	29
Figure 1-17 (A) Pulse sequence for a 2D WISE experiment ⁴⁰ B) resultant 2D WISE spectrum correlating molecular structures within a ¹³ C spectrum to the corresponding segmental mobilities through a ¹ H spectrum ⁴³	30
Figure 1-18 SEM image at the cross section of the membrane.	31
Figure 2-1 PVP 1 (left) PVP 2 (middle) and PVP 3 (right) dissolved in tetrahydrofuran at $7.5 \text{ g}\cdot\text{L}^{-1}$. Image taken at t_{initial}	41
Figure 2-2 A) Distribution of electrophoretic mobilities of methyl green in DMSO at $0.05 \text{ g}\cdot\text{L}^{-1}$ ($n = 10$). B) Zoom in the region $1.0 - 1.5 \times 10^{-8} \text{ m}^2 \cdot \text{V}^{-1} \cdot \text{s}^{-1}$	43
Figure 2-3 A) PVP 1 (blue), PVP 2 (red) and PVP 3 (black) dissolved in NB 200 at $1 \text{ g}\cdot\text{L}^{-1}$ methyl green was added as a mobility marker at $0.05 \text{ g}\cdot\text{L}^{-1}$. B) Zoomed in graph of the PVP from -3 to $1 \times 10^{-9} \times \text{m}^2 \cdot \text{V}^{-1} \cdot \text{s}^{-1}$	44

Figure 2-4 PM of PVP samples PVP 1(blue), PVP 2(Red) PVP 3 (black) with the capillary at 15°C capillary and the sample at 9 °C.....	47
Figure 2-5 Distributions of electrophoretic mobilities of PVP 1 (blue), PVP 2 (red), PVP 3 (black) dissolved in NB 200 at 1 g·L ⁻¹ with methyl green as a mobility marker. Conditions set at 15 °C in the capillary and 9 °C at the sample.	48
Figure 3-1 Normalised ¹³ C CP spectra of A) polymer A, B) polymer B, C) polymer C, D) AB membrane and E) ABC membrane.	56
Figure 3-2 ¹³ C Inversion recovery spectrum of ABC membrane at an evolution time τ of 2.08s (green) and 13.86 s (black).....	60
Figure 3-3 ¹³ C Inversion recovery spectrum of ABC membrane at a τ evolution time of 8.32 s.	61
Figure 3-4 A ¹³ C SPE spectrum of the AB membrane in quantitative conditions.	62
Figure 3-5 A quantitative ¹³ C SPE NMR spectrum of ABC membrane. localised baseline introduced from 30 to 10 ppm.....	65
Figure 3-6 2D WISE spectra of A) AB powder, B) AB membrane and C) ABC membrane.....	68
Figure 3-7 Normalised ¹ H spectra of A) AB powder B) AB membrane and C) ABC membrane extracted from the 2D WISE spectra at specific carbon structures (\approx 177.0 ppm (brown), \approx 120 ppm (red), \approx 51.6 ppm (orange), \approx 43.0 ppm (green), 31.2 ppm (black), \approx 18.0 ppm (blue). For specific ¹³ C chemical shifts of all samples, please refer to (Table 3-7).	70
Figure 3-8 FWHM in relationship to ¹³ C chemical shifts of AB powder (purple circle), AB membrane (blue square) and ABC membrane (red triangle).	73
Figure 4-1 SEM images of the AB membrane A) cross section at 200 μ m with length measurements (green lines), C) surface at 75 μ m, E) surface at 1 μ m.	

SEM images of ABC membrane B) cross section at 200 μm , D) cross section at 100 μm , F) cross section at 10 μm with pore-size calculations (green circles) (refer to scale bar for image lengths).	81
Figure 4-2 SEM-EDS analysis of the surface of A) AB membrane B) ABC membrane.....	83
Figure 4-3 ^1H SPE spectra of AB (blue) and ABC (red) membrane in dry state (dashed lines) and soaked in D_2O (solid lines).....	85
Figure 4-4 Normalised ^1H SPE spectra of AB (blue) and ABC membrane (red) soaked in D_2O in comparison with the stock solution of D_2O (grey).	86
Figure 4-5 Normalised ^1H SPE spectra of AB membrane soaked in D_2O with a repeat.....	88
Figure 4-6 Load in relation to extension of the AB membrane (blue) and the ABC membrane (red).	91
Figure 5-1 Pore-size distributions determined through liquid-liquid porometry of six industrially used membranes.	98
Figure 5-2 Overlays of the diffractograms of AB membrane (blue), ABC membrane (red) and polymer B (black dots).....	99
Figure A 1 PVP 1, PVP 2 and PVP 3 dissolved in A) NMP B) THF C) MilliQ water D) Water at pH 4 E) Water at pH 10 F) Ethanol, at $7.5 \text{ g}\cdot\text{L}^{-1}$. Images taken at t_{initial}	111
Figure A 2 CE of PVP 1 dissolved in NB200 with MG(black) and without MG (red).	113
Figure A 3 Normalised peaks of PVP 2 dissolved in NB200 at $1 \text{ g}\cdot\text{L}^{-1}$ (blue), $0.5 \text{ g}\cdot\text{L}^{-1}$ (green), $0.25 \text{ g}\cdot\text{L}^{-1}$ (red). MG $0.05 \text{ g}\cdot\text{L}^{-1}$ was used as a mobility marker.	114
Figure A 4 PM of PVP 1 (Blue), PVP 2 (Red), PVP 3 (black) at $1 \text{ g}\cdot\text{L}^{-1}$ with the capillary at 25°C	115

Figure A 5 PM of PVP 1 (blue) PVP 2 (red) and PVP 3 (black) at 1 g·L ⁻¹ with the capillary at 55 °C.....	116
Figure A 6 PM of PVP 1 (blue) PVP 2 (red) PVP 3 (black) at 1 g/L with the capillary at 15 °C.	117
Figure A 7 ¹ H SPE of polymer A (green), polymer B (black) and polymer C (gold).....	118
Figure A 8 ¹ H SPE of membrane AB (blue) and membrane ABC (red).....	119
Figure A 9 ¹³ C CP spectrum of polymer C zoomed in between 170 and 120 ppm to show signals attributed to the monomer.	120
Figure A 10 ¹³ C Inversion recovery of ABC membrane at a τ evolution time of 0.1 sec.	121
Figure A 11 ¹ H FID of the 2D WISE measurement on the ABC membrane.	121
Figure A 12 Normalised ¹ H spectra of A) AB powder B) AB membrane and C) ABC membrane.....	122
Figure A 13 SEM image of the ABC membrane indicating the general dimensions on length measurements of the inner diameter (green line), membrane wall thickness (yellow line) and outer diameter (blue line)	123
Figure A 14 SEM/EDS images of the surface of the A) AB membrane and B) ABC membrane.....	124
Figure A 15 Normalised ¹ H spectra of the ABC membrane in excess D ₂ O compared to the stock solution of D ₂ O	125
Figure A 16 ¹ H SPE spectra A) AB membrane and B) ABC membrane) pre-soaked in D ₂ O. Respective membranes were left soaking for 15 min (red line) and 30 min (green line), no observable difference in signal was observed past 30 min. AB membrane was recorded for a total of 60 min hour and the AB membrane was recorded for a total of 120 min.	126

LIST OF TABLES

Table 1-1 Ultrafiltration membranes essential and additional desired properties ⁷	13
Table 3-1 Formulations of the membranes and powder used.	54
Table 3-2 ¹³ C chemical shift assignments of the precursors.	57
Table 3-3 Relative percentages of the molecular constituents associated to the respective polymers found within membrane AB.	63
Table 3-4 Weight by weight and mole by mole ratios of the respective polymers within the AB membrane.	64
Table 3-5 Relative percentages of the molecular constituents associated with the respective polymer/s of membrane ABC.....	66
Table 3-6 Weight and mole ratio of the respective polymers in the ABC membrane.....	67
Table 3-7 FWHM of ¹ H slices at specific carbon structures for all samples use in 2D WISE measurements (Figure 3-7).....	72
Table 4-1 EDS values of the expected elements in the AB and ABC membrane.	83
Table 4-2 Averaged results of tensiometry tests of the AB membrane and the ABC membrane. Standard deviations are shown adjacent to the measured value (n=3).....	89
Table 4-3 Averaged values of tensile tests results conducted on both AB membrane and ABC membrane. SD values are found adjacent to measured values (n=5).....	92
Table 5-1 Bubble point and water permeability tests.	97

Table A 1 Electrophoretic mobilities values of methyl green in NB200 at 25 C (n = 10). Average mobility and RSD of methyl green was calculated.	112
Table A 2 Length measurements determined through SEM on the regions of interest in both the AB and ABC membrane.....	123
Table A 3 Tensiometry results on the repeats of both the AB and ABC membrane.....	127
Table A 4 Tensile strength results on the repeats of both the AB and ABC membrane.....	128

TABLE OF ABBREVIATIONS

Abbreviations	Definitions
2D WISE	Two-dimensional wideline separation
CE	Free solution capillary electrophoresis
CE-CC	Free solution capillary electrophoresis in the critical conditions
CP	Cross polarization
DAD	Diode array detector
DD	Dipolar decoupling
DMSO	Dimethyl sulfoxide
EDS	Energy dispersive X-ray spectroscopy
EOF	Electroosmotic flow
EtOH	Ethanol
FID	Free induction decay
FWHM	Full width at half maximum
HCl	Hydrchloric acid
Hz	Hertz
keV	Kilo electron volts
ld	Length to the detector
LLP	Liquid-liquid porometry
lt	Total length
MAS	Magic angle spinning
MF	Microfiltration

MG	Methyl green
MQ	Milli-Q water
NaOH	Sodium hydroxide
NB	Sodium borate
NB200	200 mM sodium borate buffer
NF	Nanofiltration
NMP	N-methyl-2-pyrrolidone
NMR	Nuclear magnetic resonance
NSW	New South Wales
PM	Pressure mobilisation
ppm	Parts per million
PSD	Pore size distribution
PVP	Poly(n-vinyl pyrrolidone)
RO	Reverse osmosis
RSD	Relative standard deviation
RSD _{SNR}	The RSD of SNR
SD	Standard deviation
SEC	Size exclusion chromatography
SEM	Scanning electron microscopy
SNR	Signal-to-noise ratio
SPE	Single pulse excitation
T ₁	Longitudinal relaxation time
t _{eof}	Migration time of EOF

THF	Tetrahydrofuran
t_m	Migration time
UF	Ultrafiltration
USA	United States of America
V	Voltage
$W(\mu)$	Weight distribution of electrophoretic mobility
WSU	Western Sydney University
μ	Electrophoretic mobility
τ	Evolution time
τ_{null}	The evolution time at which there is no signal in a inversion recovery experiment

ABSTRACT

The increase of urbanisation has caused water scarcity concerns in developed nations. Natural sources of freshwater (ground water, river water, rain fall) are becoming insufficient, requiring man-made technologies for the purification of water. Ultrafiltration membranes are currently becoming more relied upon for water purification due to their selectivity and applicability in different environments. Fabrication of some ultrafiltration membranes require the mixing of two (binary blend) or three (ternary blend) synthetic polymers to form an amphiphilic polymer blend. Overall properties of the blend are dependent on the chemical nature of the precursors; however, chemical incompatibilities between polymers causes incomplete mixing, thereby forming a partially miscible system. The presence of different domains of varying miscibility creates a complex matrix where minimal changes in local chemical composition can drastically change the membranes properties. The material becomes increasingly complex with a ternary blend. Hence, the understanding of function and composition relationship is important to the development of design and functionality.

This project aims to characterise a number of properties of ultrafiltration membranes at various stages, from fabrication to production. . In this work, industrial membranes (both binary and ternary) and their respective precursors were studied.

Difference in end groups within the system affects solubility of the precursor leading. This can lead to undissolved poly(*N*-vinyl pyrrolidone) (PVP) affecting the properties of the membrane produced. Free solution Capillary Electrophoresis (CE) was employed for the separation of PVP via end groups. Representative electrophoretic mobility distributions of different PVP samples were obtained showing the presence of different populations.

The membranes were characterised through solid-state Nuclear Magnetic Resonance (NMR) spectroscopy, providing a means to determine the

molecular structure and molecular mobility within the membranes. NMR measurements identified that polymer A is extracted out of the membrane during production and the ternary membrane is a miscible system. Deductions made contributed to interpretations on functionality

Relationships between the surface composition and the functionality of the membrane were established. Functional properties were determined through tensile strength tests and tensiometry tests. The surface composition was determined through Scanning electron microscopy / energy dispersive x-ray spectroscopy and ^1H NMR spectroscopy. Surface localisation of polymer A and polymer C affected the hydrophilicity of the membranes. It was also found the formation of macrovoids affect the tensile strength of the membrane.

In conclusion, methods were developed to determine the chemical structures of the membrane, at various stages of production, and relating it to functionality. Analysis of structure-function relationships allowed for the improvement of design to optimise membrane properties. The AB membrane was determined to have better functional properties than the ABC membrane; however, the chemical stability of the ABC membrane makes it a promising system to be used for future design. Future design proposals can incorporate different polymerisations yielding PVP with end groups that are soluble. These improved designs will not only increase performance but also allow for cost-efficient measures of membrane production.

1 BACKGROUND

1.1 The Need for Water Purification

Inadequate access to sanitised and purified water is a pervasive problem that afflicts populations globally. As a result, millions are afflicted by preventable diseases, caused by waterborne bacteria and enteric viruses, commonly associated to malnutrition, poor digestion, and death ¹. Although a problem associated with third world countries, freshwater supply deficiencies still persists in developed nations causing it to be a global problem. In Australia, conventional means of attaining freshwater cannot keep up with the demands of ever-increasing urbanisation, a statement signified by the devastation caused by the millennial drought, 2001-2009, affecting agriculture, inland rivers and livelihoods ². A large contributor to this devastation reported was the lowest average rainfall in New South Wales, Victoria, and regions within Queensland since 1900 (Figure 1-1).

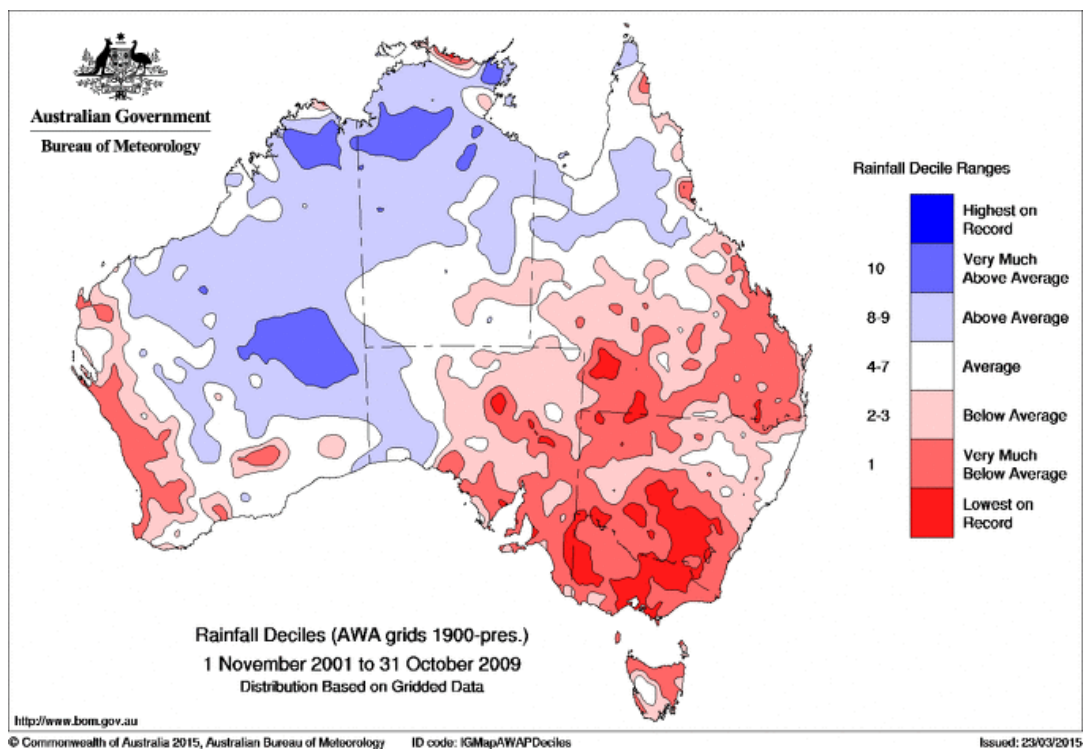


Figure 1-1 Rainfall records during the peak of the millennial drought ³.

Below average rainfall is observed across south east Australia with particular regions showing the lowest rainfall on record. Dependence towards traditional water supplies (ground water, dams) that rely on rainfall are

proving to be inconsistent for urban water planning. To ensure an adequate supply of water is available at a given time, methods able to purify water from environments outside of the hydrological cycle are required to sustain a growing population.

Current man-made purification processes (such as desalination) address many problems in terms of water supply and quality; however, it requires an extensive amount of capital and energy towards the development of large scaled systems that heavily impact the local environment. In many regions suffering from water deficiencies, current purification processes are economically and environmentally unsuitable. The practical drawbacks of current purification techniques have led to the development of new forms of filtration systems that look to minimise associated costs and improve water quality.

1.2 Conventional Methods of Water Purification

Water purification is the removal of undesirable contaminants from water. Water purification techniques aim to recycle and reclaim fouled water or extend current water supplies by improving efficiency.

1.2.1 Coagulation, Flocculation, Sedimentation and Sand Filtration

Coagulation is the chemical processes that destabilises dissolved particles and colloidal suspensions in feed water. Coagulants generally involves adding ferric sulphate, ferric chloride or different types of polymers, a common theme among all compounds is the possession of a nominal positive charge that neutralises the negative charge of dissolved and suspended particles ⁴. After coagulation, flocculation occurs as particles adhere to each other forming large clusters, also known as flocs. Flocculation consists of various mechanism such as entrapment, adsorption, and complexation ⁴. The formation of flocs increases the particles weight causing the flocs to settle to the bottom of the vessel, a process known as sedimentation.

Coagulants are primarily used for their capability to remove natural organic matter which is commonly found in ground water. Natural organic matter is known to affect other water treatment processes, both in chemical disinfection (in the formation of disinfection by-products) and membrane filtration (acting as membrane foulants) ⁴. Hence, coagulation, flocculation and sedimentation act as basic conditioning mechanisms for both conventional filtration and membrane filtration.

1.2.2 Conventional Water Filtration Processes

Conventional water filtration applies both sand filtration and chemical disinfection for the purification of water. After sedimentation, sand filtration acts as a porous medium for the removal of particulates in water. While filters are generally made up of sand, gravel and charcoal are also implemented ⁵. Sand filters are capable of filtering at sizes of ≈ 0.1 mm ⁵; however, many contaminants such as viruses, are smaller than 0.1 mm. To remove viruses within the processed water, chemical disinfection is used.

Chemical disinfection of water is one of the most important advances of public health in the last century ⁶. In the United States of America, cholera and typhoid incidence rates dropped by 90% and 80% respectively upon the introduction of chemical disinfection ⁶. Chemical disinfectants are aimed towards killing bacteria in feed water by disrupting their chemical processes, thereby deactivating or killing the microorganism. Chemical disinfectants are known to persist in purified water longer than desired and can complex with other various contaminants. Some chemical disinfectants are composed of oxidising agents able to react with contaminants to form unwanted by-products. Certain disinfection by-products can be considered as carcinogens and mutagens ⁶. The formation of disinfection by-products is a concern as they can be toxic in trace quantities.

A commonly used disinfectant is chlorine ⁷ for which the reported disinfection by-products include a variety of trihalomethanes and chloroform, a probable carcinogen ⁶. In 1976, The United States Environmental Protection agencies placed regulations, the disinfection and disinfection by-product rule, on

permissible levels of disinfection by-products within drinking water ⁶. Adherence to the regulation is difficult as feed water conditions differ between locations and time affecting the concentration of disinfection by-products in purified water ⁶. This raises public health concerns as the potential toxicity of many disinfection by-products are relatively unknown ⁶.

The drawbacks of chemical disinfection have inspired methods capable of water purification that can sustain water quality when feed water conditions differ. Technological advances in membrane technology in the past 40 years has allowed for decreases in energy consumption ⁸.

1.3 Advanced Methods of Water Purification- Membrane Based Filtration

Membrane filtration allows for the separation between two adjacent phases, feed water and purified water (Figure 1-2). Pressure is applied on the feed water, causing the feed water to permeate through the membrane. The membrane interface consists of pores that are selective towards compound sizes that are equal to or less than the size of the pore (Figure 1-2). The size of the compounds that permeate through the membrane is dependent on the membrane properties and the size selectivity.

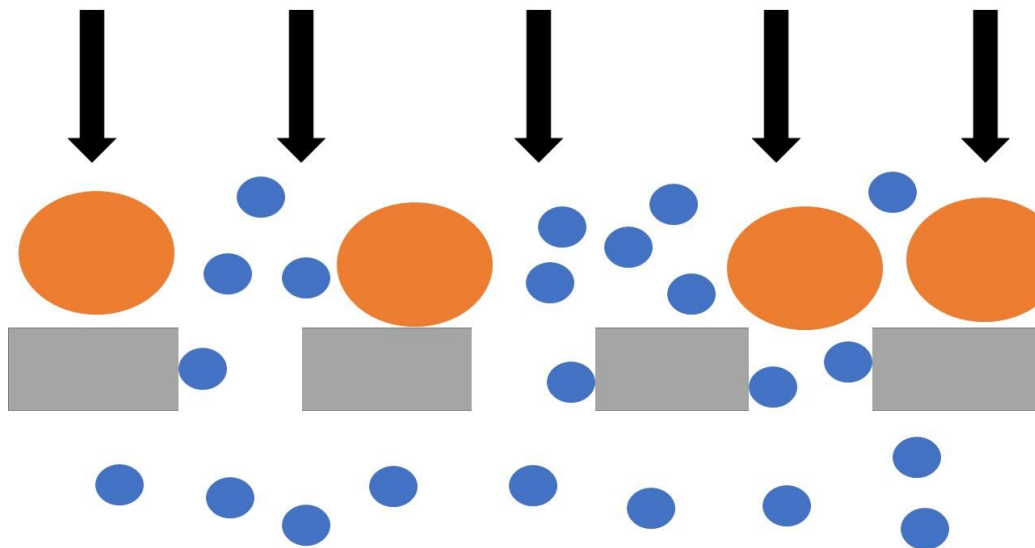


Figure 1-2 Pressure (black arrows) applied to the feed water on the porous membrane (grey). Permeation occurs for particles smaller than the pores (blue) and particles larger (orange) than the pores adhere to the membrane.

There are four types of pressure driven membrane filtration, Microfiltration (MF), Ultrafiltration (UF), Nano filtration (NF) and Reverse Osmosis (RO). They follow the same mechanism of filtration; however, the distinction between filtration techniques is dependent on the size selectivity of the membranes (Figure 1-3) ⁹. Through size selectivity, these techniques are prominently used in filtering out certain compounds as follows ⁷:

- MF can remove particulates, bacteria and turbidity (10 – 0.2 μm)
- UF can remove macro solutes, fine colloids and virus (40 – 20 nm)
- NF and RO can remove ionic species and low molecular weight organics

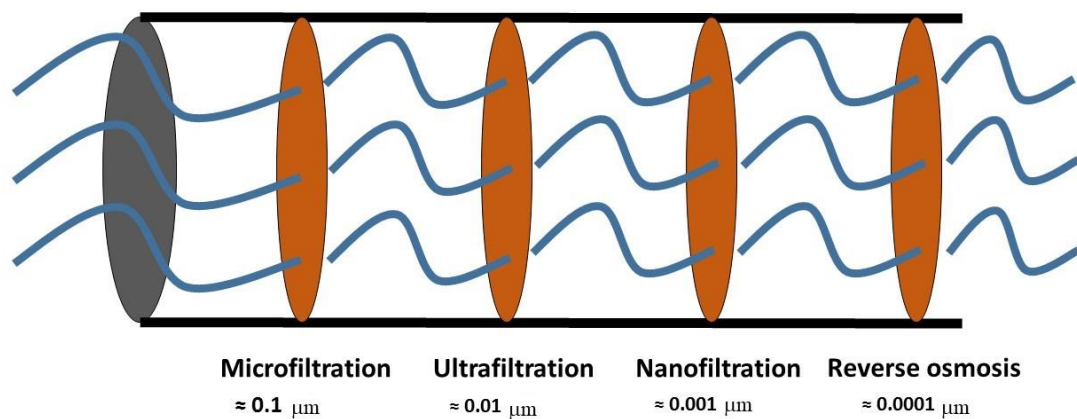


Figure 1-3 Different types of filtration process (orange circles). Length measurements given are the maximum value of the filtrates size (blue lines).

The size selectivity makes it commercially viable within a variety of fields, where applicability is dependent on the feed water. The following points are a general description of the types of membranes and the respective applications ¹⁰:

- MF: removal of particles and for sterile filtration used in medical, biotechnology industries.
- UF: for processes that involve concentration maintenance, fractionation, and purification, used in industries focusing on water treatment, food and beverages, chemicals.
- NF: potent in the separation of small inorganic salts and organic molecules. Primarily for water treatment and various other industries ⁹.
- RO: desalination, production of ultrapure water, primarily for water treatment.

Demand for membrane filtration will continue to grow as populations and water scarcity increase; however, many questions remain regarding how the molecular features of this technology affect their activity and outputs. There is a strong push by users and manufacturers to improve these membranes and the filtration processes to allow for more energy and cost-efficient separation ¹⁰.

Membranes are generally derived from two types of materials, organic and inorganic materials. Inorganic materials are highly suited for adverse environments (high temperature, an abundance of contaminants) and are usually made from different metals and ceramics ¹¹. Organic polymers are more widely used for filtration membranes. Some common types of polymers used are poly(ether sulfone), polyamide and poly(vinylidene fluoride) ¹⁰. In the determination of the membranes properties and performance, an understanding of the chemical nature is required.

1.4 Structure Variance in Polymers upon Membrane Synthesis

Certain membranes are formed through the blending of polymers. In Non-Solvent Induced Phase Separation (NIPS), a casting solution is made up of desired polymers dissolved in a poor solvent at high temperatures. The solution is quenched (generally in water) to lower temperature causing phase separation between the polymers and the solvent, forming cellular structures with pore formations ¹². Structural incompatibilities of the polymer-solvent system can lead to de-mixing, affecting the final fabrication. To analyse the effects of structural incompatibilities in the blending process, an understanding on polymer structure is required. Polymers are constructed from monomeric repeating units and the type of polymer created is dependent on the repeating monomer units (Figure 1-4).

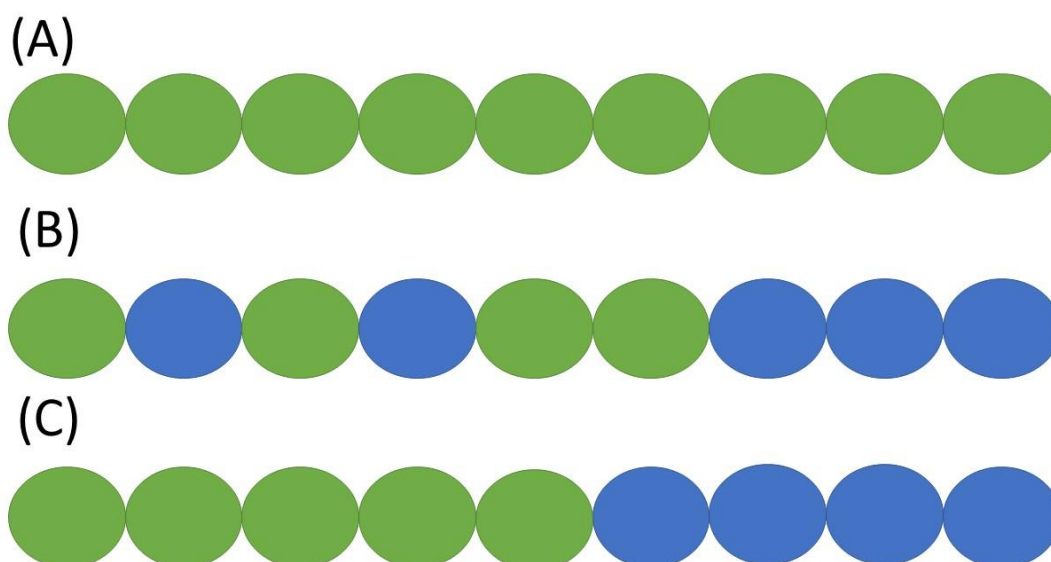


Figure 1-4: Different types of polymers composed of monomer unit 1 (green) and monomer unit 2 (blue). Compositions show a (A) Homopolymer, repeating sub units of an individual monomer unit, (B) Statistical copolymer, Monomer unit 1 and 2 exhibit a statistical ratio composition, (C) Block copolymer monomers form ‘block’ compositions respective to a monomer unit.

There are difficulties in deducing specific structure-activity relationships as polymers exist within a diverse range of structures. This is attributed to a variety of factors, including but not limited to the transfer agent, polymerisation time and the formation of different molecular shapes. Variations in molecular attributes such as molar mass, composition, type of copolymer, branching, charge and chain ends can exist within a given sample (Figure 1-5) ¹³. Each of these attributes exists as distributions, where the representative peak shape can be broad, narrow or multimodal.

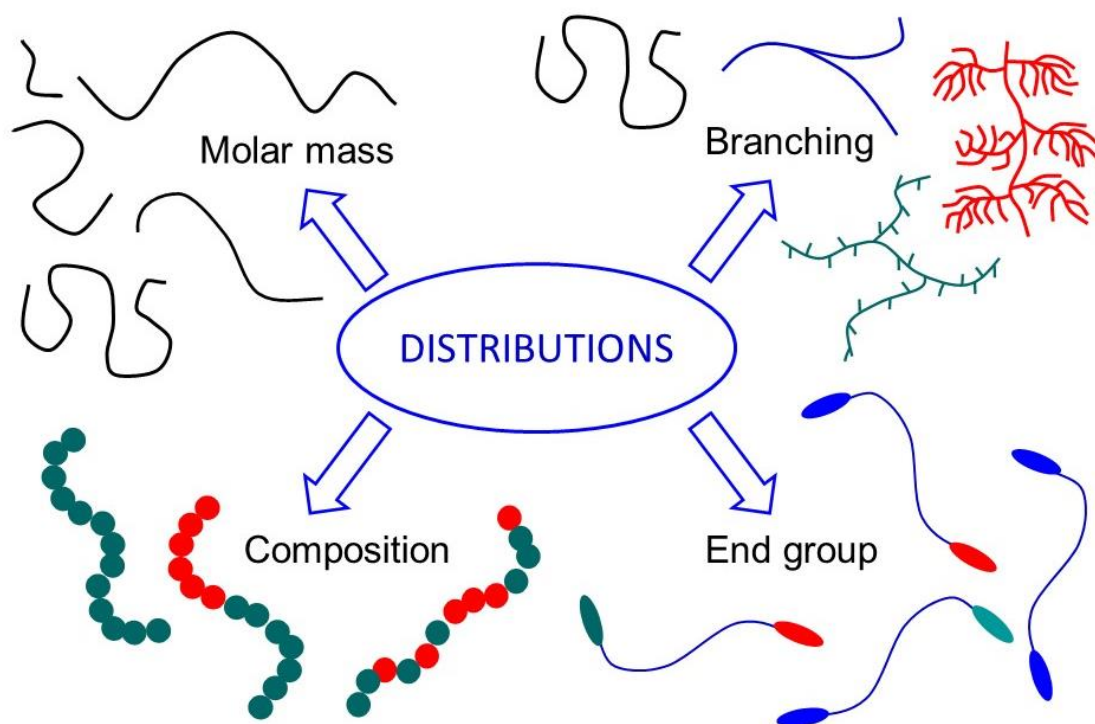


Figure 1-5 A schematic diagram showing that polymers are characterised by different types of distributions: molar mass, branching, chain ends and monomeric unit arrangement ¹⁴.

End groups are the molecular structures found at the ends of the polymer chain. The types of end groups found on the polymer chain are dependent on the initiator used and the reaction pathway. End groups have the capability of affecting numerous properties, dependent on the polymer. This makes the study of end groups complex as difficulties persist in the prediction of the specific effects of end groups. In small chain polymers, the effect of end groups is significant; however, as molecular weight of the polymer increases to large values, these effects are expected to eventually become negligible ^{15,16}.

Industrially relevant polymers exhibit chain lengths ranging from thousands to millions monomer units, making it increasingly complex to define the structure-activity relationship with end groups ¹⁵. Studies have investigated the influence end groups on solubility in small molar mass polymers ¹⁷ and hyperbranched polymers ¹⁸; however, the knowledge in large molar mass polymers with minimal branching is not as developed. The lack of a straightforward characterisation method (Section 2.1.1) creates difficulties on contributions made from end groups. Developments made within this topic

will help in the tailoring of mechanical properties in industrially relevant polymers.

1.5 Characterisation of Polymer Blends

The blending of polymers leads to materials that exhibit properties associated with each of the individual polymers ¹⁹. Typically, UF membranes employ the blending of a hydrophilic polymer with a hydrophobic polymer ²⁰. Membranes with hydrophilic surface properties allow for higher water flux and lower fouling ²⁰, where hydrophobic properties reduce the potential of membrane leaching ²⁰ and display an increase of mechanical stability in an aqueous environment ²¹. Ensuring the membrane retains the properties of the precursors requires an understanding of the miscibility of the polymers.

Blend formulations desire the individual polymers to be miscible, thereby producing materials with the desired features of its constituents. Difficulties persists with this approach as structure incompatibilities between relatively stable polymers causes polymers to phase separate into localised regions (Figure 1-6)²². Partially immiscible or fully immiscible blends exhibit reduced mechanical and functional properties in comparison to a miscible blend. A large number of industrially used blends are only partially miscible where morphology can be random throughout the membrane.

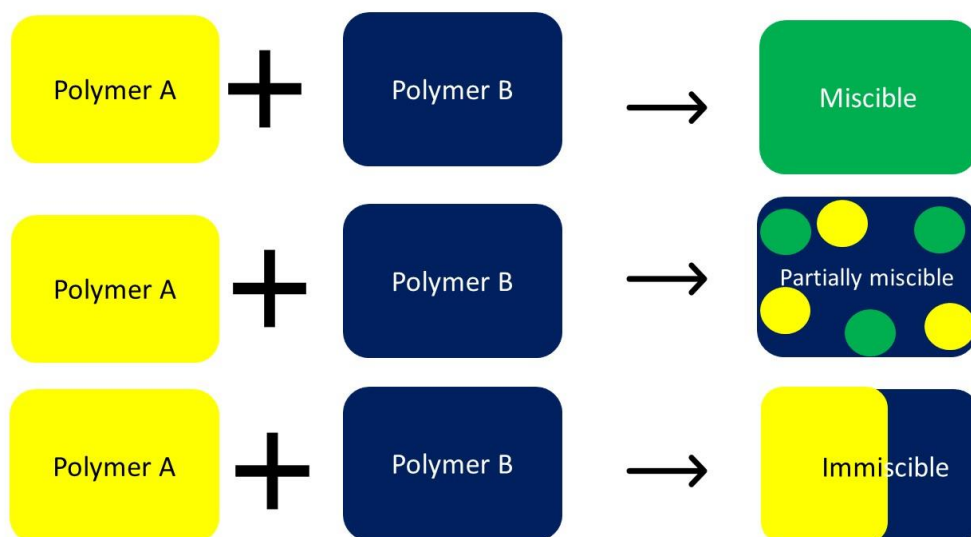


Figure 1-6 Schematic diagram of the outcomes of blending two polymers. Formation of localised regions can be seen in a partially miscible blend.

General approaches to increasing miscibility are through favourable chemical interactions (primarily hydrogen bonding) that favour mixing ²³. Ideally, polymers containing both donor sites and acceptor sites form blends that are likely to mix. These structures influence the degree of intermolecular hydrogen bonding, dipole-dipole interactions and/or ionic bonding. Blends exhibiting the aforementioned interactions are relatively stable and miscible ¹⁰. Through hydrogen bonding, physical properties can be affected within polymeric blends including the melting temperature, the temperature where molecular chain rotation is restricted (glass transition temperature, T_g), crystal structure, solubility and miscibility ²⁴.

For semi-crystalline polymer blends, these materials consist of regions of rigidity (crystalline) and regions of high mobility (amorphous). Polymers are semi-crystalline at temperatures up until the melting point indicating the importance of temperature in blend composition. Characterisation is complex as the interplay between asymmetries from polymorph variations and the presence of different polymers within the blend morphology makes data interpretations difficult ²². Thus, methodologies that correlate functional properties with miscibility have led to a rise in both industrial applications and academic interest ¹⁰.

1.6 Relationship between Structure and Physical Properties

Membrane development largely focuses on the optimisation of physical properties, one of the most important being water permeability. Water permeability is the volume of water that passes through a porous material as a function of time. Water permeability is affected by factors such as pore size distribution (PSD), particle deposits on the membrane surface (fouling) and mechanical strength under pressure. For a generalised viewpoint on the desired properties of UF membranes refer to (Table 1-1).

Table 1-1 Ultrafiltration membranes essential and additional desired properties ⁷.

Membrane	Essential properties	Desired properties
Ultrafiltration	Water permeability > 500 L m ⁻² h ⁻¹ bar ⁻¹ Mean pore sizes: 20-50 nm Robust (wide pH range) Good mechanical strength Not hydrophobic Low cost	Water permeability >10 ³ L m ⁻² h ⁻¹ bar ⁻¹ Isoporous (very narrow PSD) Anti-fouling High structural integrity Tunable (surface charge, pore size)

The PSD characterises the size and dispersity of the pore size over the membrane hence, it quantifies the heterogeneity of pore sizes found within the membrane. Commercial UF membranes often exhibit a relatively wide PSD ⁷, where ideal UF membranes are modelled to become more isoporous ¹⁰. Regularity in pore size allows for precision on the molecular weight cut off ¹⁰ and a constant water permeability. A wide PSD is prone to fouling at the

largest pore due to disproportionate flux thereby lowering the water permeability ⁷.

A prominent problem that is limiting the use of membrane filtration is membrane fouling ²⁵. Membrane fouling is influenced by undesired adsorption interactions occurring at the membrane/feed water interface causing for a decrease in performance ²⁵.

Mechanical strength is the ability for a material to sustain an applied load without deformation or breakage. Applied pressure to the feed water shares a proportional relationship with water permeability. This requires a mechanically stable membrane to retain structural integrity at high pressures for optimal water permeability. The optimisation and prediction of PSD, antifouling capabilities and mechanical strength requires an understanding on the chemical nature and composition of the membrane.

Modification of membrane composition has shown to affect the aforementioned physical properties; however, physical property optimisation can be influenced by a variety of chemical factors. For example, increasing the hydrophilicity of the membrane reduces adsorption interactions from foulants ²⁵; however, hydrophobic polymers tend to provide chemical stability and mechanical strength ²⁶. Industrial means of characterisation primarily observe the physical properties of the membrane. To develop structure-activity relationships for the improvement of membranes, characterisation methods that elucidate the chemical nature of the membrane materials are required.

1.7 Characterisation Methods

The following section includes characterisation methods used in this study detailing the theoretical principles of the method and the desired outputs.

1.7.1 Capillary Electrophoresis

Free solution Capillary Electrophoresis (CE) is a separation technique able to separate molecules based on their charge-to-friction ratio ²⁷. The migration velocity (v) is proportional to the electric field strength (E) and the electrophoretic mobility (μ) is the proportionality constant. This is expressed below (Equation 1.1)

$$v = \mu \cdot E \quad 1.1$$

In CE, a background electrolyte is introduced in a capillary tube and the sample is injected at one end of the capillary. Reservoirs of background electrolyte are connected to both ends of the capillary and an electric field is applied allowing for separation (Figure 1-7).

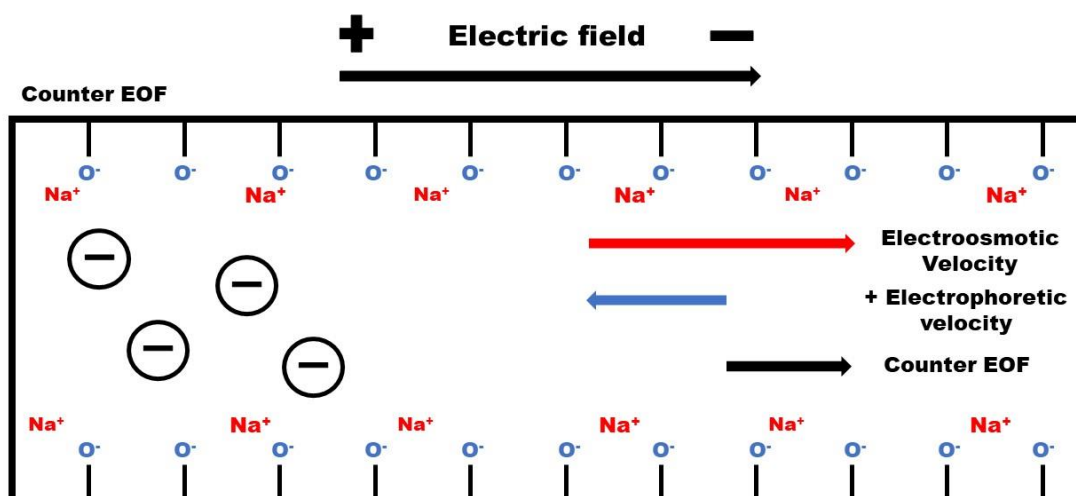


Figure 1-7 Migration of ions in CE. Vector of the ions are represented by arrows; the length of the arrow represents the magnitude of the vector.

A factor to the “net migration” of ions inside a capillary is the electroosmotic flow (EOF). The EOF is induced by the migration of ions within the background electrolyte in a capillary under the presence of an electric field, contributing towards migration of all molecules, including neutral analytes.

Identification of the electroosmotic flow velocity allows for the investigation of analytes based on the respective charge-to-friction ratio. Separation of analytes is respective to their electrophoretic velocity (V_{ep}) relative to the electroosmotic flow velocity (V_{eof})²⁷ of the background electrolyte, yielding an apparent velocity (V_{app}) within the capillary (Equation 1.2).

$$V_{app} = V_{eof} + V_{ep} \quad 1.2$$

1.7.1.1 Expressing Migration Time as Electrophoretic Mobility

EOF can be represented by the migration time of neutral species with the mobility set as 0. Migration time can be converted to electrophoretic mobility, μ_{ep} , (Equation 1.3) where L_d is the length to the detector, L_t is the total length of the capillary and V is the voltage applied on the two ends of the capillary, t_m and t_{eo} are the migration time of the samples and neutral species, or EOF marker, respectively. In this work, anode is at the inlet of the capillary and cathode is at the outlet. According to this formula, negatively charged analytes would have negative mobilities and positively charged analytes have positive mobilities.

$$\mu_{ep} = \frac{L_d \cdot L_t}{V} \cdot \left(\frac{1}{t_m} - \frac{1}{t_{eo}} \right) \quad 1.3$$

1.7.1.2 Correcting for the Analyte Velocity through the Detector

Absorbance is corrected to account for the analyte velocity through the detection window. Absorbance is corrected in relation to the time spent at the detection. This is accounted for in the conversion from time scale distributions to mobility scale distributions on the x-axis. It is to be noted that detection occurs during separation and not after it. This is shown in Equation 1.4 to Equation 1.7, where absorbance is corrected for velocity.²⁸

$$UV\ signal_{corrected} = \frac{Absorbance}{t_m} \quad 1.4$$

$$W(\mu) = \frac{UV \text{ signal}_{corrected}}{\frac{d\mu}{dt_m}} \quad 1.5$$

Transformation to weight-distribution of electrophoretic mobilities $W(\mu)$ is then done, where $\frac{d\mu}{dt_m}$ is the derivative of μ with respect to t_m

$$\frac{d\mu}{dt_m} = -\frac{L_d \cdot L_t}{V} \times \frac{1}{t_m^2} \quad 1.6$$

Combining Equation 1.6 with Equations 1.4 and Equation 1.5 provides Equation 1.7,

$$W(\mu) = Absorbance \times t_m \quad 1.7$$

Using (Equation 1.7), raw absorbance data was corrected to consider the analyte velocity and transformed from absorbance on the time scale to the mobility scale. In determination of structural features these corrections are essential.

1.7.1.3 Capillary Electrophoresis in the Critical Conditions

CE has also shown to be an effective tool for the separation of several natural and synthetic polymers based on their composition and branching in critical conditions²⁹. CE in the Critical Conditions (CE-CC) relates to the conditions sought in liquid chromatography where separation occurs in the absence of molar mass. At certain chain lengths, the electrophoretic mobility of polyelectrolytes becomes independent of molar mass (Figure 1-8)³⁰.

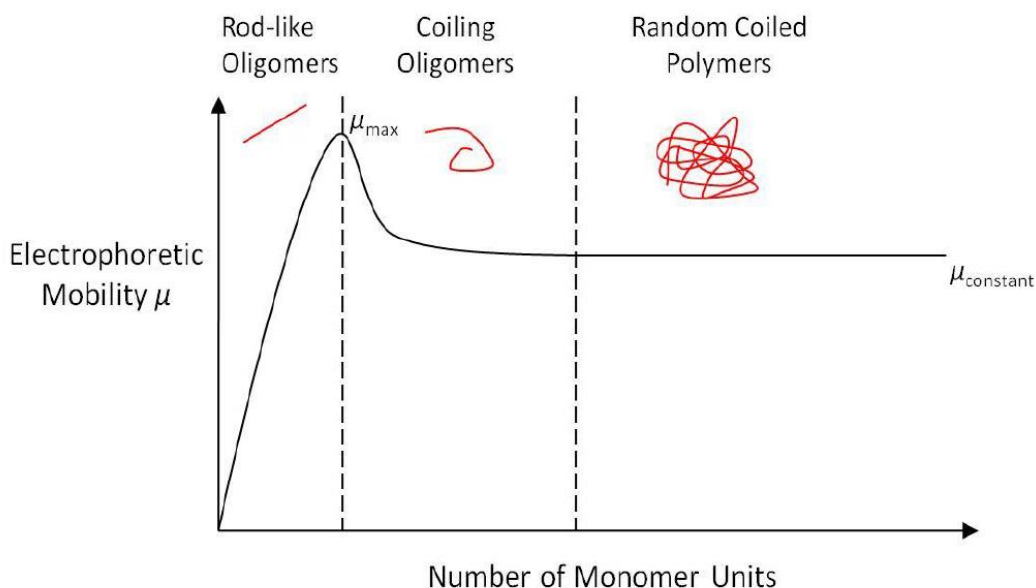


Figure 1-8 General trend of electrophoretic mobility in respect to the number of monomer units in a polyelectrolyte ³⁰

At μ_{constant} the electrophoretic mobility is independent of molar mass at a degree of polymerisation usually above 15 ³⁰⁻³². The polymer likely adopts a coiled conformation causing the electrostatic friction to have larger influence than the hydrodynamic friction ³³. Therefore, CE-CC allows for separations by composition and topology ²⁹.

1.7.2 Nuclear Magnetic Resonance Spectroscopy

Nuclear magnetic resonance (NMR) spectroscopy allows probing the molecular dynamics of a material. An attraction of NMR spectroscopy is the capability to study the molecular dynamics of the material in both the solid and solution state ³⁴. Certain literature sources have signified the importance of solid-state NMR in deducing molecular mobility ³⁵ and structure elucidation of polymeric membranes ³⁴. To obtain a detailed knowledge on what information can be obtained through NMR spectroscopy, an understanding of the theoretical principles is required.

1.7.2.1 Introduction to NMR theory

NMR spectroscopy is a form of absorption spectrometry capable of analysing the nucleus of atoms within a sample. Under the influence of an external magnetic field, a sample absorbs electromagnetic radiation in the radio frequency (rf) region. Angular momentum (P) of a spinning nucleus produces a magnetic moment (u), which is influenced by the charge and the motion of the charge ³⁶ as described below (Equation 1.8)

$$u = \gamma P \quad 1.8$$

where γ is the magnetogyric ratio, a constant value for each nuclide. Both magnetic moment and angular momentum are considered vector quantities. In an external static magnetic field (B_0) the nuclei magnetic moments align themselves relative to the field in a discrete number of orientations as the energy states are quantised.

Atomic nuclei are characterised through a nuclear spin quantum number (I) which is a multiple of $\frac{1}{2}$. Nuclei with $I = 0$ possess no nuclear spin and are not NMR active; therefore, ^{12}C is not NMR active but the ^{13}C isotope is NMR active. A spin of magnetic quantum number I , exists as $2I + 1$ possible spin states. For a spin $\frac{1}{2}$ nucleus such as ^1H and ^{13}C , there are two possible spin states $+\frac{1}{2}$ and $-\frac{1}{2}$ considered as “spin up” and “spin down” respectively.

A spin $\frac{1}{2}$ nucleus can be considered to orientate itself parallel (known as spin up), or anti parallel (known as spin down) to the static field. Spin states parallel to the magnetic field consist of lower energy, resulting in a positive magnetogyric ratio. In terms of classical mechanics, the magnetic field imposes a torque on the magnetic moment, causing the moment to precess about the applied field (Figure 1-9), termed as Larmor precession. Angular velocity of the precession is described below (Equation 1.9):

$$\omega = -\gamma B_0 \quad 1.9$$

the frequency of precession is termed as Larmor frequency (ν) and is described below (Equation 1.10),

$$\nu = \omega/2\pi \quad 1.10$$

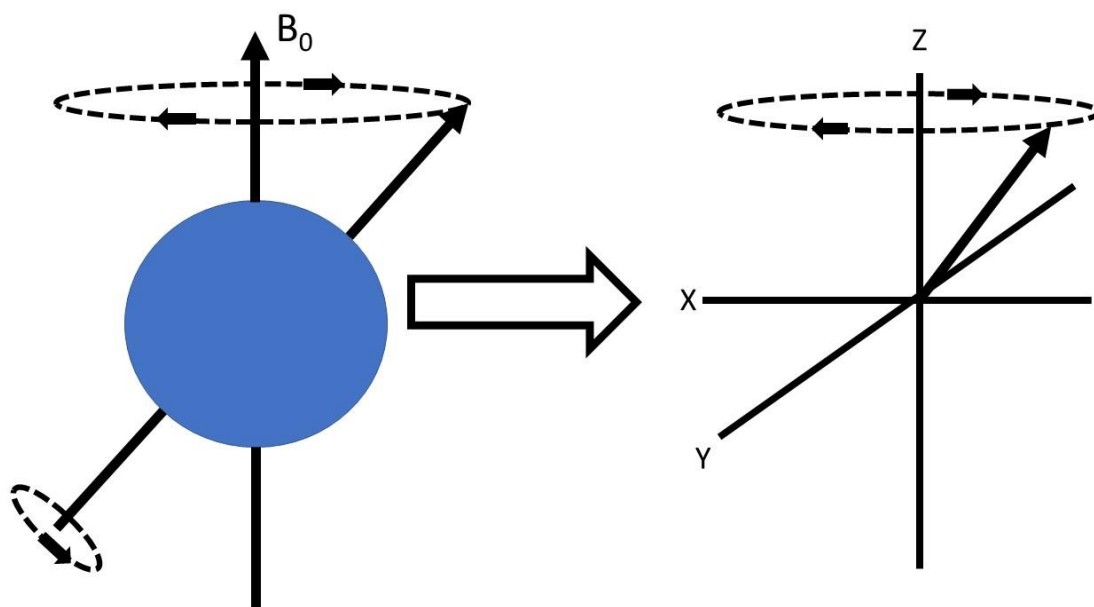


Figure 1-9 Precession of a single nucleus affected by a static magnetic field B_0 . B_0 is directed along the z-axis and the nucleus motion is represented as a vector moving in a pattern similar to the surface of a cone.

The spin down nuclei are in slight excess; however, the difference between energy levels are small. The population differences between the two energy states are small, approximately 1 spin to 10^4 spins at the highest ³⁷. The excess nuclei spins are distributed around the precessional cone, resulting in a bulk magnetisation vector along the z-axis at equilibrium (Figure 1-10). The tiny population of excess nuclear spins is part of the reason NMR is considered insensitive compared to other spectroscopy techniques (infrared spectroscopy and ultraviolet spectroscopy).

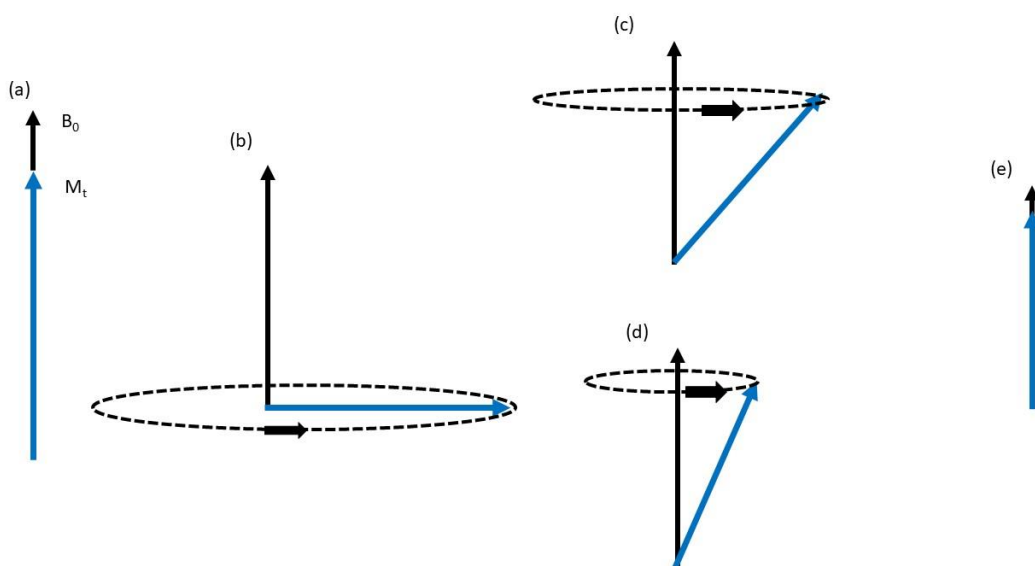


Figure 1-10 Bulk magnetisation of the sample in a pulsed NMR experiment; (a) and (e) at equilibrium, (b) at the time of acquisition, (c) and (d) during the relaxation delay.

Signal is attained when the nucleus changes spin state and absorbs electromagnetic radiation at a frequency matching the Larmor frequency of the nucleus. Nucleic spins in different chemical environments exhibit different Larmor frequencies. The difference in Larmor frequencies appear in the resultant spectrum (as a difference of chemical shifts). Chemical shift differences are recorded in the ppm range relative to the Larmor frequencies thereby producing a spectrum of the sample.

1.7.2.2 Introduction to Solid-State NMR Spectroscopy

The previous section is applicable in both solution and solid-state NMR spectroscopy. Solution-state NMR spectroscopy is considered as a prominent tool for characterisation of organic molecules; however, dissolving the sample can restrict determinations made on the sample. Dissolution affects the structural integrity of the sample and introduces a foreign compound generally not seen in the application state. Representations made on the application state cannot be determined, thereby causing difficulties when developing relationships between structure and functionality. Solid-state NMR spectroscopy operates without the use of a solvent allowing for structure and mobility determinations made on the sample in its application state.

In solution-state NMR spectroscopy, dissolution through a solvent, induces an increased molecular mobility of the atoms. In the liquid state, molecular tumbling averages the interactions affecting line shapes, dipolar coupling, forming relatively well resolved signals. In the solid-state, chemical shift anisotropy, dipolar coupling and quadrupolar effects are not averaged causing a broadening of line shapes ³⁸. As such, solution-state NMR spectroscopy is considered the attractive choice for molecular structure determinations due to the high resolution it can attain. While signals are not as well resolved in solid-state NMR spectroscopy, it gives an accurate representation of the molecular mobility of the sample allowing for techniques, such as Two Dimensional Wideline Separation (2D-WISE), that probe molecular mobility. Determinations on molecular mobility allows for deductions on species that are mobile or immobile within the sample. The determination of mobility is primarily conducted through the interpretation of line shapes and line widths.

1.7.2.3 Line Shapes and Line Widths

NMR spectra of solid samples are usually quite broad due to anisotropic nuclear interactions. In order to increase resolution, Magic Angle Spinning (MAS) can be used. The MAS procedure rotates the sample at an axis inclined at the angle $54^{\circ}44'$ relative to the direction of the static magnetic field (Figure 1-11) ³⁹. Rapid isotropic motion at this angle eliminates anisotropic interactions ³⁹. This leaves only isotropic shift interactions and isotropic J-couplings on NMR spectra, similar to the interactions found in NMR spectra of liquids ⁴⁰. Spinning sidebands should appear on the spectrum at multiples of the spinning frequency.

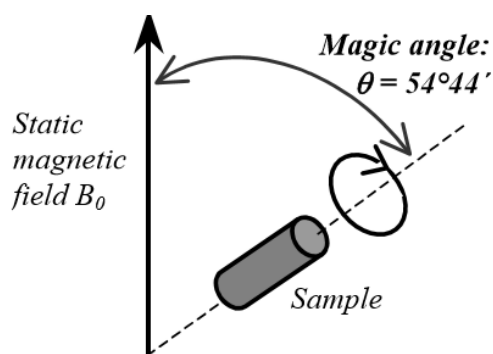


Figure 1-11 Magic angle spinning (MAS) of a solid-state NMR sample. taken from ⁴⁰.

1.7.2.4 Pulse Programs: Solution and Solid-state NMR Spectroscopy

The following pulse programs are applicable to both solution and solid-state NMR spectroscopy. All the following techniques are applied in solid-state NMR throughout this thesis.

1.7.2.4.1 Single Pulse Excitation

Single Pulse Excitation (SPE) can be performed on all NMR-active nuclei; however, this work will mainly focus on ¹³C and ¹H. SPE on the ¹H channel is considered as the simplest NMR experiment. The pulse scheme of a ¹H SPE is displayed below (Figure 1-12).

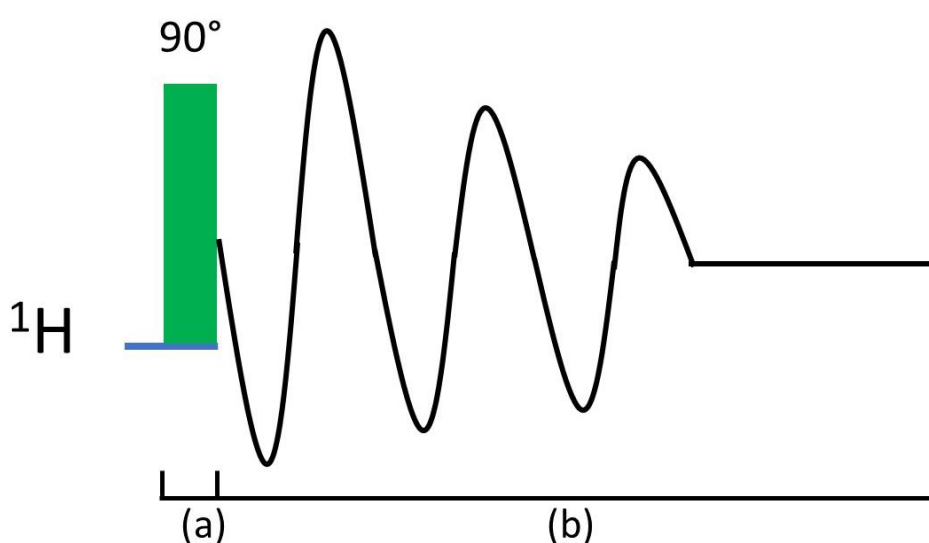


Figure 1-12 ¹H single pulse excitation pulse scheme. Adapted from ⁴⁰.

Initial bulk magnetisation is at equilibrium in reference to the static magnetic field. A 90° pulse is applied to direct bulk magnetisation to the xy plane which is orthogonal to the main magnetic field (a). Magnetisation is recorded at the xy plane, producing a Free Induction Decay (FID) which is converted into a spectrum after Fourier transform (b). The pulse sequence of a ^{13}C SPE experiment is displayed in (Figure 1-13).

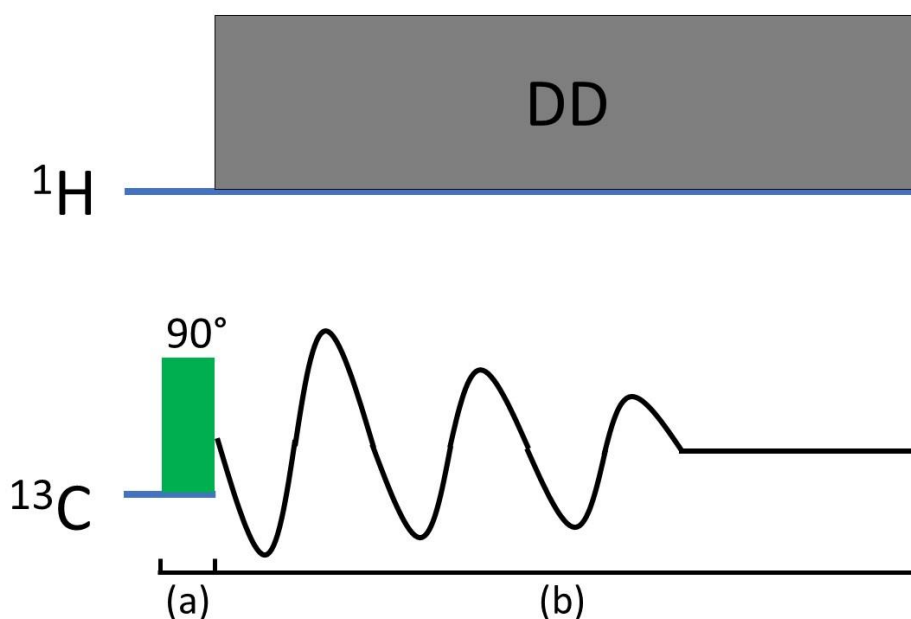


Figure 1-13 Pulse scheme of a ^{13}C SPE experiment. Adapted from ⁴⁰.

Initial bulk magnetisation of carbon nuclei is at equilibrium in reference to the static magnetic field. (a) a 90° pulse is applied to direct the bulk magnetisation to the xy-plane which is perpendicular to the static magnetic field. (b) Upon data acquisition, the ^1H nuclei surrounding the measured carbon nuclei are irradiated with a continuous rf field causing dipolar decoupling (DD) between the protons and carbons. This heteronuclear decoupling process minimises line broadening influenced by strong dipole-dipole coupling between ^{13}C and ^1H .

Quantification studies are possible through SPE as shown in various studies using sample systems such as polymer resins ⁴¹ and coal ⁴² to name a few. To ensure a quantitative spectrum, the sample nuclei need to be in thermal equilibrium prior to pulsing, therefore requiring techniques able to determine the relaxation time to reach thermal equilibrium.

1.7.2.4.2 Longitudinal Relaxation

Pulse excitation of the spin system moves the bulk magnetisation vector away from thermal equilibrium, +z axis, causing a discrepancy in spin populations. Recovery to magnetisation along the +z axis, termed longitudinal relaxation, is dependent on equilibrium populations being re-established. Partial longitudinal relaxation leads to an overall loss of energy in the spins. The loss of energy is transferred to its environment in the form of heat causing for partial signal attainment. To obtain quantifiable spectra, determination of the longitudinal relaxation is required. This is expressed by the Bloch theory of NMR (Equation 1.11).

$$M_z = M_0(1 - e^{-t/T_1}) \quad 1.11$$

Where (M_z) is the recovery of the +z magnetisation, M_0 is the magnetisation at thermal equilibrium and T_1 is the time constant for relaxation. The Bloch theory proposes longitudinal relaxation follows an exponential trend, a model well documented for $\frac{1}{2}$ spin nuclei (refer to Figure 1-14)³⁶.

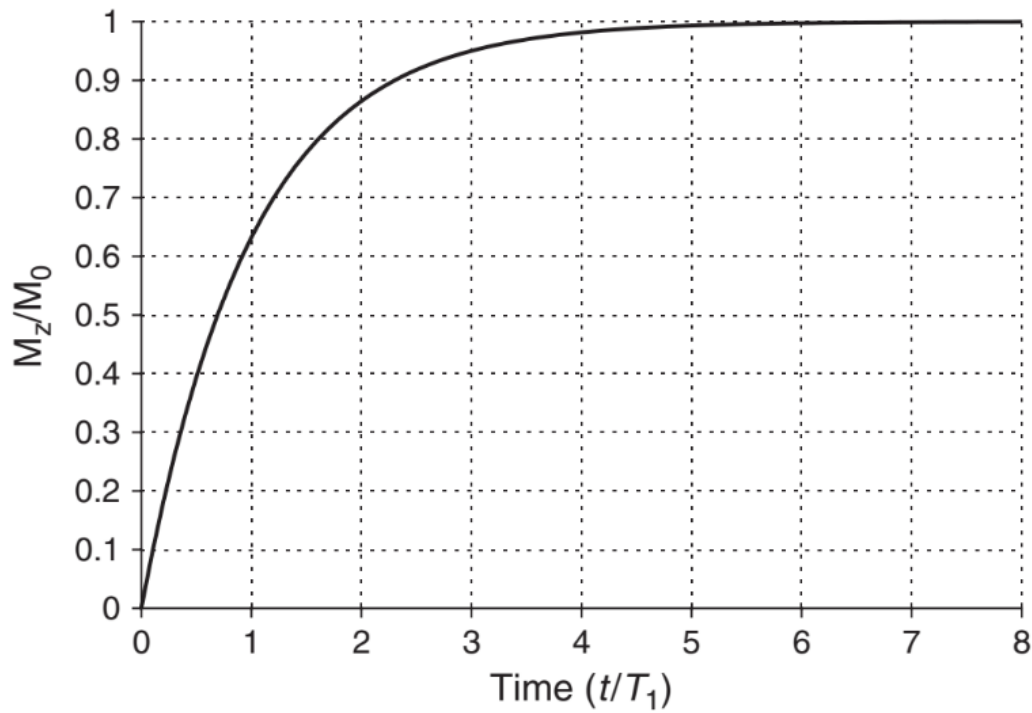


Figure 1-14 Longitudinal relaxation dictated by the time constant (τ/T_1) and magnetisation approaching thermal equilibrium. Longitudinal relaxation is considered complete at a period of $5T_1$. Image taken from ³⁶.

The exponential growth of longitudinal magnetisation is considered 99.33 percent recovered after a period of $5T_1$ (Figure 1-14) which ranges from a few seconds to many tens of seconds in carbon. It is noted that Figure 1-14 was determined through SPE; however, SPE is not conventionally used to determine longitudinal relaxation as it is considered inefficient ³⁶. To determine longitudinal relaxation, the most common method applied is inversion recovery ³⁶.

1.7.2.4.3 Determining Longitudinal Relaxation through the Inversion Recovery Sequence

Inversion recovery perturbs the spin system from thermal equilibrium and determines the rate of recovery back to thermal equilibrium as a function of time. Complete relaxation between two pulses allows for a maximum positive signal recorded; thereby, allowing for quantitative measurements through ^{13}C single pulse excitation. This discussion will focus mainly on inversion recovery being applied to carbon; however, this technique can be applied to

all nuclei. The pulse sequence of a ^{13}C inversion recovery experiment is displayed in (Figure 1-15).

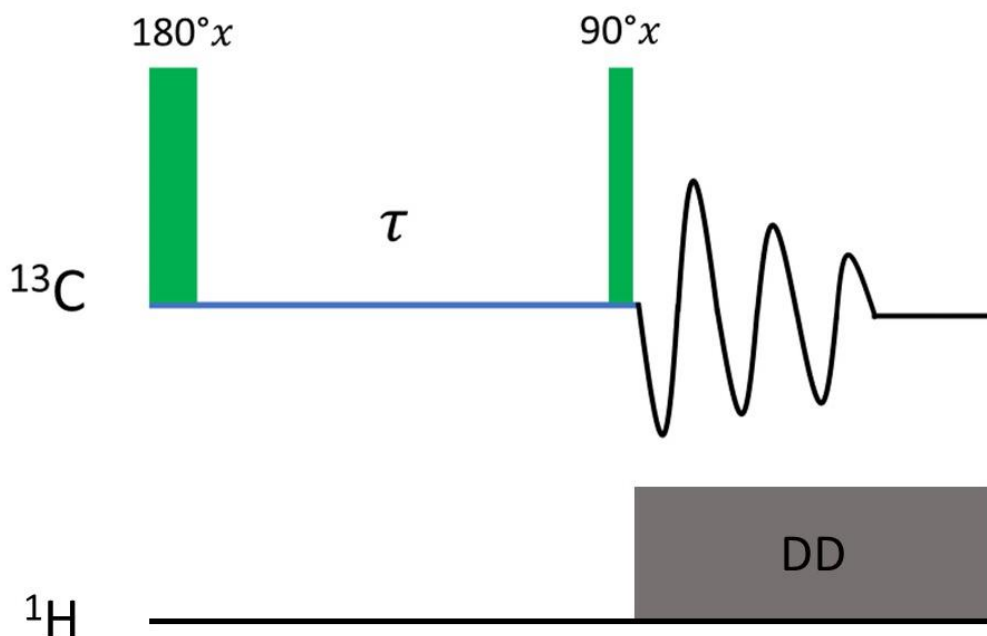


Figure 1-15 Pulse scheme of a ^{13}C inversion recovery experiment.

Inversion recovery follows a two-pulse sequence. The initial carbon magnetisation is inverted through a 180° pulse which flips the magnetisation from the $+z$ axis to $-z$ axis. During the evolution time (τ), the magnetisation then gradually reverts back to the $+z$ axis at a rate dictated by the longitudinal relaxation time (T_1). Magnetisation along the z -axis is unobservable, therefore a 90° pulse places the magnetisation vector along either the $+y$ axis or $-y$ axis dependent on the T_1 .

$$M_t = M_0(1 - 2e^{-\tau/T_1}) \quad 1.12$$

At τ equals zero, the intensity of the magnetisation vector, M_t , aligns itself along the $-y$ axis at full intensity producing an inverted spectrum using conventional spectrum phasing (Equation 1.12) ³⁶. At large τ values the intensity of the magnetisation vector aligns along the $+y$ axis producing a positive signal, an indicator of complete longitudinal relaxation between

acquisitions. The τ value required to equate $M_t = 0$ is considered the null condition, thus defining τ_{null} . The null condition is expressed in (Equation 1.13).

$$T_1 = \frac{\tau_{null}}{\ln 2} = 1.443\tau_{null} \quad 1.13$$

At τ_{null} , the T_1 can be determined; however, the value is considered an estimate ³⁶. Errors may be introduced through inaccurate 180° pulses and insufficient waiting periods between acquisitions ³⁶ requiring τ values larger than τ_{null} . Complete relaxation between two pulses allows for a maximum positive signal recorded; thereby, allowing for quantitative measurements through a ¹³C SPE pulse program.

1.7.2.5 Pulse Programs: Applied Only in Solid-State NMR

The following pulse schemes are only applicable solid-state NMR

1.7.2.5.1 ¹³C Cross Polarization

The low natural abundance of ¹³C nuclei ³⁶ has led to the developments of techniques designed to increase the sensitivity in ¹³C spectra. CP increases sensitivity in the dilute nucleus (¹³C), through indirect transfer of magnetisation from the abundant nuclei (¹H). T_1 relaxation of hydrogen nuclei is (in most cases) shorter than carbon nuclei allowing for higher polarization and an increase in signal. The pulse sequence of a CP experiment is displayed in (Figure 1-16).

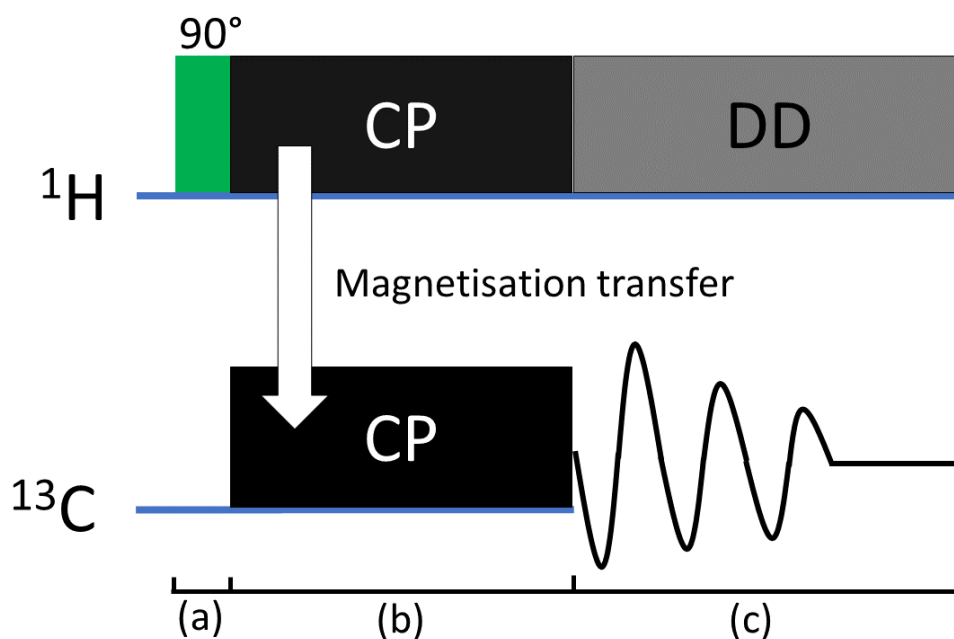


Figure 1-16 Pulse scheme of a ^{13}C cross polarisation experiment. Adapted from ⁴⁰.

In the initial stages (a) of the experiment, a 90° pulse is applied to drive ^1H magnetisation towards the xy-plane. Thereafter (b) CP is conducted through a defined contact time, TCP, where magnetisation is transferred from the ^1H nuclei to the ^{13}C nuclei. (C) The FID of the ^{13}C nuclei is detected as dipolar decoupling occurs with the ^1H nuclei.

1.7.2.5.2 Two-Dimensional Wideline Separation

In obtaining specific information towards favourable interactions between individual polymers, advanced techniques such as 2-Dimensional Wideline SEparation (2D WISE) can be implemented. 2D WISE measurements correlate a ^{13}C NMR spectrum with a ^1H NMR spectrum to determine the segmental mobility of individual carbon sites (Figure 1-17) ⁴³. The distinction between segmental mobility pertaining to specific functional groups gives information on favourable polymer-polymer interactions that affect miscibility.

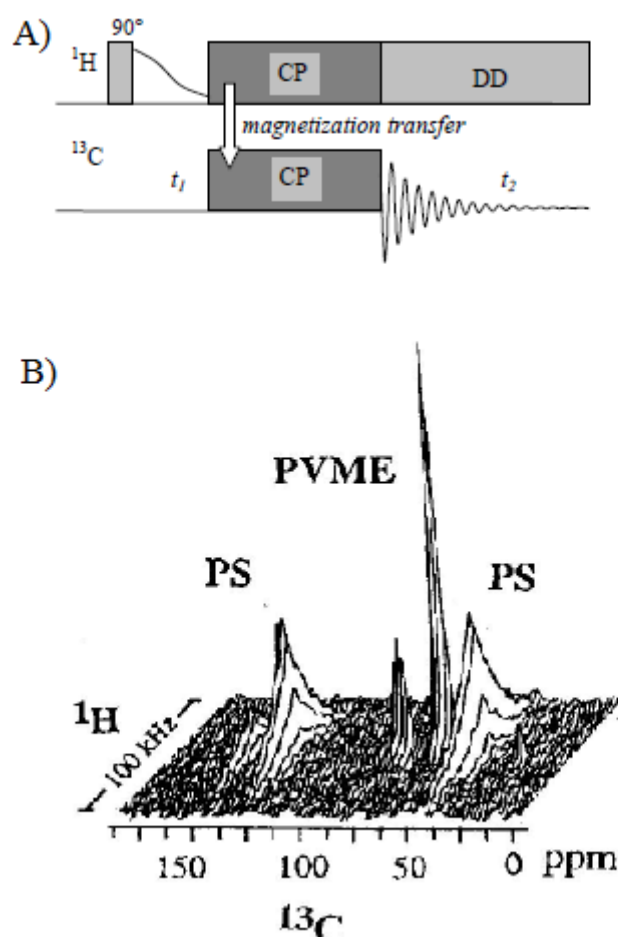


Figure 1-17 (A) Pulse sequence for a 2D WISE experiment ⁴⁰ B) resultant 2D WISE spectrum correlating molecular structures within a ^{13}C spectrum to the corresponding segmental mobilities through a ^1H spectrum ⁴³.

The pulse sequence of a 2D-WISE experiment is similar the pulse sequence to CP pulse sequence; however, transformations of the FID results in a 2D spectrum. In terms of defining the pulse sequence of a 2D WISE (Figure 1-17A), a 90° radiofrequency pulse is applied to flip the magnetisation of the hydrogens to the xy-plane ⁴⁰. Magnetisation of hydrogens is transferred to the carbons within the sample through dipole-dipole couplings under the Hartmann-Hahn conditions during the CP contact time ⁴⁴. After carbon magnetisation, the resulting magnetisation is detected using ^1H dipolar decoupling during t_2 .

Since conventional CP is only able to directly acquire 1 dimensional data, 2D data is recorded indirectly ⁴³. To acquire a 2D FID, several 1D FID are

assembled at increasing t_1 (indirect dimension) values ⁴³. ^1H signal intensity after t_1 is encoded to the FID recorded during t_2 . Correlation of the different FIDs results in a 2D dataset where 2D Fourier transform is applied for a 2D spectrum (refer to Figure 1-17B) ⁴³.

1.7.3 Scanning Electron Microscopy

Scanning Electron Microscopy (SEM) is a microscopy technique that applies a focused beam of electrons on a sample to produce an image. Preparation of the technique involves mounting a sample in the chamber where the sample is put under vacuum. At the top of the column, electrons are produced and accelerated to the surface of the sample. The beam of electrons passes through a combination of condenser lenses that focus the electron beam. Upon interaction with the sample, secondary electrons, backscattered electrons and characteristic X-rays are produced and detected to form an image (Figure 1-18).

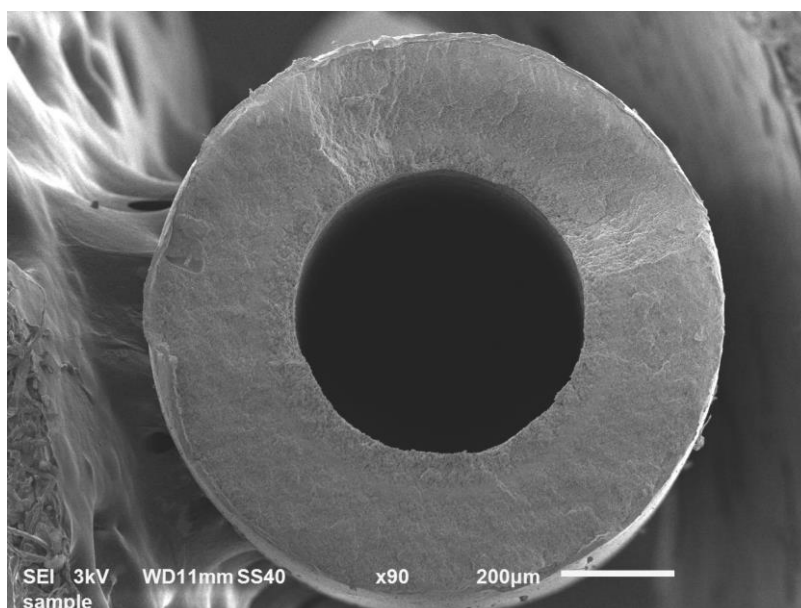


Figure 1-18 SEM image at the cross section of the membrane.

SEM has been extensively used to characterise UF membrane surface properties, both qualitatively and quantitatively (e.g. pore size, pore shape and porosity) ⁴⁵. Qualitative determinations allow for deductions made on the membrane surface, membrane cross section and fouling layers ⁹.

1.8 Aims and Objectives

This project aims to develop structure property relationships for the improvement of ultrafiltration membranes. The ultrafiltration membranes used are provided by an industrial sponsor and are primarily made from the blending of two or more polymers. This project will:

- Assess the impact of polymer end groups on solubility.
- Characterise UF membranes and the respective precursors at the molecular scale
- Identify relationships between functional properties and surface composition of UF membranes.

In regard to the impact of end groups on solubility, the objectives are:

- Understanding the effect of end groups on the solubility of poly(*N*-vinyl pyrrolidone) (PVP) through solubility tests and to use CE as a method to separate polymers through end groups.

In regard to miscibility characterisation of the ultrafiltration membranes, the objectives are:

- To determine the chemical structures making up the composition of the membrane and affecting miscibility through solid-state NMR spectroscopy,

In regard to analysing current methodologies used to optimise towards functionality and surface composition, the objectives are:

- To analyse the surface composition of UF membranes through SEM and NMR.
- The determination of the functional properties through tensiometry and tensile strength tests.
- The Identification of relationships between surface composition and functional properties.

1.9 Chapters and Potential Publications Overview

An in-depth characterisation of the polymers used in UF membranes is presented in this thesis. Structural information of polymers within membranes enables knowledge to develop links to membrane performance. An enhanced understanding of the molecular behaviour will help improve design and optimise methods of membrane manufacturing. This thesis is divided into three chapters which are discussed individually below (Sections 1.9.1.1 to 1.9.1.3)

1.9.1.1 Characterisation of Poly(N-vinyl pyrrolidone) End Groups through Capillary Electrophoresis (chapter 2).

The second chapter delves into the influence of end groups on solubility in blends with PVP, a polymer commonly used in membrane manufacturing and a variety of other industries. This work will use CE as a characterisation method to separate polymers due to differences in end groups.

This chapter is a publication in preparation with 6 authors including myself as the second author. The author Dr Marion Gaborieau and the last author Dr Patrice Castignolles conceptualised the scientific ideas. The first author, Dr Joel Thevarajah, the author Dr Marion Gaborieau, the last author Dr Patrice Castignolles and I carried out the interpretation of results. The third author Hai Feng, the fourth author Fiona Lai and I carried out all experiments in the chapter. All solubility tests and CE experiments at optimal conditions were carried out by myself. Dr Joel Thevarajah and I drafted the complete manuscript with other co-authors reviewing the manuscript.

1.9.1.2 Molecular Characterisation of Ultrafiltration Membranes (chapter 3)

The third chapter investigates the extent of miscibility of the blended polymers used within industrially relevant UF membranes. Quantitative measurements on the molecular constituents in each polymer allow for

determinations on the percentage yield of the polymers found in the final product (UF membranes) which was compared with the synthetic formulations. Furthermore, solid-state NMR measurements allowed for an understanding on how well the individual polymers are mixing at the molecular level.

The preparation of this chapter was helped by various individuals. Dr Marion Gaborieau, Dr Patrice Castignolles conceptualised the scientific ideas. Dr James Oliver, Dr Joel Thevarajah, Dr Marion Gaborieau, Dr Patrice Castignolles and I carried out the interpretation of results. Dr Marion Gaborieau's NMR spectroscopy expertise allowed for consultations on demanding NMR topics. Lastly, Joel Thevarajah and I conducted the 2D WISE experiments. All other experiments, data processing and writing of the chapter was conducted by myself.

1.9.1.3 Relation of Surface Composition to Functionality (chapter 4).

The fourth chapter investigated that surface composition and functionality of UF membranes through a variety of characterisation tools. The chapter established relationships between surface composition and functionality.

The making of this chapter was helped by various individuals. Dr Geoffrey Johnston-Hall, Dr Marion Gaborieau, Dr Patrice Castignolles conceptualised the scientific ideas. Dr Geoffrey Johnston-Hall, Dr Marion Gaborieau, Dr Patrice Castignolles Dr James Oliver and I carried out the interpretation of results. Dr Geoffrey Johnston-Hall expertise on SEM, tensiometry and tensile strength tests allowed for consultations on functionality tests. Lastly, I conducted all experiments, data processing and writing of the chapter.

2 CHARACTERISATION OF POLY(N-VINYL PYRROLIDONE) END GROUPS THROUGH CAPILLARY ELECTROPHORESIS

Joel J. Thevarajah^{1,2}, Kevin P. Dizon^{1,2}, Hai Feng^{1,2}, Fiona Lai^{1,2}, Marion Gaborieau^{1,2}, Patrice Castignolles¹

¹Western Sydney University (WSU), Australian Centre for Research on Separation Science (ACROSS), School of Science and Health, Locked Bag 1797, Penrith 2751, NSW, Australia

²Western Sydney University (WSU), Medical Sciences Research Group, Locked Bag 1797, Penrith, 2751, NSW, Australia

2.1 Introduction

Poly(*N*-vinyl pyrrolidone) (PVP, also called povidone) is a non-toxic hydrophilic polymer used in a variety of industries. Its amphiphilic nature and unique functionality allow it to be used in a variety of industries including cosmetics ⁴⁶ and pharmaceuticals ⁴⁷. In the production of ultrafiltration membranes, PVP is used influence membrane properties such as pore structure, mechanical stability, thermal stability, hydrophilicity, water flux and rejection capabilities ⁴⁸. In certain industries, understanding the structural features that affect polymer solubility (such as PVP) allows for design improvements on membrane production.

End group compositional differences have been shown to affect solubility in smaller molar mass polymers ¹⁷ and hyperbranched polymers ¹⁸; however, the field is not as well developed when detailing the effects in large molar mass polymer ($\geq 10,000$) with minimal branching. In small molar mass polymers, end groups heavily affect the properties of the polymer ¹⁶; however most industrial relevant polymers consist of large molar masses. One such reason is that polymers consisting of molar masses larger than 10,000, retain strong durable mechanical properties ⁴⁹. In large molar mass polymers, the properties of the polymer are primarily determined by the monomers that contribute to the vast majority of the weight ⁴⁹, considered as the bulk. Mole ratios of end groups are comparatively small compared to the bulk; however, studies have shown its influence towards solubility in hyperbranched polyetherimides ⁵⁰ crystallinity in polyesters ⁵¹ and cloud points in polyethers ⁵². The knowledge in this area is lacking as characterisations on end groups is complex. Hence techniques able to discern compositional differences between the bulk and end groups are required to determine the impact of end groups in polymers with large molar masses.

2.1.1 Means of Characterisation

Size Exclusion Chromatography (SEC) is heavily relied upon as the standard separation method for the characterisation of polymers ^{32, 53}. However, SEC separates polymers based on hydrodynamic volume ⁵⁴. SEC columns are capable of undesired interactions with the separated polymer, causing adsorption which potentially alter polymer retention volumes ⁵³, requiring a well dissolved system for an accurate characterisation. This separation mechanism limits the characterisation of PVP based on end groups as compositional differences may lead to concerns of complete dissolution. Liquid chromatography in critical condition is an alternative method that can be used to separate and characterise polymers based on end groups ⁵⁵, but it is tedious to establish conditions where separation is achieved by a difference in end groups and not molar mass and it is reported to have low recovery ^{55, 56, 57}. This study intends to develop a method that could characterise the end groups of PVP through the distributions of electrophoretic mobility. The results of this work could be the first step in correlating end groups of large molar mass PVP to solubility.

Free solution Capillary Electrophoresis (CE) is a characterisation technique which involves the separation of an analyte in a capillary filled with only buffer. Charged species are separated based on their charge-to-friction ratio (Section 1.7.1). It is performed in the absence of a stationary phase, thus minimizing the impact of adsorption or interactions with the stationary phase ^{29, 58}. Moreover, the technique requires little to no sample preparation and a much smaller volume of sample compared to common chromatography techniques.

To allow the characterisation of PVP by end groups, separation needs to take place without an influence of molar mass. CE in the Critical Condition (CE-CC) of polymers with evenly distributed charges along the backbone leads to an analogous separation to liquid chromatography in the critical conditions (Section 1.7.1.3) ^{29, 59}. This allows the separation to be independent of molar mass and dependent on other factors such as composition ^{13, 60}, branching or

end groups⁶¹. Therefore, it has potential to be used as a tool for the characterisation of PVP end groups.

From the principle of CE, separation only occurs if the dissolved samples are charged. PVP is neutral in aqueous solution and therefore is required to be charged before characterisation by CE. PVP complexes with various inorganic salts and low molar mass compounds^{62, 63}. Therefore, using the ions of the CE background electrolyte, it is possible to complex PVP and induce a charge to allow separation. This complex formation has been previously studied in the case of CE of carbohydrates^{64, 65}.

To allow for accurate characterisation, the appropriate data treatment is required^{66, 67}. Comparisons of electropherograms in migration time are prone to instrumental errors (current variance, capillary length,) which can significantly affect migration rates between samples. Instrumental error can be normalised through the conversion of migration time to electrophoretic mobility (μ) (Equation 7.1). Absorbance can be influenced by the difference of velocities of the analytes through the detector, thus the conversion to weight-average electrophoretic mobility $W(\mu)$ is required (1.7.1.2). $W(\mu)$ distributions are determined to account for variations between measurements to improve reproducibility and precision. Therefore $W(\mu)$ is representative of the distribution of the end groups of PVP¹³.

In CE, adsorption reduces the relative motion of the analyte, where separation is not respective solely to the electrophoretic mobility creating concerns on its applicability with analytes that consist of a soluble/insoluble matrix under non-optimal conditions. To understand the effects of adsorption Pressure Mobilisation (PM) is applied.

2.1.2 Pressure Mobilisation

PM is not a separation technique as it involves pushing the analytes through the capillary in the absence of an electric field. The structural differences at the interface between the background electrolyte and the capillary can cause the analyte to adsorb to the capillary. Interactions with the capillary wall

decreases the migration rate, causing tailing. If no interactions with the capillary surface occurs, then a Gaussian peak is observed where symmetrical peak broadening is due only to the diffusion of the analyte ⁶⁸.

2.2 Materials and Methods

2.2.1 Chemicals

The PVP samples studied were obtained from different suppliers: PVP 1 and 2 were supplied by BASF, Australia and PVP 3 was supplied by Sigma-Aldrich, Australia. All PVP samples have a theoretical number-average molar masses $> 10,000 \text{ g} \cdot \text{mol}^{-1}$ ⁶³. Hydrochloric acid (HCl, 32%), Methyl Green (MG), boric acid ($\geq 99\%$), Sodium hydroxide (NaOH) pellets and dimethyl sulfoxide (DMSO, 99 %) were purchased from Sigma-Aldrich, Australia. Tetrahydrofuran (THF, 99%) was obtained from Ajax chemicals, Australia and ethanol (EtOH, 95%) was obtained from Thermo Fischer Scientific, Australia. *N*-methyl-2-pyrrolidone (NMP, 93%) was acquired from BASF. All water used was Milli-Q quality (from Q-Grad[®] 1 filter), HCl and NaOH were used to make up water solutions to a pH of 4 and 10 respectively.

2.2.2 Dissolution of PVP

All PVP samples were dissolved in different solvents (THF, Milli Q water (MQ), water solution at a pH of 4, water solution at a pH of 10, NMP, HCl, EtOH) at a concentration of 7.5 g/L to test their solubility. Pictures were taken at specific time intervals (0 min, 30 min, 60 min, 120 min, 300 min, 1 day).

2.2.3 Sample and Buffer Preparation

Sodium borate (NB) buffer (200 mM, NB200) was prepared from 0.5 M boric acid in Milli-Q water and titrated to pH 9.2 with 10 M sodium hydroxide. This was used as the background electrolyte and was sonicated for 5 min and filtered with a Millex-GP polyethersulfone (PES) syringe filter (0.22 μm) before use. PVP was prepared at $10 \text{ g} \cdot \text{L}^{-1}$ in Milli-Q water or NB200 and left to dissolve overnight. The samples were then diluted with Milli Q water for

CE experiments and NB200 for PM experiments at different concentrations (1, 0.5, 0.25 g·L⁻¹). Before analysis, methyl green (0.05 g/L) was added as a mobility marker. 10 µL of 10% v/v DMSO was added as an electroosmotic flow (EOF) marker. NaOH 1 M solutions were prepared fresh on the day of the experiment.

2.2.4 Capillary Electrophoresis Analysis

Separations were carried out on Agilent Technologies 7100 CE (Agilent Technologies, Waldbronn, Germany), with a Diode Array Detector (DAD) monitoring at a wavelength of 195 nm with bandwidth of 10 nm and a voltage of 30 kV. All samples were injected hydrodynamically by applying 60 mbar of pressure for 40 s. Before each series of experiments, the capillary was flushed for 10 min with 1 M NaOH, 5 min with 0.1 M NaOH, 5 min with MQ water and 5 min with NB200. Preconditioning between injections involved a 2 min flush with 1 M NaOH, followed by a 5 min flush with NB200. Each day of experiment, the CE instrument and capillary were validated by measuring the electrophoretic mobility of the peaks of an oligo(acrylic acid) standard^{32, 69}.

All separations were carried out in triplicates in NB200 buffer using a 50 µm ID fused silica capillary (Polymicro, IL, USA) with a total length of 150.0 cm (effective length 141.5 cm). After the final separation, the capillary was flushed for 10 min with 1 M NaOH, 4 min with 0.1 M NaOH, 10 min with MQ water and 10 min with air. CE experiments were conducted at room temperature unless stated on the caption. Chemstation A.10.01 was used for data acquisition. Data treatment was conducted using OriginPro 9.0.

2.2.5 Pressure Mobilisation Analysis

Pressure mobilisation experiments were carried out on the same instrumentation and detection as the CE analysis. Samples were injected at 40 mbar for 30 s at different concentrations (1, 0.5, 0.25, 0.125 and 0.0625 g·L⁻¹) and there was no applied electric field. All other conditions were identical

as the CE analysis. Following the injection, 100 mbar of pressure was applied for each run.

2.3 Results and Discussion

2.3.1 Qualitative Observations of PVP Dissolution

Dispersion of a polymer in a compatible solvent allows for visual observations on solubility^{13, 70, 71}. This technique was applied as a screening method to identify solvents able to distinguish the extent of dissolution of the 3 PVP samples.



Figure 2-1 PVP 1 (left) PVP 2 (middle) and PVP 3 (right) dissolved in tetrahydrofuran at 7.5 g·L⁻¹. Image taken at t_{initial} .

Most solvents showed no discernible differences between PVP samples (Figure A 1), except when dissolved in tetrahydrofuran (Figure 2-1). t_{initial} is defined as the time taken between the sample mixing with the solvent and the photo taken. Samples were observed to have been partially dissolved in THF as evident by the white precipitate found at the bottom of the vial. Discernible differences were found between samples. PVP 1 and PVP 3 exhibited noticeable precipitate, the precipitate in PVP 1 is more abundant than in PVP 3 and PVP 2 was observed to have minimal precipitate.

Empirical methods to monitor dissolution are subject to a significant degree of error. The time difference at $t_{initial}$ varied from 5 to 15 seconds between all samples which will affect comparisons made between solvents. Also, dissolution is determined through the observed precipitate: however, observations of a transparent liquid is not an indicator of complete dissolution as shown in starch suspensions ^{72, 73}. These factors could significantly affect the accuracy of the monitoring thus analytical techniques able to probe the differences in end groups are necessary. For an accurate representation of end group differences between PVP samples, CE was employed.

Since all experiments deal with PVP samples with molar masses $> 10,000 \text{ g} \cdot \text{mol}^{-1}$, the assumption made is that CE separations occur in the critical conditions. CE-CC allows for separations to occur independently from the contributions of the hydrodynamic friction caused by the size of the chain. Therefore, end group characterisation is possible through CE as molar mass differences between end groups will influence the hydrodynamic friction of the analyte.

Challenges persist with this approach as PVP is an uncharged molecule. To induce a partial negative charge, allowing for separations, borate is complexed with PVP upon injection. Complexation produces a weak charge and complete complexation is not guaranteed. This could create concerns in the conversion of migration time to electrophoretic mobility as the analyte may comigrate with the EOF marker. To allow for conversion to electrophoretic mobility, the identification of an appropriate mobility marker is required.

2.3.2 Selection of an Appropriate Mobility Marker

Utilisation of a mobility marker allows for the determination of μ (Section 0). Identification of an appropriate mobility marker requires known electrophoretic mobilities, high selectivity and no interactions occurring with PVP. The electrophoretic mobility of methyl green was determined from repeated CE injections utilizing DMSO as an EOF marker (Figure 2-2) and results were tabulated (Table A 1).

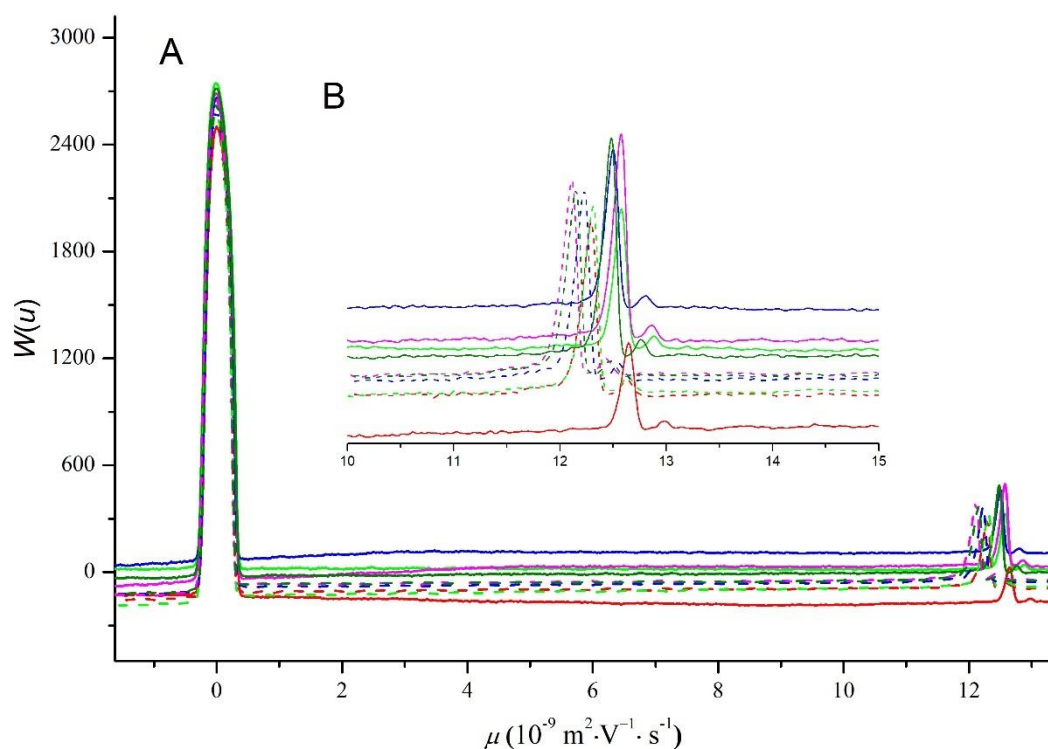


Figure 2-2 A) Distribution of electrophoretic mobilities of methyl green in DMSO at 0.05 g·L⁻¹ (n = 10). B) Zoom in the region 1.0 – 1.5 × 10⁻⁸ m² · V⁻¹ · s⁻¹.

Methyl green has a positive nominal charge, hence, a higher migration rate than DMSO in this counter-electroosmotic flow mode. The electrophoretic mobility at the apex of the largest methyl green peak (Figure 2-2B) was averaged to $1.26 \cdot 10^{-8} \times \text{m}^2 \cdot \text{V}^{-1} \cdot \text{s}^{-1}$ with a RSD value of 0.63% (Table S-1); therefore, the electrophoretic mobility of methyl green is repeatable. Electrophoretic mobility calculations were conducted using DMSO as an EOF marker (Section 0). The mobilities of methyl green are thus repeatable as in PNaA (RSD = 1.63%)⁶¹. CE of methyl green added to the PVP samples was conducted to test if the interactions occurred between analytes (Figure A 2). In terms of selectivity, methyl green is appropriate as a mobility marker in PVP separations as it is completely resolved from PVP (Figure 2-3).

2.3.3 Determination of the Distribution of Electrophoretic Mobilities of Different PVP Samples

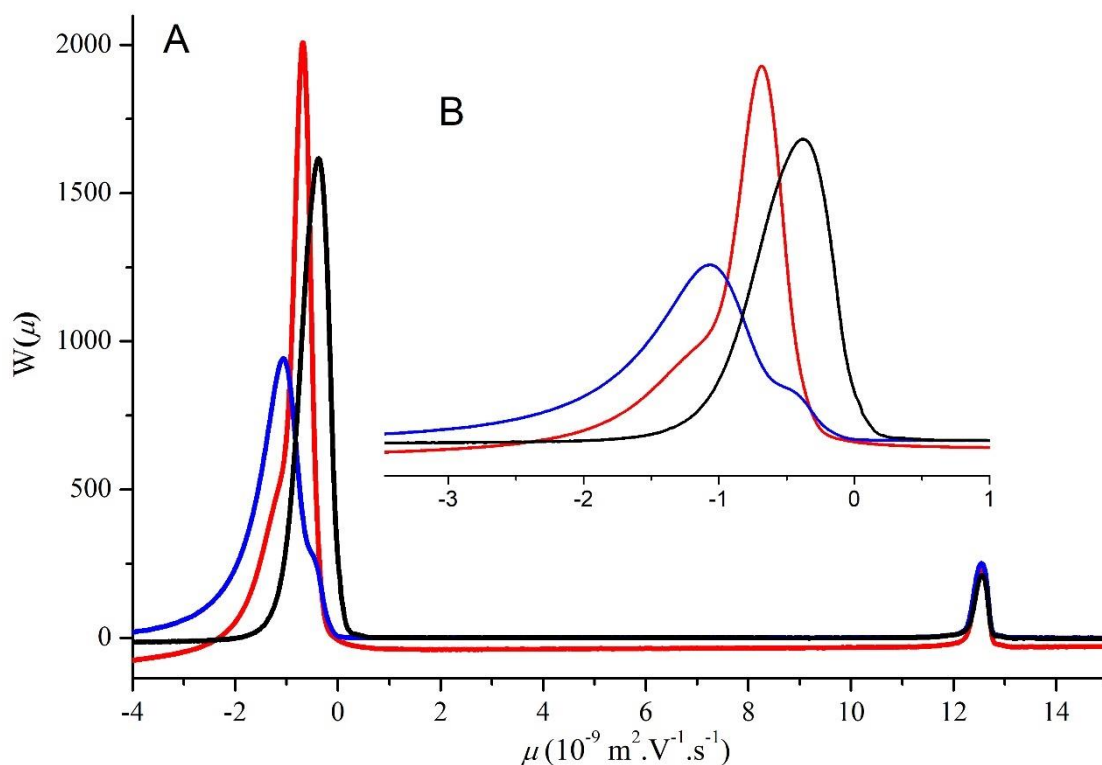


Figure 2-3 A) PVP 1 (blue), PVP 2 (red) and PVP 3 (black) dissolved in NB 200 at 1 g·L⁻¹ methyl green was added as a mobility marker at 0.05 g·L⁻¹. B) Zoomed in graph of the PVP from -3 to $1 \times 10^{-9} \times \text{m}^2 \cdot \text{V}^{-1} \cdot \text{s}^{-1}$.

Methyl green peaks in all PVP sample injections were found at $1.26 \times 10^{-8} \times \text{m}^2 \cdot \text{V}^{-1} \cdot \text{s}^{-1}$ allowing for highly precise CE measurements (Figure 2-3 A). The sodium borate buffer is used extensively in CE for the ability of borate to form complexes with polymers to induce a partial negative charge^{65,61}. PVP has no nominal charge; however, it is able to form complexes⁶², indicating the potential application of borate buffers to impart a charge. Negative electrophoretic distributions of PVP samples demonstrates borate complexation allowing for determinations of end group populations (Figure 2-3B). A population at 0 can be found in PVP 3 indicating the presence of large end-groups than for the rest of the PVP or that most PVP is affected by adsorption or overloading leading to an over-estimated electrophoretic mobility (Figure 2-3). The electrophoretic mobility distributions of PVP 1 and

2 exhibit shoulders and tailing is observed in PVP 1. Both could be due to either smaller end groups, or the influence of adsorption to the capillary wall (Figure 2-3B).

Sample overloading, overloading was tested by performing CE at different PVP concentrations (Figure A 3). It was found that higher resolution can be obtained at lower concentrations; however, 1 g·L⁻¹ was kept for all CE and PM experiments in this chapter due to time constraints. The experiment was conducted at the latter portion of the thesis year and does not show a significant improvement in resolution; hence, it is considered as future work to be completed.

Adsorption of the PVP sample onto the capillary wall during CE analysis could lead to problems such as an unstable EOF, poor resolution and long migration times ^{74, 75} thus overestimated electrophoretic mobilities in this case. Therefore, it is necessary to confirm whether adsorption exists and eliminate its effect. To identify conditions to minimise the effects of adsorption, PM was used.

2.3.4 Adsorption and Solubility of PVP

In PM, Interpretation of the shapes of the signals allows information regarding adsorption ^{76, 77}. PM experiments were first conducted at 25 °C (Figure A 4).

Tailing is present in the elugram of PVP 1 and the peak from PVP 2 is slightly asymmetric. PVP 3 produced non-repeatable results and the peak shape produced is evident of significant adsorption and desorption ⁷⁶. All samples exhibited adsorption with the sample and capillary at 25 °C. To reduce the interactions of PVP with the capillary walls and to increase the solubility of PVP, different temperatures were tested. At 55 °C (Figure A 5). extensive tailing, due to adsorption, is still noted.

There is a link between the shape of the signal time profile and different types of adsorption based on the time of adsorption ⁷⁶, t_{ad} , time of desorption, t_{de} and

the time taken for the sample to be detected, t_{det} ⁷⁶. At 25 °C, the signal shape of PVP 1 and PVP 2 indicates that the t_{ad} , t_{de} and t_{det} are similar. The shape of PVP 3 indicates that the t_{ad} is around $\frac{1}{4}$ of the t_{det} and $\frac{1}{2}$ of the t_{de} .

At 55 °C, there are peak splits shown in the profile of all the samples. This suggests that the t_{ad} values of all the samples are around $\frac{1}{4}$ of the t_{det} and $\frac{1}{2}$ of the t_{de} . Given that the t_{det} value of all experiments are similar, the changes in the shapes of the signal time profile indicate the time it takes for the samples to be adsorbed on the capillary wall decreases with the decrease of temperature. Therefore, it is possible to reduce the effects of the sample adsorption by decreasing the temperature during the experiment.

The PM experiment was then carried out at 15 °C (Figure A 6). The repeatability notably improved compared to the higher temperature experiments. Slight adsorption is still seen for PVP 1 and 3 whilst PVP 2 exhibited a symmetrical peak. This is an indication that the effect of sample adsorption of PVP 1 and PVP 3 have been greatly reduced and that of the PVP 2 is eliminated. One factor which may influence adsorption is solubility and the fact that PVP's solubility may increase when temperature decreases. The PVP samples had been kept at 25 °C whilst the capillary temperature had been varied. The PM experiments were then repeated at 15 °C with the sample temperature lowered to 9 °C (Figure 2-4)

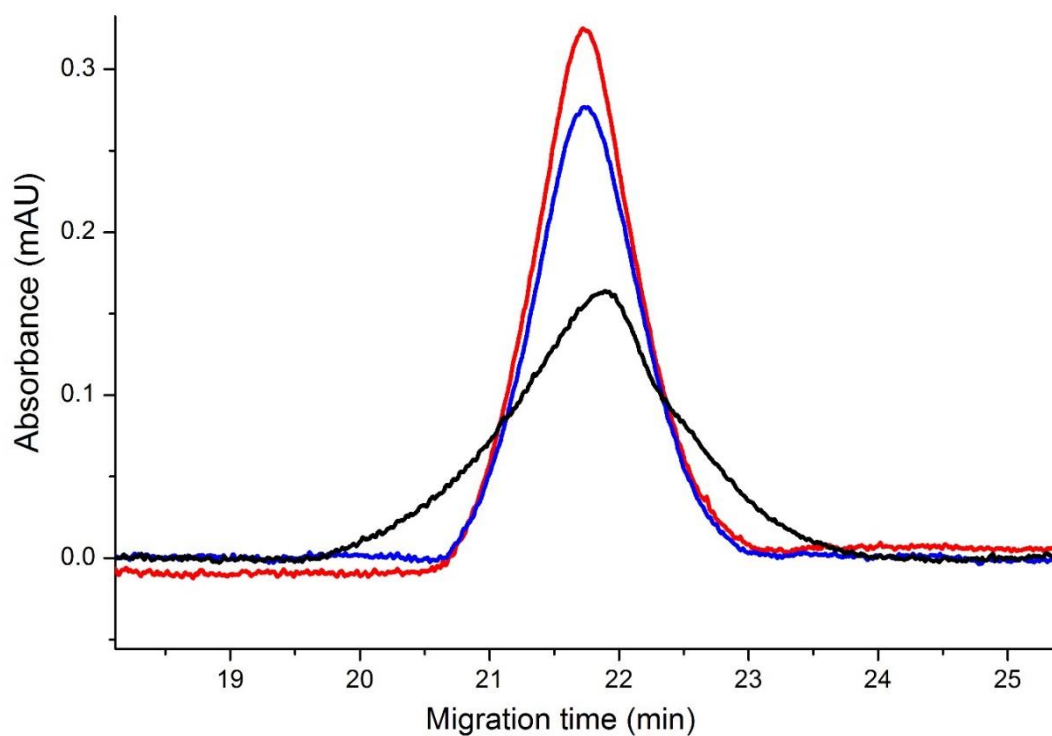


Figure 2-4 PM of PVP samples PVP 1(blue), PVP 2(Red) PVP 3 (black) with the capillary at 15°C capillary and the sample at 9 °C.

It is observed that the adsorption of the PVP is eliminated. This is indicated by the symmetrical peaks in each of the elugrams. Therefore, to allow an accurate characterisation of PVP using CE, the above conditions were employed.

2.3.5 Characterisation of PVP End Groups

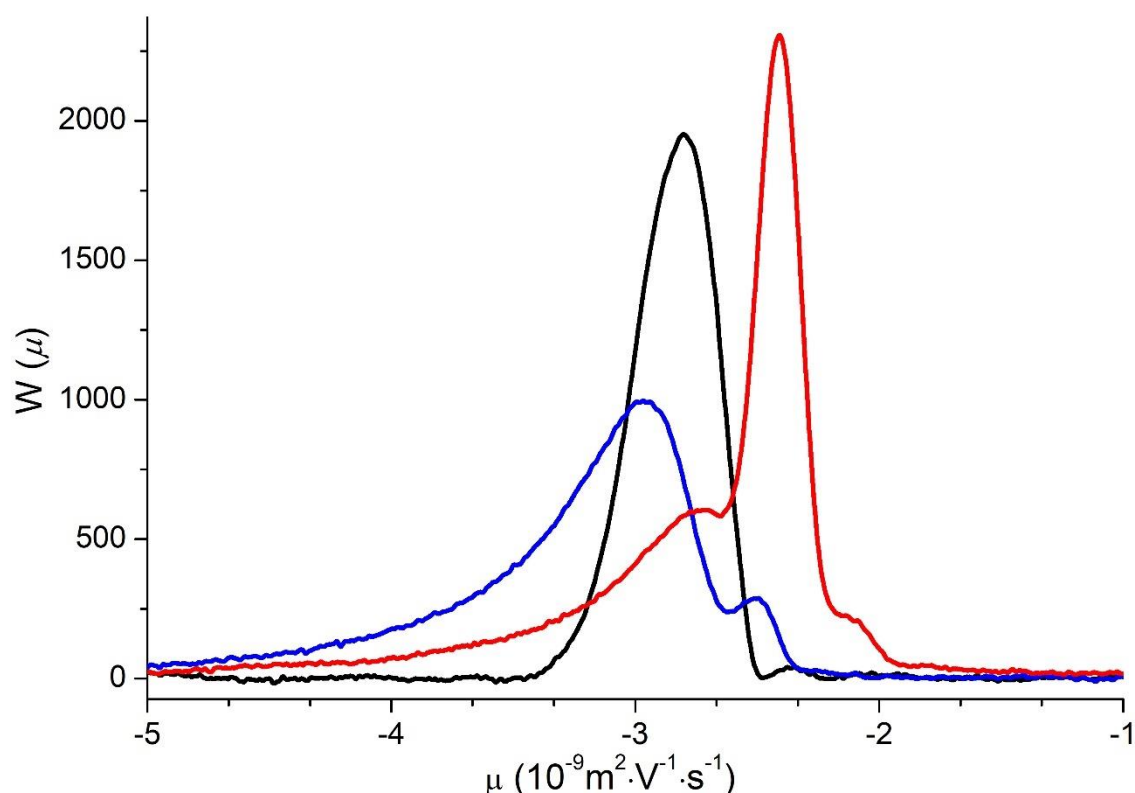


Figure 2-5 Distributions of electrophoretic mobilities of PVP 1 (blue), PVP 2 (red), PVP 3 (black) dissolved in NB 200 at 1 g·L⁻¹ with methyl green as a mobility marker. Conditions set at 15 °C in the capillary and 9 °C at the sample.

The electrophoretic mobility range of the PVP samples range from -2.0 to -5.0 $\times 10^{-9} \text{ m}^2 \cdot \text{V}^{-1} \cdot \text{s}^{-1}$ which is considerably small as poly(sodium acrylate) has shown of consist mobilities of 3.49 to 3.61 $\times 10^{-8} \text{ m}^2 \cdot \text{V}^{-1} \cdot \text{s}^{-1}$ {Maniego, 2013 #157}. Hence, all PVP populations possess a partial negative charge (Figure 2-5). PVP samples under optimised conditions depict end group population differences between samples. PVP 3 consists of a symmetrical gaussian peak, shoulder peaks are found in PVP 1 and PVP 2. The presence of shoulders in the electropherogram indicates the presence of different end group populations within the sample. In comparison to shoulders peaks found in (Figure 2-3B), the shoulder peaks are better resolved on both PVP samples and a new distinct population is found in PVP 2. Tailing is observed in PVP 1 and PVP 2 under conditions with minimal adsorption. This can be deduced as a heterogeneity in terms of end-groups.

Determinations on end group solubility can be made in reference to (Figure 2-1). The large distribution of end group structures found in PVP 1 (in the form of tailing) will lower the dissolution rate. A large distribution of end group structures, due to differences in charge and molar masses, will consist of partially soluble fractions that dissolve slower. PVP 3 consists of a distribution of structures found in the same mobility range as PVP 1. This indicates the presence of partially soluble fractions in PVP 3 may be present in PVP 1. PVP 2 has minimal peak overlapping with in the partially soluble fractions of PVP 1 and PVP 3, thereby consisting of minimal precipitate in (Figure 2-1).

2.4 Conclusion

The influence of end-groups in large molar mass polymers is not well established in the literature. This may be due to the lack of a straightforward separation method in obtaining this information. In this study, we compared three different commercially available PVP samples. PVP is a neutral compound; however, the complexation of PVP with borate allows for separation to occur based off the analytes charge-to-friction ratio. Further, CE-CC allows separation to take place without the influence of the hydrodynamic friction contributed by the polymer chain. Hence, separations are a result of end group compositions. The employment of PM and a mobility marker allowed for an improvement in resolution and precision in CE separations. Electrophoretic mobility distributions of PVP samples are observed to have varying end group populations. Future research opportunities will use CE for end group characterisations in different systems. In an industrial setting, the difference of end group populations in a given polymer may lead to poor solubility, producing UF membranes with lowered physical properties.

*3 MOLECULAR
CHARACTERISATION OF
ULTRAFILTRATION MEMBRANES*

3.1 Introduction

Polymeric membranes have been used in a wide range of industrial applications such as water filtration, haemodialysis, food processing ⁷⁸ to name a few. The common concept on the application of polymer membranes is the capability to allow for selective transportation of compounds across a medium (Section 1.3). In water filtration systems, production of porous membranes with well-defined pore shapes, domains, and distributions on the surface are highly desired. Formulations consisting of diverse barrier structures and properties can be designed from polymeric materials ¹⁰, namely polymer blends. A brief understanding of polymer blends is provided in Section 1.5. While polymer blends can incorporate more than two polymers (ternary system), this introduction will refer to systems with two polymers.

One way to design porous membranes is the addition of a macromolecular additive with a pronounced surface segregation to ensure minor influence onto the bulk ¹⁰. Certain hydrophilic polymers such as poly(ethylene oxide) ⁷⁹ and poly(ethersulfone) ⁸⁰ segregate to the surface through blending. These types of modification are not necessarily stable as the miscibility gap between the surface and the bulk can cause de-mixing leading to membrane leaching. In haemodialysis, membrane leaching can affect membrane integrity and lead to significant damage within the human host ^{10,81}. To optimise membrane formulations for specified functionality, an understanding of the blend miscibility of the system is required.

3.1.1 Optimising Functionality through Miscibility

Certain Ultrafiltration (UF) membrane formulations are designed to incorporate a hydrophilic and a hydrophobic polymer within the blend ²⁰. Polymer blends of this nature are generally partially miscible, and predicting properties raises questions on the phase separated morphology, interfacial properties and the dependence of properties of each phase on composition ⁸². Polymer blend functional properties are heavily reliant on their macromolecular composition. Hydrogen bonds and ionic bonds between the

two networks allow for mechanical stability; however, an increase in surface area interactions leads to an increase in repulsive forces between the two polymers ⁸³. Hence, formulations are generally limited to blends that are primarily composed of one polymer with minimal contributions from the other component.

A common practice in minimising immiscibility is the use of a compatibilizer to help mitigate the energy phase boundary between the polymer networks, allowing larger surface area interactions while maintaining bond interactions between the two networks ⁸³. However, the addition of a compatibilizer inherently makes the system more complex as the binary system converts to a ternary system. The added compound may affect desired functional properties and complicate design procedures that incorporate a compatibilizer.

Functional properties of polymer blends are dependent on the interrelation between morphology, performance and mixing parameters. To develop accurate representations of complex systems, methods that can analyse, and thus help predict, the morphological progression of the blending stage and the final polymer blend are required.

3.1.2 Characterisation of Polymer Blends through NMR Spectroscopy

NMR techniques have played an extensive role in understanding the morphology of amphiphilic polymer blends ^{84 85}. Solid-state NMR provides details on the system at length scales ranging from 0.5 to 30 nm, encompassing the crystalline dimensions ⁸⁵ and chain dimensions ⁸⁶ of polymers. An advantage of solid-state NMR is the capability to analyse the sample in the application state (generally solid) without the need for a solvent.

Other advantages are evident within the spectral separation of bulk material (carbon backbone) from interfacial groups (functional groups) where differences of structural properties affect chemical shifts, relaxation times

and line shapes allowing for structure determination at the molecular level. In solid-state NMR, structure elucidation through ^1H Single Pulse Excitation (SPE) NMR is affected by poor spectral resolution from strong anisotropic spin interactions⁸⁷; therefore, ^{13}C NMR spectroscopy is used for structure identification. Obtaining signal in the ^{13}C channel is time consuming as the natural abundance of ^{13}C nuclei is low³⁶. To alleviate issues of sensitivity, ^{13}C Cross Polarisation (CP) NMR is generally used (Section 1.7.2.5.1). CP transfers magnetisation of ^1H nuclei to ^{13}C nuclei (Hartmann-Hahn conditions) allowing for higher polarization and an increase in signal. It is important to note that ^{13}C CP is biased to the mobility of a molecule. In rigid segments of ^{13}C nuclei in the sample, the magnetisation transferred to quickly to the ^{13}C nuclei; however, mobile segments will exhibit a slower magnetisation transfer, hence a lowered intensity. At a high enough mobility, certain ^{13}C nuclei would not be observable in the spectrum.

Modern solid-state NMR methods can provide quantitative information on semi-crystalline blend systems, generally without the need for any form of isotropic labelling or probe molecule perturbations⁸⁶. To obtain a quantitative spectrum, the ^{13}C SPE pulse scheme (Section 1.7.2.4.1) is used as opposed to the ^{13}C CP pulse scheme. The bias in CP applies a significant degree of error in signal intensity when quantifying molecular constituents with varying molecular mobilities. ^{13}C SPE is impartial to varying molecular mobility populations; however, the technique is considered less sensitive than ^{13}C CP and therefore requires more accumulated scans for increased sensitivity.

Solid-state NMR techniques are able to probe the molecular dynamics of a material providing representations on the miscibility of the system. ^1H SPE NMR is a qualitative characterisation method to probe the molecular mobility⁴³. However, it is not sufficient when characterising complex samples, as superimposition is present of both mobile and immobile components⁴³. Multidimensional NMR of polymer blends can help in portraying an accurate representation of a complex system. Two-dimensional (2D) WIdeline SEparation (WISE) correlates chemical structure to segmental mobility by

yielding a proton spectrum for all resolved carbon signals (Section 1.7.2.5.2). In a miscible system all molecular constituents would have the same mobility.

This study looks to characterise industrially used membranes probing information regarding structure, polymer composition and miscibility through a variety of NMR techniques. Samples used in the study are industrially used samples where the membrane consists of either a binary or a ternary blend. Results of this study will help contribute to the development of methods able to probe the molecular dynamics of complex systems and the design improvement of UF membranes. This work is done in collaboration with an industry sponsor: hence, certain aspects of the project are considered confidential and not shared within this document.

3.2 Materials and Methods

3.2.1 Chemicals

Membranes and the precursors were provided by the industrial collaborator except for the polymer AB powder which is both polymer A and polymer B mixed as received into a powder at 50/50 ratio (Table 3-1). Ethanol (99 %) and adamantane (99 %) were acquired from Sigma Aldrich. Membranes were washed in excess Milli-Q water with periodical rinsing every day for 4 days and dried at 70° C for 1 h.

Table 3-1 Formulations of the membranes and powder used.

Precursors	Polymer based formulations
polymer A + polymer B	Membrane AB
polymer A + polymer B + polymer C	Membrane ABC
polymer A + polymer B	Powder AB

3.2.2 NMR Analysis

All ^1H SPE, and ^{13}C CP NMR spectra were recorded on a Bruker Avance DPX200 spectrometer operating at Larmor frequencies of 200 MHz and 50 MHz, respectively. ^{13}C Inversion recovery, ^{13}C SPE (in quantitative conditions) and 2D WISE experiments were conducted on a Bruker DRX300 spectrometer operating at Larmor frequencies of 300 MHz and 75 MHz for ^1H and ^{13}C , respectively. Commercial double resonance probes supporting zirconia MAS rotors with a 4 mm outer diameter and a 3 mm inner diameter were used. Powders and blends were spun at 10 kHz at the magic angle. 2D WISE spectra were recorded using a 90° pulse at 4.50 μs , a 2 s relaxation delay, a CP contact time of 500 μs . Acquisition time of ^1H channel is set 0.002 s to a total of 200 increments. Acquisition time of ^{13}C channel is set to 0.02 s with 1240 scans accumulated. 2D WISE and CP experiments were optimized using a mixture of three singly ^{13}C -labelled alanines. The ^1H and ^{13}C chemical shifts scales were externally referenced using adamantane by setting the CH resonance to 1.64 ppm and 38.48 ppm, respectively⁸⁸. Rotors were rinsed with ethanol and dried before packing. Precursors were packed as received and membranes were cut into small pieces before being packed.

3.3 Results and Discussion

3.3.1 Molecular Structure Identification

To allow for comparative studies, peak assignment of the precursor materials is necessary. Peak assignment allows for the elucidation of structure where interpretations can be made on the incorporation of the precursors within the membranes.

To determine if high mobility populations exist within the membranes, preliminary, ^1H single pulse excitation (SPE) NMR spectra were recorded of the precursors (Figure A 7) and membranes (Figure A 8). ^1H SPE measurements allow for empirical determinations of molecular mobility through signal broadness. All spectra exhibit a single peak consisting of a narrow signal (mobile region) superimposed on top of a broad signal (rigid

region). The lack of a significantly narrow signal allows for the assumption that all molecular constituents are observable in ^{13}C CP NMR spectra for both the membranes and the precursors (Figure 3-1).

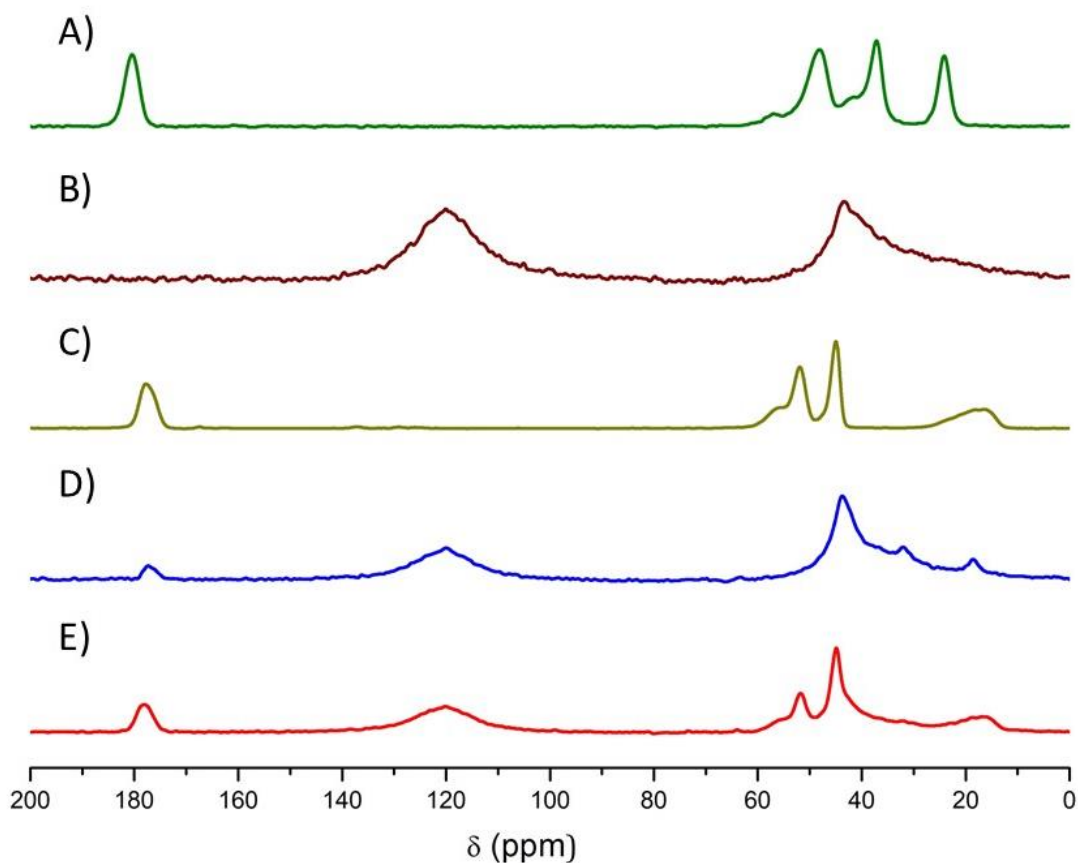


Figure 3-1 Normalised ^{13}C CP spectra of A) polymer A, B) polymer B, C) polymer C, D) AB membrane and E) ABC membrane.

^{13}C CP spectra of the membranes and the respective precursors are shown in (Figure 3-1) and chemical shift assignments of the precursors were tabulated in (Table 3-2). Chemical shift values were determined at the apex of the signal. All precursor polymers consist of all molecular constituents found in literature sources. Observed chemical shift values are slightly different from literature values due to a cumulation of instrumental precision, sample variations and spectrum processing. Both membranes (Figure 3-1D and Figure 3-1E) exhibit all signals found in their respective precursors (Table

3-2); however, structures found in the aliphatic region (60 – 0) ppm are not fully resolved.

Table 3-2 ^{13}C chemical shift assignments of the precursors.

Sample	Observed δ (ppm)	δ (ppm) ⁸⁹	Structure assignment
Polymer A	180.9	178.0	Carbonyl
	48.1	46.0	Cyclic aliphatic, aliphatic
	41.9	40.0	Aliphatic
	37.1	34.0	Cyclic aliphatic
	24.1	21.0	Cyclic aliphatic
Polymer B	120.1	119.5	Halogenic
	43.4	43.2	Aliphatic
Polymer C	177.6	178.1	Carbonyl
	53	52.2	<i>O</i> -methyl
	51.9	52.2	Quaternary carbon
	45.0	45.2	Aliphatic
	17.3	16.7	Aliphatic

In all samples (Figure 3-1), the aliphatic region suffers from poor resolution. Poorly resolved signals in the aliphatic region are due to chemical shift anisotropy, dipolar coupling and quadrupolar effects resulting in line broadening (Section 1.7.2.3). Furthermore, aliphatic structures corresponding to the carbon backbone are sensitive to conformational change because crystalline carbons adhere to the trans conformation while bond rotation is more prevalent in amorphous region ⁹⁰. Alteration of bond rotation is a γ -gauche interaction allowing for a shielding effect with a noted chemical difference of 2-3 ppm difference ⁹¹. Regarding the membranes (Figure 3-1D and Figure 3-1E), structure elucidation of the aliphatic region is complex as

different phases of the material create γ -gauche interactions between the two materials thus altering structure conformation ⁹⁰. Identification of polymorph variations inherent within the precursors and the membranes through X-ray diffraction would help in depicting the different phases present within the material. This is considered as future work (Section 5.2.2).

All samples exhibit a carbonyl signal except for polymer B (Figure 3-1). The carbonyl signal in the ABC membrane is broader than that of the AB membrane suggesting the carbonyl peaks from polymer A and C are superimposed. Sharing similar structural characteristics between polymers leads to lowering the phase boundary repulsive forces between both polymers in the blend and increasing miscibility between the two polymers ⁹². Hence, Polymer C may be having a compatibilizing effect in the ABC membrane allowing for the formation of miscible domains. However, this determination is not conclusive and will need further tests to strengthen the determination made.

It is to be noted the presence of weak signals is found between 170 and 120 ppm in the CP of polymer C (Figure A 9). These signals align with the residual monomer and are considered impurities within the compound ⁹³. Monomers within the membrane will affect blend morphology; however, signals attributed to the residual monomer were not present within both membranes (Figure 3-1D and Figure 3-1E) indicating the extraction of the monomer during the manufacturing process. Expulsion of the monomer may be due to structural incompatibilities upon blending or the dissolution of the monomer in a solvent, which may also be the case for the precursors. Understanding the effects of expulsion within the membrane will help contribute to deducing polymers that poorly blend. Expulsion of certain polymers will show in the composition of the membrane, when compared to the initial formulation. To better understand the composition of the membrane, quantitative analysis through NMR spectroscopy can be applied (Section 3.3.2).

3.3.2 Semi Quantitative Analysis of Precursor Content

Quantitative analysis of the membrane allows for comparisons between the initial mixture of the membrane and the final composition bearing results on the relative weight percentages. Comparisons of weight percentages ascertains claims made on polymer expulsion of the membrane. To obtain conditions for quantification, determination of the membranes longitudinal relaxation times (T_1) is required.

A significant reason conventional NMR spectra are considered qualitative is due to partial longitudinal relaxation which affects signal intensity respective to the molecular constituent (Section 1.7.2.4.3). To determine all molecular constituent's longitudinal relaxation times, ^{13}C inversion recovery is used. A spectrum consisting of all positive signals identifies conditions for full relaxation in all molecular constituents. ^{13}C Inversion recovery experiment was performed on the ABC membrane at τ evolution times of 2.08 s and 13.86 s (Figure 3-2).

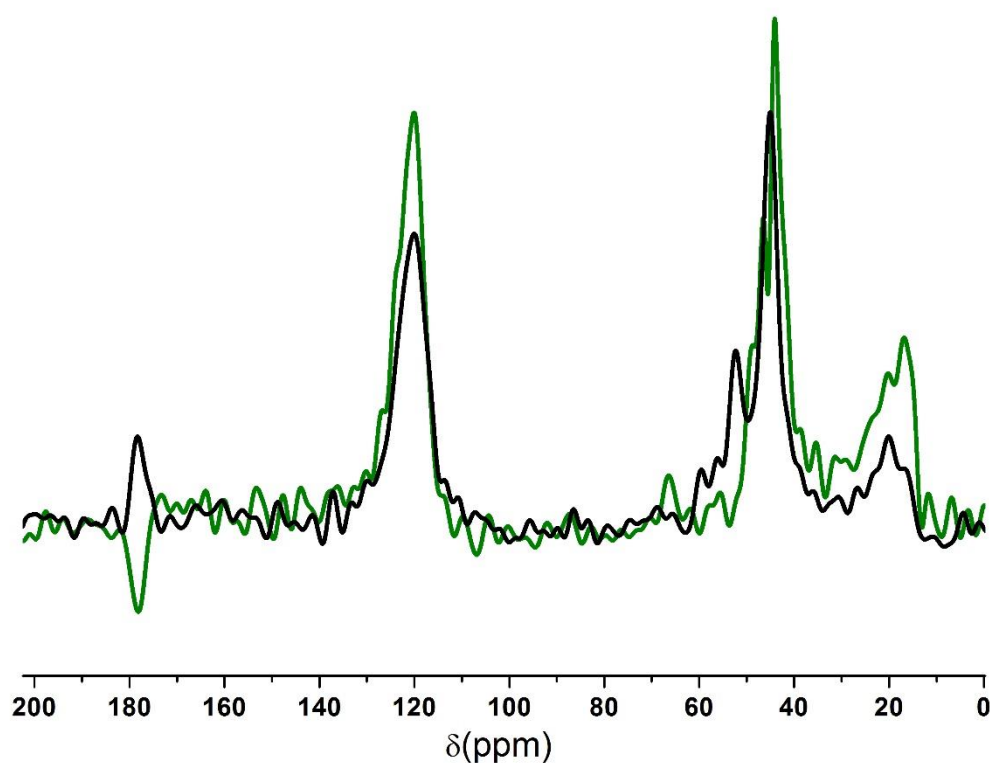


Figure 3-2 ^{13}C Inversion recovery spectrum of ABC membrane at an evolution time τ of 2.08s (green) and 13.86 s (black).

The ^{13}C inversion recovery spectra of the ABC membrane at τ evolution time of 2.08 s and 13.86 s are shown in Figure 3-2. To ensure the phasing was correct (negative signals for short evolution times and positive signals for long evolution times), phasing parameters were optimised for a ^{13}C SPE spectrum in the same experiment series and applied to all ^{13}C inversion recovery spectra. The carbonyl signal is observed to be negative at a τ evolution time of 2.08 s indicating partial relaxation whereas all other structures exhibit a positive signal. Comparisons with a τ evolution time of 13.86 s shows the carbonyl signal to be positive. Therefore, the conditions are considered quantitative ($1.443 \tau \geq T_1$) and the T_1 value were determined to be lower than 20 s. The ^{13}C SPE spectrum at a τ evolution time of 13.86 s can be can be optimised for a shorter time between scans. The evolution time of the ABC membrane was optimised for 8.32 s (Figure 3-3).

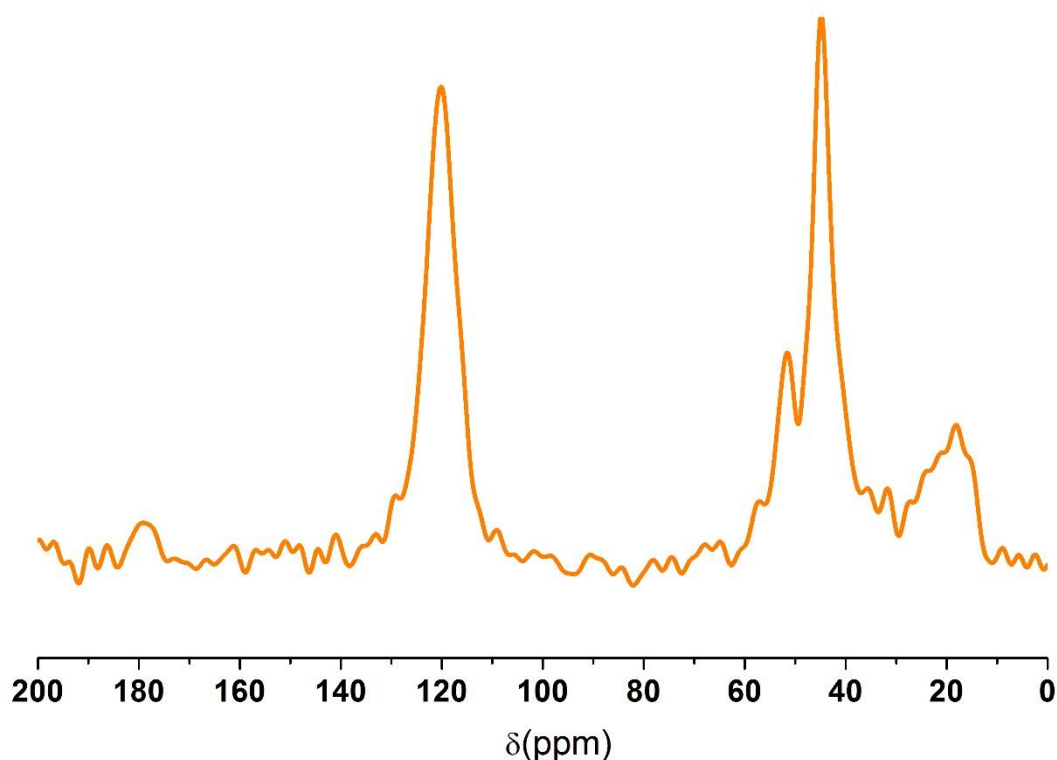


Figure 3-3 ^{13}C Inversion recovery spectrum of ABC membrane at a τ evolution time of 8.32 s.

All signals in the resultant spectrum are observed to be positive. While positive, the carbonyl signal suffers from poor sensitivity which is indicative that the τ value is similar to the τ_{null} conditions ($1.443\tau = T_1$). At τ_{null} conditions, the T_1 can be determined; however, it is considered an estimate as inaccurate 180° pulses and waiting periods between acquisitions start to have a larger impact on the determined value. Nonetheless, we assume the overestimated T_1 value of 12 s is sufficient to optimise acquisition parameters for a quantitative ^{13}C SPE spectrum.

It needs to be noted that ^{13}C inversion recovery experiments were not conducted on the AB membrane. The AB membrane is a similar system to the ABC membrane; moreover, the ABC membrane is considered more complex as it is a ternary system. Therefore, ^{13}C inversion experiments of the AB membrane were not carried out as it was assumed that a given component has the same T_1 value in the binary and ternary mixtures. A relaxation delay

of 60 s was set to take into account T_1 of less than 12 s to obtain a quantitative ^{13}C SPE spectrum of the AB membrane (Figure 3-4).

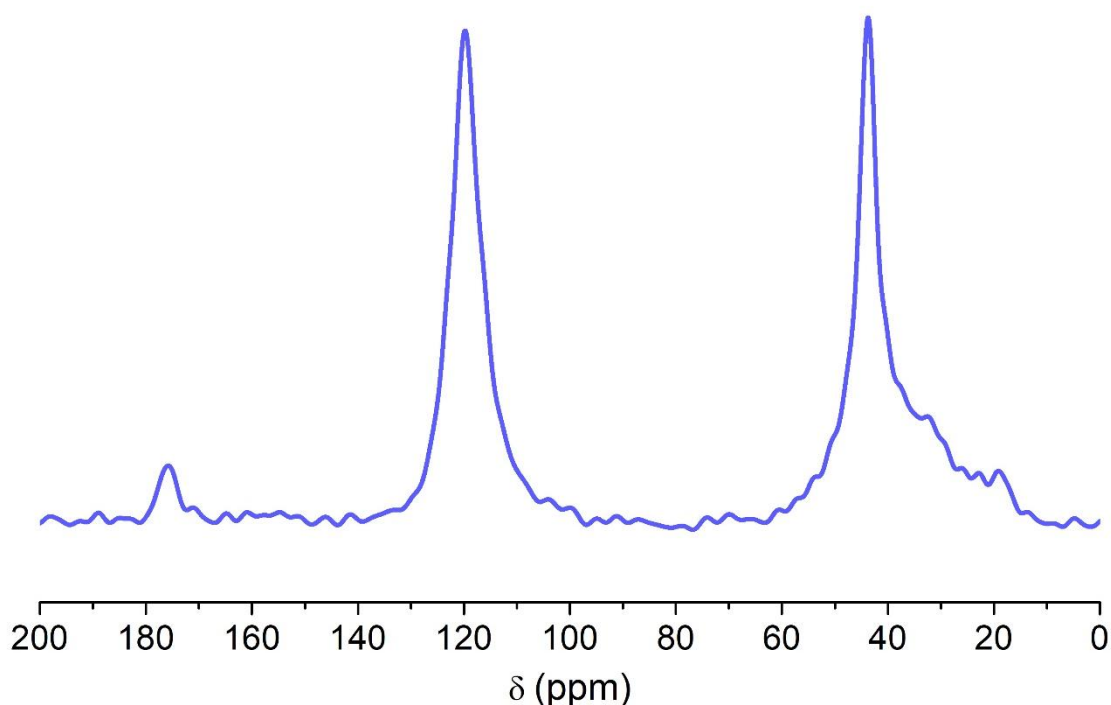


Figure 3-4 A ^{13}C SPE spectrum of the AB membrane in quantitative conditions.

The ^{13}C SPE spectrum of the AB membrane in quantitative conditions (Figure 3-4) exhibits all molecular constituents attributed to the precursors identified in previous measurements (Table 3-2). Integration of the spectrum allowed for determinations of the relative percentages of all molecular constituents (Table 3-3). The carbonyl signal suffers from the lowest SNR (SNR= 9), causing for the highest RSD value among all molecular constituents. At low signal to noise ratios (SNR), it is important to assess the precision of quantification ⁷³. Precision due to poor SNRs can be estimated through their relative standard deviation RSD_{SNR} (Equation 3-1) ⁹⁴.

$$\text{RSD}_{\text{SNR}}(\%) = \frac{238}{\text{SNR}^{1.28}} \quad 3-1$$

There are certain aspects not considered or overlooked when using (Equation 3-1). The value of 1.28 was experimentally determined for polyolefin compounds ⁹⁵; however, it is material specific ⁹⁴. Also, the calculated RSD value does not consider errors introduced

from phasing, which can be considered significant when SNR values are poor ⁷³. Errors introduced from phasing can be considered through comparisons of several data sets by several different users ⁷³.

Identifying structures that are solely contributing towards an individual polymer provides a mean for quantification studies. Molecular constituents found in the aliphatic region suffer from poor resolution, due to superimposition, leaving it unsuitable to pinpoint structures solely specific to a precursor polymer. Structures to take note of are the carbonyl group and the halogen group. Both the carbonyl and halogen signals are highly selective and exclusive to both polymer A and polymer B respectively. Relative percentages of the halogen and carbonyl signal were calculated in respect to the stoichiometric ratio to determine the weight and mole ratio percentages of the precursor polymers (Table 3-4).

Table 3-3 Relative percentages of the molecular constituents associated to the respective polymers found within membrane AB.

Molecular structures	Chemical shift range (ppm)	Relative percentage (%)	Polymer attribution
Carbonyl	180 to 173	2.7± 0.24	Polymer B
Halogenic	135 to 105	44.6*	Polymer A
Aliphatic	60 to 10	52.6*	Polymer A, Polymer B

*SNR too high for a significant RSD value

The weight by weight (w/w) and mole by mole (n/n) fractions were calculated for both polymer A and B (Table 3-4). When compared to the initial mixture (weight and mole fraction are not given for confidentiality reasons), Polymer

A exhibits a significantly smaller w/w and n/n ratio and polymer B exhibits a significantly larger w/w and n/n ratio where the difference is larger than the precision errors introduced. These results may be indicative of the extraction of immiscible domains in polymer A during the manufacturing process. Polymer A consists of polar molecular constituents; therefore, it is likely to segregate to the surface of the membrane where it is susceptible to interactions with water when quenched. This could explain the loss in polymer A content within the membrane.

The ABC membrane includes of an added polymer C which was previously identified to consist of similar structural features to both polymer A and polymer B. The added polymer may act as a compatibiliser between both polymers, promoting the formation of miscible domains. To better understand the contributions made from polymer C, a quantitative ^{13}C SPE NMR spectrum of the ABC membrane was recorded (Figure 3-5).

Table 3-4 Weight by weight and mole by mole ratios of the respective polymers within the AB membrane.

Sample	w/w %	n/n %
Polymer A	10.8	7.2
Polymer B	89.2	92.8

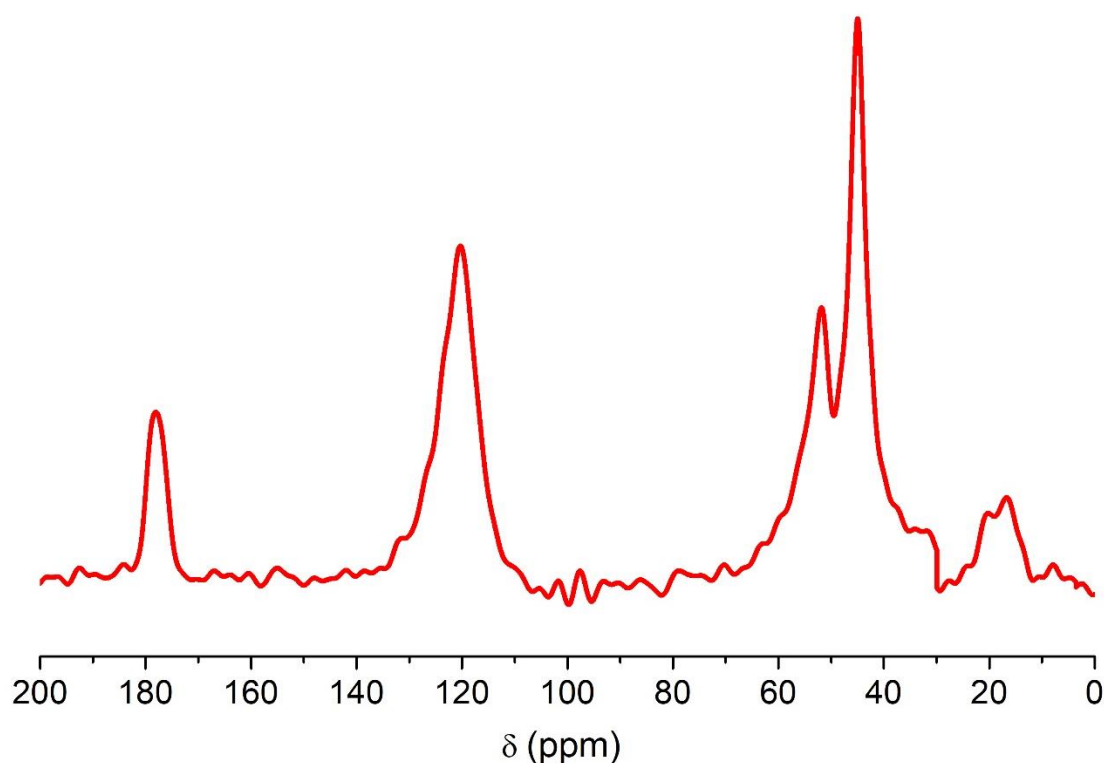


Figure 3-5 A quantitative ^{13}C SPE NMR spectrum of ABC membrane. localised baseline introduced from 30 to 10 ppm.

A ^{13}C SPE spectrum of the ABC membrane was recorded under quantitative conditions (Figure 3-5). Signal integration and determination of the RSD was conducted to calculate relative percentages of the molecular constituents found within the ABC membrane (Equation 3-1) (Table 3-5). Structures solely contributing to an individual precursor for quantification studies is more complex in the ABC membrane. The halogen signal is solely attributed to polymer B; however, the carbonyl signal consists of superimposed signals from both polymer A and polymer C.

The aliphatic structure at 22 ppm to 10 ppm consists of superimposed signals from polymer B and polymer C; however, the signal contribution from polymer B is the tail end of a broad signal (Figure 3-1B) suggesting the contribution is minimal. Hence, it is assumed the structure is mainly attributed to polymer C. A localised 2-point baseline was introduced from 30 to 10 ppm (Figure 3-5) for the integration of the aliphatic structure at 22 ppm

to 12 ppm, minimising the signal contribution from polymer B and providing the relative percentage contributing to polymer C.

The obtained percentage was used towards determining the relative percentage of the carbonyl signal solely attributed to polymer A (1.8%) (Table 3-5). All molecular constituents deemed exclusive to a precursor were calculated to determine the weight and mole ratio percentages of the precursor polymers (Table 3-5).

Table 3-5 Relative percentages of the molecular constituents associated with the respective polymer/s of membrane ABC.

Molecular structure	Chemical shift range (ppm)	Relative percentage (%)	Polymer attribution
Carbonyl	183 to 173	7.9 ± 0.5	Polymer A Polymer C
Halogenic	132 to 107	31.9*	Polymer B
Aliphatic	68 to 30	54.1*	Polymer A Polymer B Polymer C
Aliphatic	22 to 12	6.1 ± 1.3	Polymer C

*SNR too high for a significant RSD value

The weight by weight (w/w) and mole by mole (n/n) ratios were calculated for all precursor polymers (Table 3-6). Polymer B exhibits the highest w/w and n/n fractions within the system whereas polymer A exhibits the lowest highest w/w and n/n fractions. In comparison to the AB membrane, quantification of polymer A exhibits a RSD value of 100% suggesting the

relative amount of polymer A is similar in both membranes. To improve precision of quantification, more scans are required of the ABC membrane spectrum which is considered to be future work. In comparison to the initial mixture, Polymer A exhibits a significantly smaller w/w and n/n and both polymer C and polymer B exhibits a significantly larger w/w and n/n. The low relative amount of polymer A in comparison to the initial mixture suggests that expulsion within the ABC membrane is occurring, due to reasons stated previously on the AB membrane.

While polymer C consists of polar constituents, Polymer C is observed to be retained within the membrane. Many interpretations can be made from this deduction such as polymer C forms homogenous domains and does not segregate to the surface where it is susceptible to interactions with water upon quenching. It could also be assumed that polymer C is lost upon quenching, not to the same extent as polymer A, thereby increasing the relative percentage of polymer C when compared with the initial mixture. Moreover, Polymer C may be forming miscible domains with the other precursors; however, it is not well known if interactions are with polymer A due to the high SD value. To have a better understanding of the contributions of polymer C regarding miscibility, 2D WISE measurements were conducted.

Table 3-6 Weight and mole ratio of the respective polymers in the ABC membrane.

Sample	w/w %	n/n %
Polymer A	7.6 ± 7.6	5.0 ± 5.0
Polymer B	66.8 ± 1.6	76.3 ± 1.0
Polymer C	25.6 ± 6	18.7 ± 6

3.3.3 Miscibility Determinations through 2D WISE NMR Spectroscopy

Determinations of miscibility, allows for representations on how well the precursors are mixing within the system. 2D WISE NMR spectra allows for inferred deductions on miscibility by analysing the molecular mobility at certain carbon nuclei. If all carbon nuclei exhibit the same mobility, it can be inferred the system is miscible at the molecular level.

This experiment set introduces a powder of polymer A and polymer B (AB powder) as a representation of the system when the precursors are phase separated. Comparisons between the powder and the membranes will allow for deductions on the miscibility of the precursors and the molecular constituents inducing miscibility. 2D WISE measurements were conducted on the AB powder, AB membrane and ABC membrane (Figure 3-6).

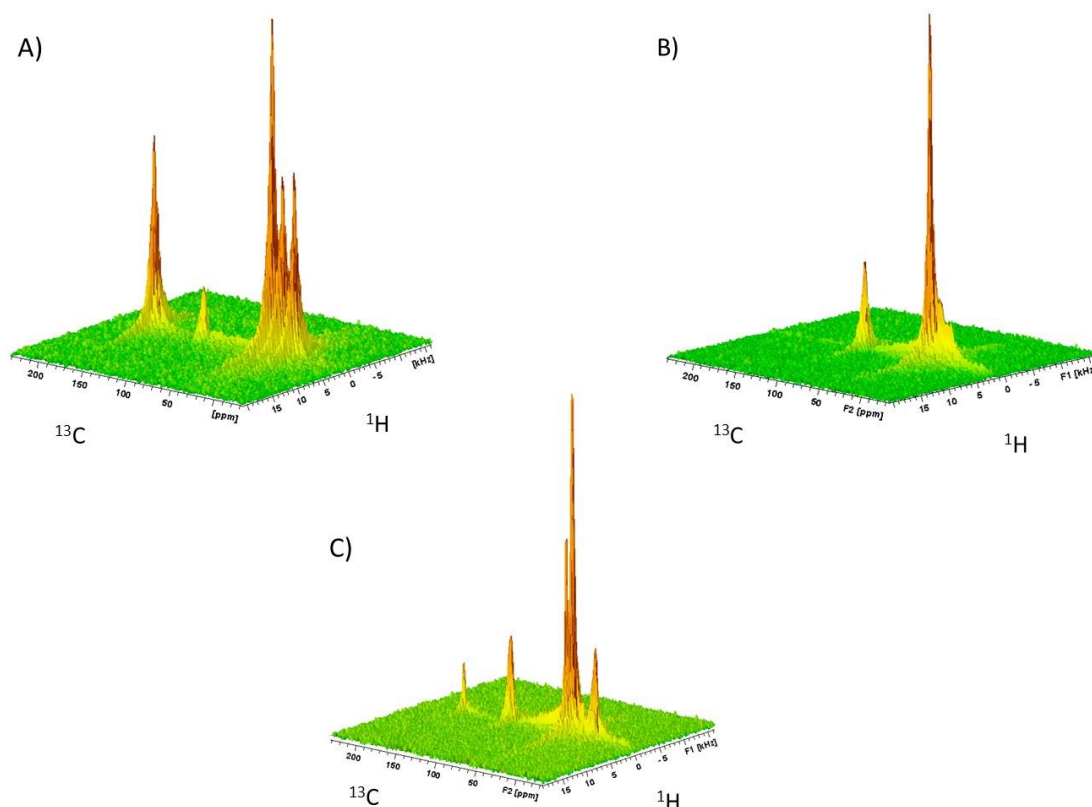


Figure 3-6 2D WISE spectra of A) AB powder, B) AB membrane and C) ABC membrane.

2D WISE spectra of the AB powder and ABC membrane (Figure 3-6A and Figure 3-6C) consists of all carbon signals in the respective precursors which has been previously determined (Table 3-2). The AB membrane spectrum (Figure 3-6B) lacks a discernible carbonyl signal indicating poor sensitivity. This may be due to the relatively low fraction of polymer A within the membrane (10.8%, Figure 3-4) and the low natural abundance of carbonyl groups within polymer A. Moreover, magnetisation transfer may not be slow due to a lack of a bounded hydrogen the carbonyl structure. Hence, polarisation is lowered due to the dependence on weak interactions from remote hydrogens ⁹⁶. Nonetheless, determinations on molecular mobility can still be made as aliphatic signals observed in polymer A are present within the system.

To better understand molecular mobility, slices of the ¹H spectrum were taken at specific ¹³C chemical shifts. ¹H slices were made at the apex of the intended ¹³C signal. All ¹H spectra of all significant carbon nuclei were normalised to highlight the differences in signal width (Figure 3-7).

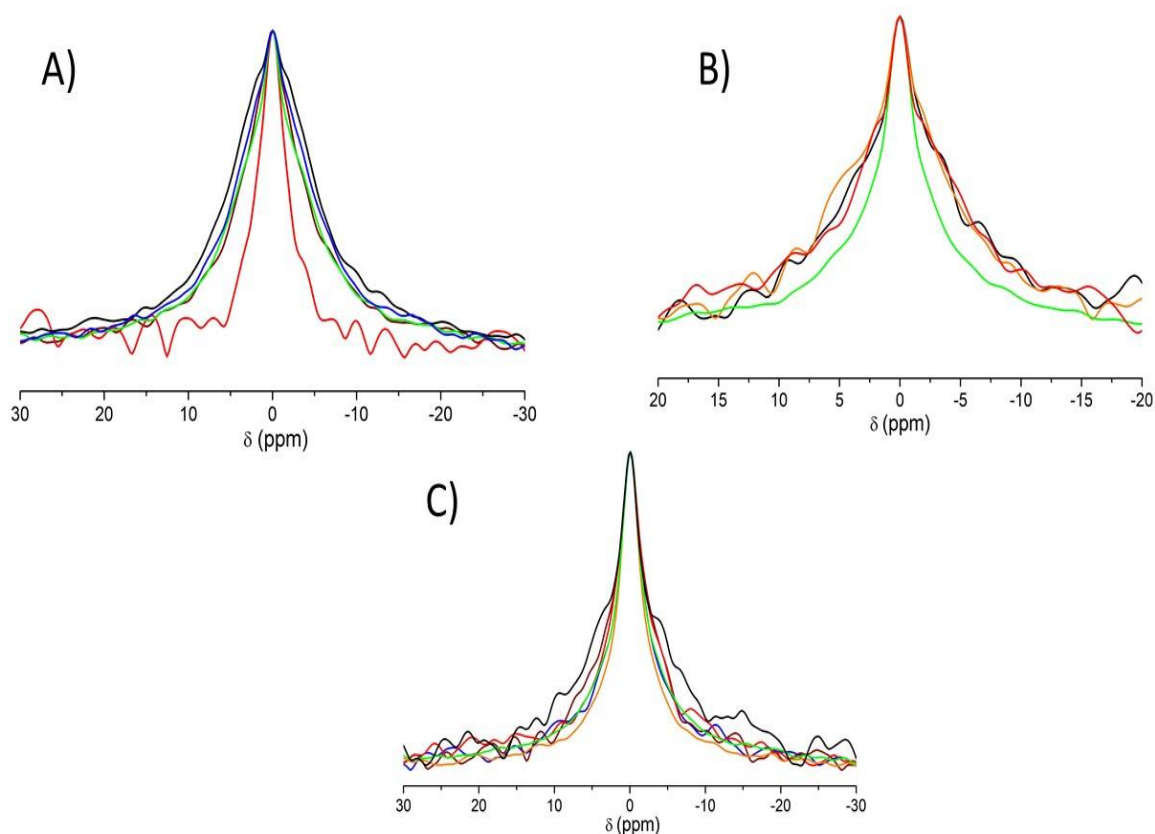


Figure 3-7 Normalised ^1H spectra of A) AB powder B) AB membrane and C) ABC membrane extracted from the 2D WISE spectra at specific carbon structures (≈ 177.0 ppm (brown), ≈ 120 ppm (red), ≈ 51.6 ppm (orange), ≈ 43.0 ppm (green), 31.2 ppm (black), ≈ 18.0 ppm (blue). For specific ^{13}C chemical shifts of all samples, please refer to (Table 3-7).

^1H spectra of the 2D WISE spectra of all samples were extracted and compared at notable carbon sites for all samples (Figure 3-7). Signal broadness was quantified by determining the width of the signal at half of the maximum intensity, Full Width at Half Maximum (FWHM) (Table 3-7). A low FWHM corresponds to a narrow signal, hence a high molecular mobility.

It is important to note the factors that affect the precision of the FWHM values (Table 3-7). The acquisition time set is short causing the Free Induction Decay (FID) to abruptly end (Figure A 11) among all 2D WISE measurements. Cutting the FID short results in strong oscillations in the spectra (Figure A 12), affecting FWHM values. A Gaussian window function was applied to reduce the oscillations; however, line broadening reduces the differences in signal width among all molecular constituents affecting

comparative studies. To reduce the effects of oscillation, a higher acquisition time needs to be set.

Regarding the AB powder (Figure 3-7A), the FWHM of all structures is assumed similar except the halogen which is observed to have a low FWHM value. The presence of a population with heightened mobility indicates homogenous domains respective to both precursors which is expected within the AB powder. When compared to the AB membrane, the halogen signal consists of similar FWHM values to most of the molecular constituents observed. It is hypothesised that interactions could be occurring at the halogen, which may be inducing domains of miscibility.

However, the aliphatic structure at 43.8 ppm consists of a noticeable lower FWHM indicating a higher mobility. This structure consists of superimposed signals from both polymer A and polymer B where it can exist within miscible domains and homogenous domains of both polymers. The different chemical environments that the aliphatic structure can potentially be in should broaden the ^1H signal; thereby, increasing the FWHM. However, this is not the case; thus, the low FWHM value may be due to the precision of the experiment as oscillations are seemingly minimal at 43.8 ppm of the AB membrane (Figure 3-7).

Regarding the ABC membrane, all molecular constituents consist of relatively the same FWHM indicating a miscible system. The addition of polymer C could be inducing interactions towards miscibility, hence acting as a compatibilizer between the two components. For comparative studies between samples, the FWHM in relation to the ^{13}C chemical shift was plotted for all samples (Figure 3-8).

Table 3-7 FWHM of ^1H slices at specific carbon structures for all samples use in 2D WISE measurements (Figure 3-7).

Sample	^{13}C δ (ppm)	Molecular structure/s	FWHM (Hz)
AB powder			
	177.0	Carbonyl	2464
	120.6	Halogenic	1159
	43.0	Cyclic Aliphatic/ Aliphatic	2536
	31.2	Cyclic aliphatic	3188
	17.9	Cyclic aliphatic	2826
AB membrane			
	120.8	Halogenic	2246
	43.8	Cyclic Aliphatic/ Aliphatic	1159
	31.1	Cyclic aliphatic	2464
	18.0	Cyclic aliphatic	2391
ABC membrane	179.0	Carbonyl	1636
	120.5	Halogenic	1449
	51.7	O-methyl	1014
	44.4	Cyclic Aliphatic/ Aliphatic	1159
	30.5	Cyclic aliphatic/ aliphatic	1884
	15.5	Cyclic aliphatic/aliphatic	1159

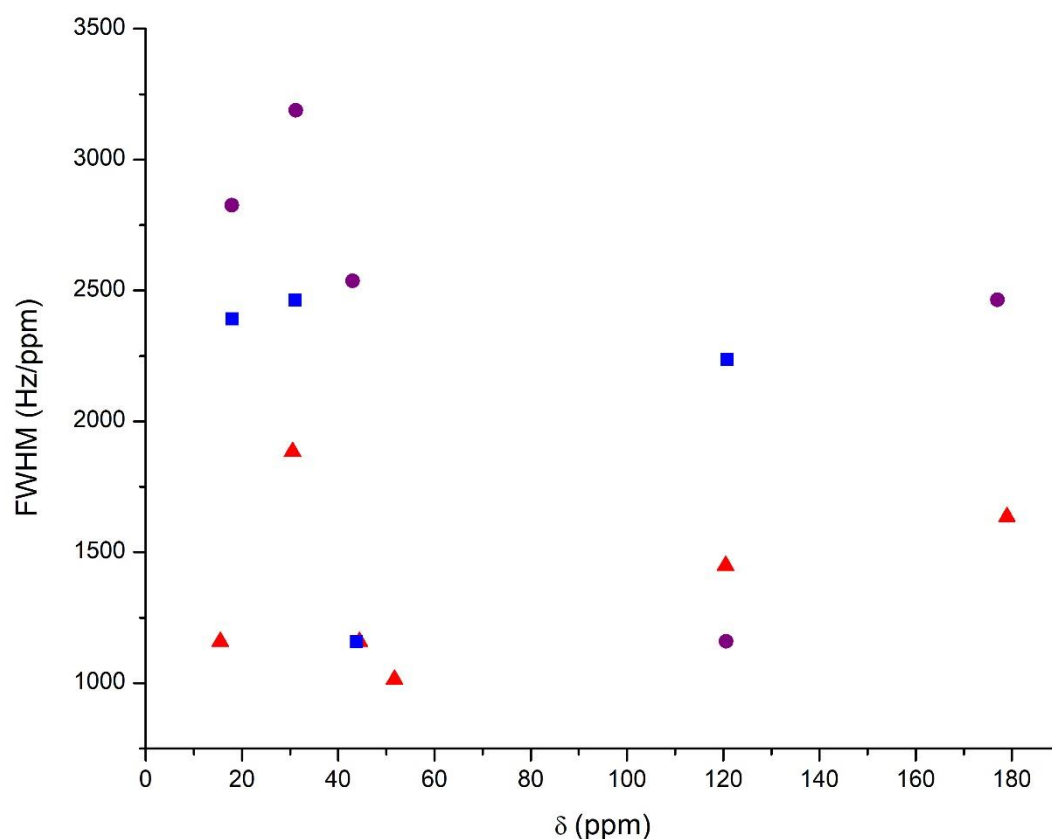


Figure 3-8 FWHM in relationship to ^{13}C chemical shifts of AB powder (purple circle), AB membrane (blue square) and ABC membrane (red triangle).

Both the AB powder and the AB membrane have molecular constituents (120.6 ppm and 43.8 ppm respectively) with lower FWHM values. As previously mentioned, this may be due to the precision of the experiments. In the assumption that the both species are more mobile than all molecular constituents in their respective system, it suggests the presence of homogenous domains between other molecular constituents. Regarding the ABC membrane, the FWHM is seemingly constant throughout all molecular constituents and has an overall lower FWHM (in most molecular constituents) than the other systems. It should also be noted that polymer C is less mobile than the other precursors, previously determined by the ^1H SPE of polymer C (Figure A 7). Homogenous domains of polymer C should increase FWHM across all molecular constituents; however, the relatively low FWHM of the ABC membrane suggests it is primarily composed of miscible domains. The high FWHM of the aliphatics in AB powder and AB membrane may be

due to the presence of homogenous domains thereby increasing the number chemical environments the structure; hence, broadening the signal.

More tests are required to strengthen determinations made on miscibility. 2D WISE experiments at a longer acquisition time need to be conducted for more precise FWHM values. To probe interactions in Polymer C, 2D WISE experiments can be conducted on a powder containing polymer A,B and C, allowing for comparative studies with the ABC membrane. The CP component of the 2D WISE experiment (refer to introduction section) can be altered to Lee-Goldburg cross polarisation parameters causing for homonuclear decoupling ⁹⁶. Minimised homonuclear interactions will increase resolution in the 2D WISE spectrum and differences in ¹H line widths become more distinct.

3.4 Conclusion

The characterisation of polymer blended ultrafiltration membranes provided detailed knowledge on the molecular characteristics through a variety of NMR spectroscopy techniques. Samples included both a binary blended and ternary blended ultrafiltration membrane. Structure elucidation of the membranes and their respective precursors allowed for determinations on molecular constituents exclusive to a precursor within the membranes. Identification of individual constituents allowed for quantitative analysis of the membranes composition after optimisation was conducted through ¹³C inversion recovery experiments. The results showed that polymer A is expelled or out or was never incorporated within the membrane. This could be due to poor miscibility within the system or an issue of solubility. 2D WISE measurements were carried out to determine miscibility at the molecular level. Interpretations suggest that AB membrane may not be a completely miscible system. The ABC membrane may be a miscible system due to the contributions of Polymer C. 2D WISE measurements were subject to errors of precision, primarily due to cutting the FID short, requiring optimisation of the technique. Future research opportunities can investigate the chain dynamics within the membranes for further deductions on miscibility ⁹⁷.

Characterisations made allow for studies that establish links between chemical structure to membrane functionality.

4 THE RELATION OF SURFACE COMPOSITION TO FUNCTIONALITY

4.1 Introduction

Membrane filtration is currently used in a variety of applications including seawater desalination ⁹⁸, biotechnologies ⁹⁹, petrochemical wastewaters ¹⁰⁰. Application in a variety of environments requires the design of membranes to finely tune for functionality. This approach is considered limited, as functionality is determined by the chemical structures present. To widen the scope of membrane design methods, the development of functionality and chemical structure relationships are required.

4.1.1 Surface Structure Composition

Most membranes have an asymmetric composition, where the surface and the bulk form distinct layers. In a polymer blend membrane, the polymer with the lowest surface energy migrates to the surface, primarily forming the surface ¹⁰¹. It was previously discussed that hydrophilic polymers generally migrate to the surface (Section 1.5) in certain membrane designs. These polymers dictate the surface properties, hence, properties like fouling ⁷⁹, pore-size distributions ¹⁰ are dependent on the hydrophobic/hydrophilic interactions occurring at the surface ⁷⁹. Analyses of the polymer composition at the surface allows for the identification of functional properties affected by the composition.

4.1.2 Functional Properties

Certain functional properties of water filtration membranes has been previously discussed (Section 1.6). Most reported research on membrane filtration is based on antifouling properties ^{102, 103} and molecular dynamics simulations ^{104, 105}. However, the mechanical behaviour of porous membranes is rarely reported ¹⁰⁶. Based on the Scopus database, publications that investigate mechanical properties of desalination and water treatment membranes constitute less than 5 percent of desalination and water treatment membrane publications annually ¹⁰⁶. Analysis of loading conditions on examining mechanical properties not only allows for design improvements on membrane structure but also for the prediction of failures ¹⁰⁶. Hence, real

life application of filtration membranes requires an understanding of their mechanical properties ¹⁰⁷.

This study aims to determine how the surface composition affects functionality within a system consisting of a binary and ternary membrane system. Contact angle tests and tensile tests were used to determine the functional properties, ¹H NMR spectroscopy and Scanning Electron Microscopy (SEM) were used to determine the polymer composition and physical features found at the surface of the membrane. Analysis with a wide variety of techniques allowed for representations of functionality and how surface composition may dictate functionality for our systems.

4.2 Materials and Method

4.2.1 Chemicals

AB Membranes and ABC membranes were supplied by an industrial sponsor (Section 3.2.1). The membranes were preconditioned through soaking in excess MQ water for 3 days, membranes were rinsed daily. The membranes were dried at 70 °C for 1 hour in an oven. Propan-2-ol (99.5%) was purchased from Chem supply, ethanol (99.7%) was purchased from Analar. Deuterium Oxide (99.9%) was purchased from Cambridge Isotope Laboratories, USA.

4.2.2 Scanning Electron Microscopy

Samples were freeze fractured in liquid nitrogen, then coated with gold using a Cressington sputter coater (Ted Pella). The sample chamber was purged with argon. 20 kV was applied for a coating time of 1 minute. A JEOL JSM-6010LA scanning electron microscopy was used, with an EDS detector. Images were taken at accelerated voltages between 5 and 15 kV used along with a spot size of 28 – 35 at a working distance of 9 – 10 mm. InTouchScope was used for data acquisition and data treatment.

4.2.3 NMR Spectroscopy

Membranes were cut into three separate fibres of equal length and soaked in D₂O for 1 hour prior to packing in a rotor. 10 µl of D₂O was added to the rotor and left to dry for 15 min before analysis. Rotors were rinsed with ethanol and dried before packing.

All ¹H SPE spectra were recorded on a Bruker Avance DPX200 spectrometer operating at a Larmor frequency of 200 MHz. A commercial double resonance probe supporting zirconia MAS rotors with a 4 mm outer diameter and a 3 mm inner diameter was used. Measurements were carried out in the absence of spin (static conditions). ¹H SPE spectra were recorded using a 90° pulse of 3.6 µs, an acquisition time of 0.15 s and a relaxation delay of 9.8 sec. The ¹H chemical shifts scale was externally referenced using adamantane by setting the CH resonance to 1.64 ppm ⁸⁸.

4.2.4 Tensiometry Tests

A DCAT11 Dataphysics was used for advancing and receding contact angle measurements. Samples were tested in water with all results reported the average of 3 replicate measurements. The Washburn method was used for all contact angle calculations ¹⁰⁸.

4.2.5 Tensile Strength Tests

An Instron mechanical tester SS65 was used for all mechanical testing. Five replicate samples were tested for each reported membrane. A set sample length of 100 mm was used, with a travel rate of 150 mm·min⁻¹. Instron Bluehill software was used for data acquisition and data treatment.

4.3 Results and Discussion

4.3.1 Membrane Surface Analysis

4.3.2 Physical Features and Element Identification

SEM is a method that provides visual information at varying length scales. The theory of SEM has been previously discussed (Section 1.7.3). SEM can be used as an identification tool, to determine the presence of physical features within the membrane. Scanning Electron Microscopy coupled with Energy Dispersive X-ray Spectroscopy (SEM/EDS) can provide element information at localised areas, allowing for surface composition information. SEM images of the AB and ABC membrane were taken for the identification of physical features (Figure 4-1).

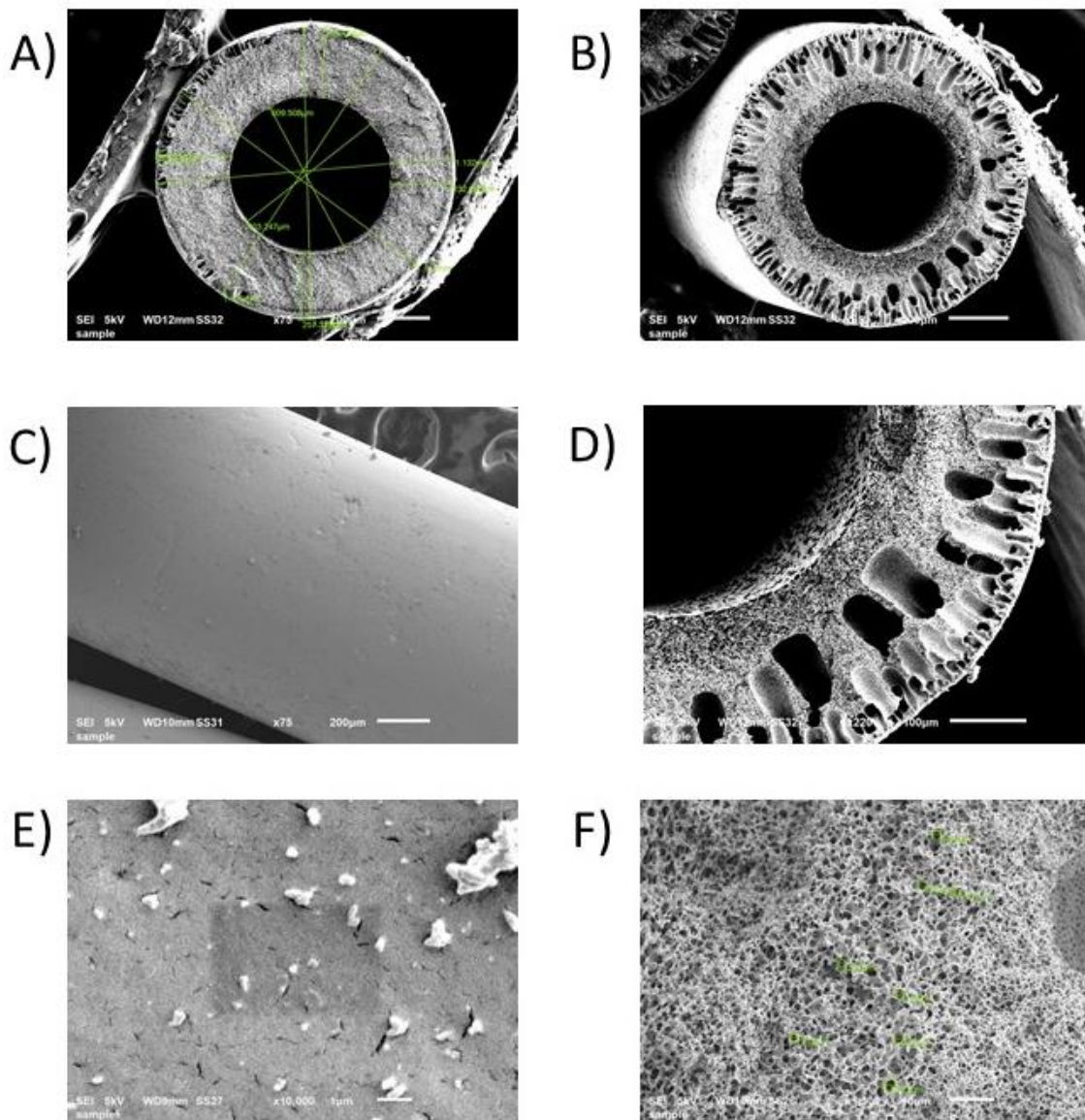


Figure 4-1 SEM images of the AB membrane A) cross section at 200 μm with length measurements (green lines), C) surface at 75 μm , E) surface at 1 μm . SEM images of ABC membrane B) cross section at 200 μm , D) cross section at 100 μm , F) cross section at 10 μm with pore-size calculations (green circles) (refer to scale bar for image lengths).

SEM images of both the AB and ABC membrane were taken at varying length scales at the cross section and the surface (Figure 4-1). The cross section of the AB and ABC membranes allows for the determinations of physical features (Figure 4-1A and Figure 4-1B) within the membrane. In both membranes, there are regions of interest used to help identify physical structures and calculate values for other characterisation tool. The inner diameter corresponds to the black region in the middle of the membrane, the

membrane wall is the region outside of the inner diameter and ends at the membrane surface and the outer diameter corresponds to the outside of the membrane wall. A graphical interpretation on identifying the regions of interest was made (Figure A 13). Length measurements on the regions of interest were conducted and tabulated (Table A 2). Length measurements were used for calculations relating to tensile strength (Section 4.3.4.2).

Important physical structures to note is the presence of macrovoids in the membrane wall of both membranes. Macrovoids are observed as the oval shaped structures observed closest to the surface of the membrane (Figure 4-1D). Macrovoids are generally considered weak mechanical points within the system ^{109,110} and are usually undesired. While the formation mechanism is not well understood ¹¹⁰, poor miscibility between polymers at the membrane surface can influence the development of macrovoids ¹¹¹. Previous determinations on miscibility (Section 3.3.3) shows the ABC membrane to be more miscible system than the AB membrane at the molecular scale; however, partial miscibility can be observed at length scales larger than the molecular scale. This indicates that more studies need to be conducted on the chemical interactions that induce macrovoids formation.

Pores were found in both membranes in the membrane wall allowing for a pore-size analysis (Figure 4-1F). Pore sizes in the membrane wall were between 1 and 2 μm . Pore-sizes in the membrane wall do not determine size selectivity of the membrane; however, they allow for transport of the filtrate to the inner diameter. To compare the pore-sizes in the bulk and the surface, SEM images of the ABC membrane surface were taken (Figure 4-1C) and showed no observable pores (Figure 4-1E). Due to the expected small sizes of the pores within the surface, roughly 0.1 μm , the gold coating may have clogged the pores. To determine pore-size and pore-size distribution at the surface, porometry techniques can be applied which is discussed in chapter 5 (5.2.1). To determine the components found within the surface of both membranes, SEM/EDS was conducted (Figure 4-2).

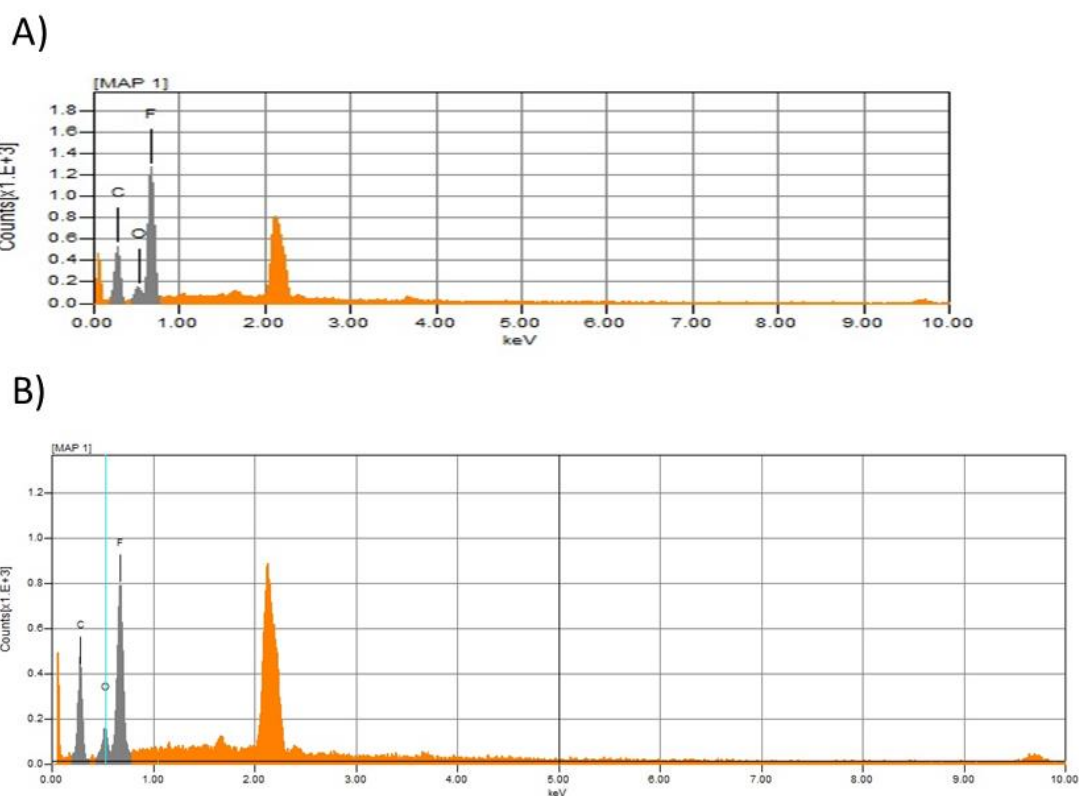


Figure 4-2 SEM-EDS analysis of the surface of A) AB membrane B) ABC membrane.

SEM-EDS analysis was conducted on the surface of the AB membrane and ABC membrane (Figure 4-2), for images of the area of analysis refer to Figure A 14. Results are in preliminary stages; hence certain elements are not marked in the figure; however, the energy of the expected element found have been tabulated (Table 4-1).

Table 4-1 EDS values of the expected elements in the AB and ABC membrane.

Element	(keV)
Carbon	0.28
Nitrogen	0.39
Oxygen	0.53
Fluorine	0.68
Gold	2.12

Identification of a fluorine group is surprising as well as the absence of nitrogen in polymer A. The presence of fluorine is mainly attributed to polymer B (Section 3.3.1) which is expected to primarily compose the bulk of the membrane. While SEM is considered a surface analysis tool, depth penetration of SEM/EDS is roughly 1 μm to several μm ¹¹² and the wall thickness is roughly 250 μm . The area of analysis may include part of the bulk of the membrane, hence explaining the fluorine peak. This is not conclusive and further tests are required on understanding the length scale of the surface. The absence of nitrogen may have been attributed to the poor sensitivity of the technique as the oxygen peak may consist of superimposed nitrogen peaks.

Both membranes exhibit a peak at 2.2 keV which is assigned to be gold. The presence of this element may be due to gold coating of both membranes. This deduction is primarily based on the higher keV value, indicating its more electronegative, and that the peak shape and intensity is similar between samples.

Identification of both carbon and oxygen are attributed to both polymer A and polymer C (Section 3.3.1). Interpretations suggest polymer A is found within the surface, deduced from the AB membrane. These results are not conclusive with polymer C as peak contributions in the ABC membrane may primarily be from polymer A. For a further understanding on the surface composition, ¹H SPE NMR spectroscopy was applied.

4.3.3 Determination of Surface Composition through ¹H Static NMR Spectroscopy

While NMR spectroscopy is generally considered a bulk analysis tool, the surface composition of the membrane can be determined through the addition of an agent that increases mobility at the surface. By inducing mobility, resolved signals could be attained creating a large contrast between the immobile and mobile segments of the membrane. This study proposes the use of D₂O as a swelling agent. D₂O should not permeate through the membrane

as the bulk is primarily hydrophobic, therefore swelling occurs mainly at the surface . To further observe the differences in mobility through NMR spectroscopy, ^1H SPE in static conditions were employed. The absence of MAS allows for larger contributions of anisotropic interactions ³⁶; thereby broadening the signal and causing the rigid segments of the membrane to be hidden within the broad baseline. ^1H SPE NMR spectra in static conditions for both membranes dry conditions and soaked in D_2O conditions (Figure 4-3)

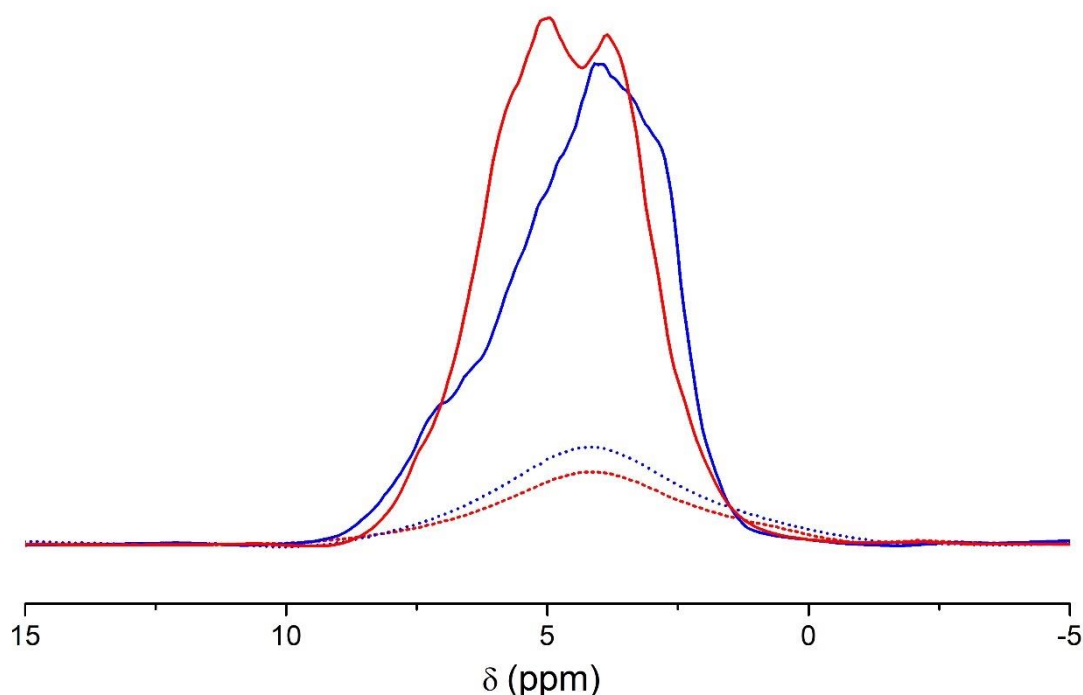


Figure 4-3 ^1H SPE spectra of AB (blue) and ABC (red) membrane in dry state (dashed lines) and soaked in D_2O (solid lines).

^1H SPE spectra of the AB and ABC membrane were recorded in both a dry state and pre-soaked in D_2O (Figure 4-3). Under dry conditions, both membranes exhibit broad signals which are poorly resolved. This is expected as anisotropic interactions (due to the absence of Magic Angle Spinning, MAS) and the rigidity cause signal broadening. Comparisons when pre-soaked in D_2O show both membranes exhibit distinct line shapes. Pre-soaking both membranes in D_2O is observed to cause an increase in intensity and resolution due to the heightened molecular mobility of the sample.

A distinct population in the ABC membrane is observed (5 to 8 ppm) when compared to the AB membrane. This population might be due to the contributions of polymer C indicating that polymer C might be found at the surface of the membrane. The polymer C signal cannot be clearly identified due to poor resolution. One method to strengthen this determination is to employ comparative ^1H NMR measurements of the precursor polymers soaked in the same amount of D_2O to provide information if this population is attributed to polymer C. This is considered as future work.

The ^1H spectra of both AB and ABC membrane (Figure 4-3) may consist of superimposed signals from the residual HOD in D_2O . While D_2O has no direct hydrogen, the deuterium-hydrogen exchange with atmospheric hydrogen ¹¹³ and the membrane creates a signal, potentially affecting both the line shape and area. To understand the signal contribution of the residual HOD in D_2O , the stock solution of D_2O was measured (Figure 4-4).

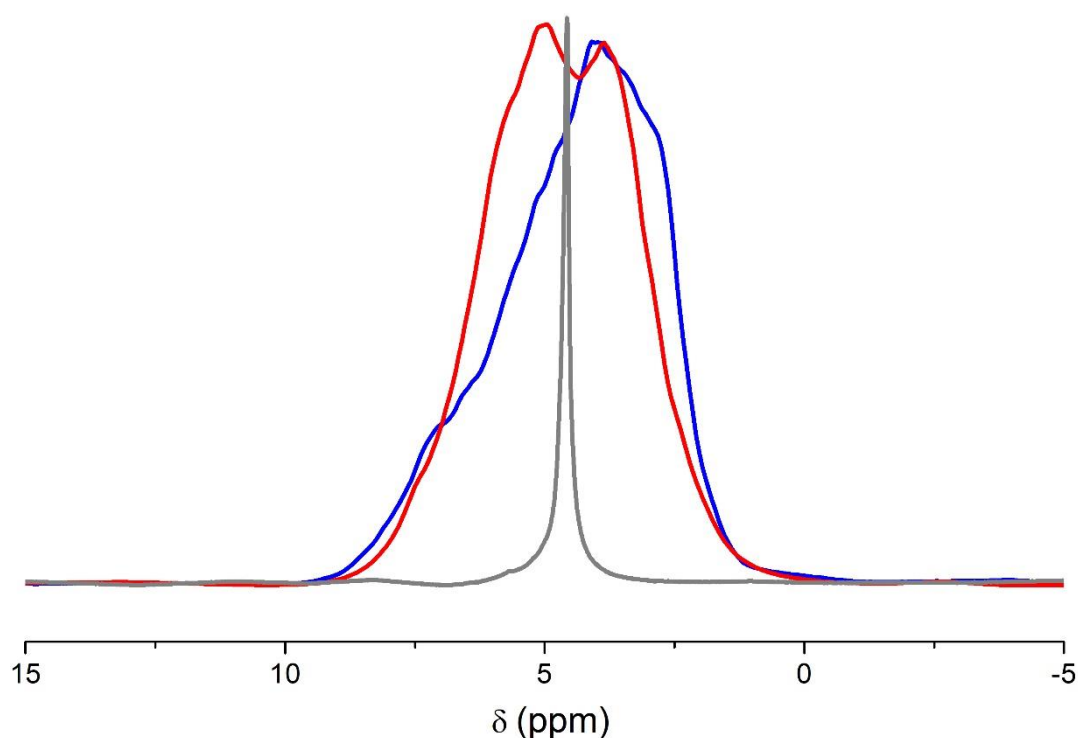


Figure 4-4 Normalised ^1H SPE spectra of AB (blue) and ABC membrane (red) soaked in D_2O in comparison with the stock solution of D_2O (grey).

The AB membrane and ABC membrane pre-soaked in D₂O were compared with the D₂O stock solution (Figure 4-4) and it was observed that the D₂O stock solution signal is considerably narrower than that of both membranes. These results suggest that broad signals from both membranes are primarily attributed to swollen segments of the membrane. Hence, the D₂O stock solution contributes minimally to the line shape of both membranes. It is important to mention the effect sample preparation can have on this method. In the presence of excess D₂O, the resultant signal is primarily attributed to free HOD (Figure A 15). However, reducing the amount of D₂O may only cause partial swelling on the surface of the membrane, affecting line shapes. Comparisons between ¹H static measurements with varying amounts of D₂O added provides detail on the optimal conditions for swelling the membrane surface without the loss in resolution.

While it is not known that swelling the membrane surface is achieved with the current sample preparation, partial swelling can be observed through line shape differences in relation to time. ¹H static measurements of the membranes in D₂O at different time intervals were conducted to see the effects of swelling (Figure A 16). Observations showed no significant difference in terms of line shape. Hence, we assume that if the membrane surface is partially swollen, ¹H static measurements will not be affected by the kinetics of further swelling. To understand other factors that may influence line shape, measurements were repeated(Figure 4-5).

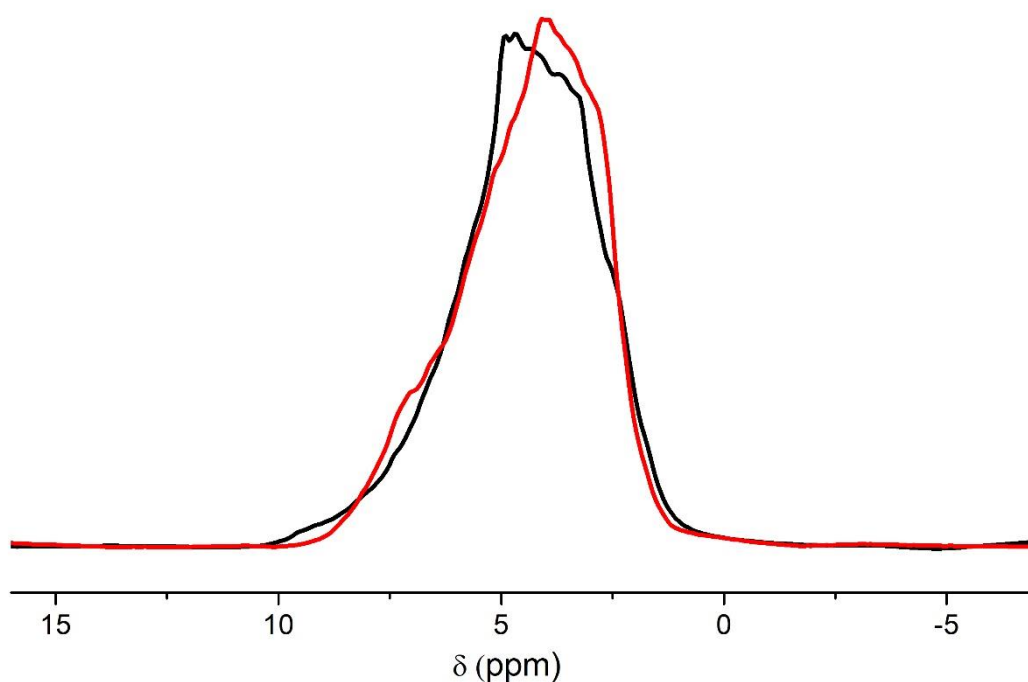


Figure 4-5 Normalised ¹H SPE spectra of AB membrane soaked in D₂O with a repeat.

¹H SPE measurements were conducted on the AB membrane pre-soaked in D₂O and a repeat (Figure 4-5). Upon comparison, there is an observable difference in line shapes indicating that line shape may be poorly repeatable. The difference in line shape can be due to varying surface composition within samples. The random nature of blending polymers may cause compositional differences in a given area. The compositional differences will show within the resultant spectra, affecting comparisons made between samples. Adding more membrane fibres to the rotor can normalised the compositional differences between samples.

In terms of quantification, the two measurements of the peak area of the AB membrane has a difference of 3.5% indicating the consistency of the method. These results are promising for the precision of quantification studies; however, more repeats are required for meaningful determinations.

Overall, compositional differences can be identified through addition of a swelling agent. Interpretations can infer the structure of a population,

however the poor resolution, and poor repeatability on signal shape requires further method optimisation. Nonetheless, there is an observed population difference on the surface of both polymers, and it is assumed it is the contributions of polymer C to allow for deductions on functionality.

4.3.4 Functionality Measurements

Functionality measurements are used to understand the properties of the membrane in its application state. Contact angle determinations were conducted in the presence of water and tensile strength tests are used to emulate the pressure applied on the membranes.

4.3.4.1 Contact Angle Determinations through Tensiometry Tests

The contact angle is the angle at which the membrane meets the interface of water. Measurements of contact angle are applied to evaluate the hydrophilicity of the material ¹¹⁴. Hydrophilicity determinations can help elucidate information on membrane fouling and water flux ⁷⁹. Measurements of the advancing angle and the receding angle help in determinations of hydrophilicity. The advancing angle is considered the maximum possible contact angle produced from the wetting of the membrane and the receding angle is the angle taken on the course to de-wetting. Hydrophilic materials exhibit contact angles less than 90° whereas hydrophobic materials exhibit contact angles of over 90°

Table 4-2 Averaged results of tensiometry tests of the AB membrane and the ABC membrane. Standard deviations are shown adjacent to the measured value (n=3).

	Average dry advancing angle (°)	Average wet advancing angle (°)
AB membrane	85.2 ± 1.9	81.1 ± 3.7
ABC membrane	96.4 ± 1.9	92.9 ± 2.1

Tensiometry tests of both membranes were conducted in triplicates (Table 4-2). Refer to Table A 3 for the raw data. Upon comparison the average dry advancing, and average wet advancing angles are higher in the ABC membrane when compared to the AB membrane. Localisation of Polymer A at the surface may be contributing towards the overall hydrophilicity of the membrane. The larger contact angle of the ABC membrane suggests it is more hydrophobic. The higher hydrophobicity may be interpreted as the contributions of polymer C. Polymer C primarily consist of molecular structures considered hydrophobic (Section 3.3.1). This strengthens determinations made in Section 4.3.3 that polymer C may be localised at the surface of the membrane.

The contact angle in both membranes show the average wet advancing angle to be within the SD of the average dry advancing angle. Water filtration membranes in dry conditions show different morphological features than in its application conditions (wet) ¹¹⁵. Hence, more repeats are required for precise contact angles allowing for accurate determinations on the contact angle difference between the dry and wet state.

4.3.4.2 Tensile Strength Determinations

Tensile tests analyse the strength of a material by applying force on the material. Tensile testing determines the average properties over a large specimen cross-section where the specimen dimensions usually do not interfere with fundamental length scale ^{106, 116}, hence it is considered a bulk analysis technique. The results of tensile testing are essential to product design as results provide data support for material specifications. Tensile strength tests were conducted on the AB and ABC membrane (Figure 4-6).

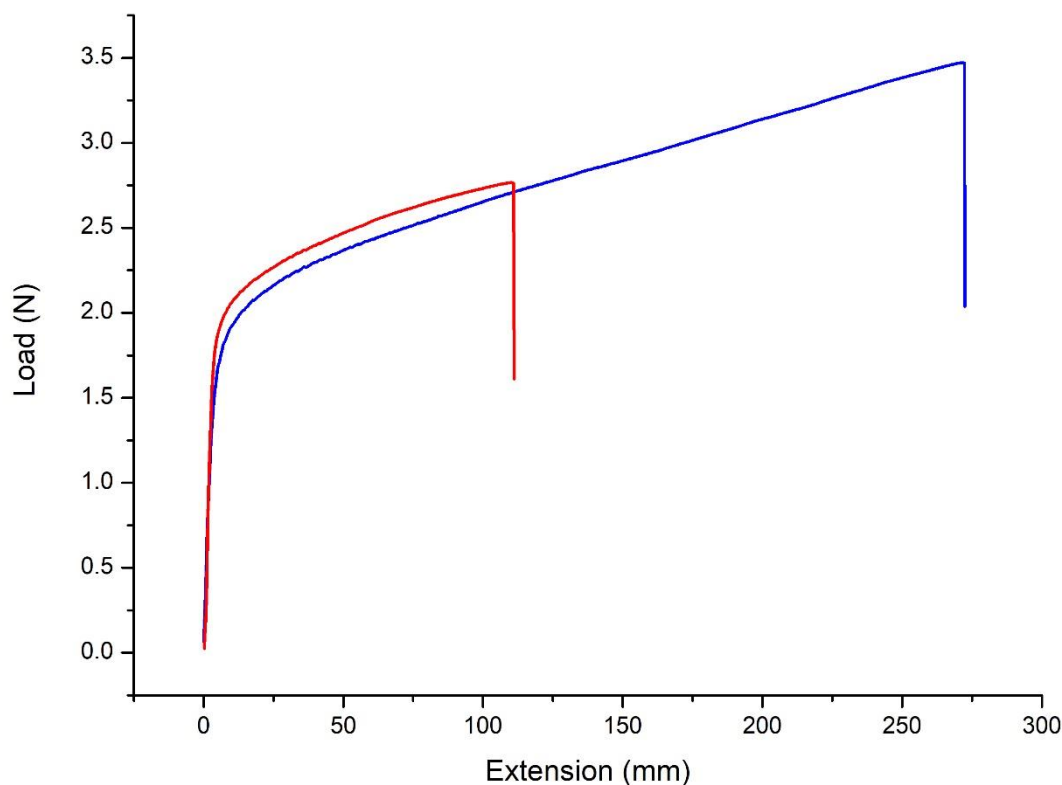


Figure 4-6 Load in relation to extension of the AB membrane (blue) and the ABC membrane (red).

Tensile strengths tests were conducted on both the AB membrane and the ABC membrane (Figure 4-6). Membranes were stretched until breakage (load at break) indicated by a sudden drop in load. 5 repeats were conducted on both membranes (Table A 4) and show similar functions as shown in (Figure 4-6) respective to the membrane. All results were averaged and tabulated (Table 4-3). Calculations on tensile tests required length measurements on specific regions within the membrane, measurements were previously determined through SEM (Table A 2). The AB membrane shows higher values on the load at break and the break extension which is expected. Previous measurements on the bulk membrane composition (Section 3.3.2) and macro void formation (Section 4.3.2) shows the AB membrane to exhibit fewer macrovoids and a higher content in polymer B. Polymer B contributes to the overall tensile strength of the membrane as it is primarily composed of

hydrophobic molecular features (Section 3.3.1). Both factors will contribute to the overall higher tensile strength in comparison to the ABC membrane.

Table 4-3 Averaged values of tensile tests results conducted on both AB membrane and ABC membrane. SD values are found adjacent to measured values (n=5).

Sample	Load at break (N)	Break extension (mm)
AB membrane	3.41 ± 0.31	270.60 ± 3.79
ABC membrane	2.43 ± 0.12	98.2 ± 2.05

4.4 Conclusion

Measurements relating to surface composition and functionality were applied to both the AB and ABC membrane. Deductions on surface composition from ^1H NMR spectroscopy and SEM revealed that structures pertaining to polymer A and C are observed in their respective membranes. Hence, it was inferred that polymer A and polymer C are localised near the surface of the membrane. Contact angle measurements suggest the hydrophilic nature of the AB membrane surface is primarily due to polymer A whereas polymer C is contributing to the hydrophobic nature of the ABC membrane surface, further strengthening the deduction that the two polymers are localising at the surface. Identifying the surface composition will help in work relating to functional properties on the membrane surface such as pore-sizes and fouling. SEM allowed for the identification of macro voids near the membrane surface where macro voids were found to be more prominent in the ABC membrane. Comparisons of tensile tests revealed that AB membrane had a higher tensile strength and interpretations suggest this was due to the minimal formation of macro voids and a higher polymer B content. The conclusions made allow for the identification of relationships between functionality and surface chemical composition. Identification of relationships will allow for better

design principles and provide reasoning on the properties of the membrane in its application state.

5 CONCLUSION AND FUTURE RESEARCH OPPORTUNITIES

This thesis delved into both the physical and chemical properties of ultrafiltration (UF) membranes. In-depth characterisation allowed for comparative studies between two different types of membranes, AB membrane and ABC membrane. Not only were the membranes investigated, but this thesis highlights how different analytical techniques can complement each other. Developments made can be the basis towards a promising means for the characterisation not limited to those investigated in this work but also for other complex systems.

5.1 Interpretations and Comparisons of UF Membranes

The comparisons between both AB and ABC membrane allows for achieving the ideal membrane. The AB membrane is shown to have better functional properties than the ABC membrane as it is mechanically stronger and more hydrophilic at the surface. However, the ABC membrane is considered to be a more chemically stable compound.

While the AB membrane is more suited to water purification, improvements in membrane formulations should still be explored. The chemical stability of the ABC membrane provides a framework to improving functionality. Some of the functional deficiencies of the ABC membrane can be linked towards the chemical properties of the membrane. The formation of macrovoids may be an indication of incomplete solubility of polymer A during membrane production. Also, the surface of the ABC membrane is hydrophobic; however, future design can incorporate more of polymer A. Incorporation of different polymerisations yielding polymer A with end groups that are soluble can lead to minimal expulsion of the precursor out of the membrane. Not only will lower amounts of the precursor be used during production, the membrane surface becomes more hydrophilic allowing for higher water flux. This will allow for the production of more cost-efficient membranes and reduce waste produced.

There are certain aspects of the ABC membrane that is not completely understood such as expulsion of polymer A. At the molecular scale, the AB membrane consist of structures that induce miscible; however, structural

incompatibilities are still present. It is surprising that interpretations of the ABC membrane consider it to be the more miscible system. The lowered functionality of the ABC membrane requires other analytical techniques to strengthen interpretations made on miscibility at different length scales as well as establish links towards structure and functional properties.

5.2 Methods to Characterise Membranes

Solid-state NMR was used as it is able to understand the molecular dynamics and structures of the material; however, equipment purchase is costly and applying the technique requires an extensive amount of technical expertise. ^1H static Solid-State NMR measurements is relatively simple and can be applied with a benchtop NMR, making the technique more accessible and affordable. Additionally, the membrane can be studied in various conditions through solid-state NMR allowing for determinations on foulants and membrane degradation.

CE was shown to separate polymers by different end group populations and is considered an inexpensive analysis method. This makes CE an attractive tool for industries as it can be applied to species with a charge. Drawbacks to be considered is the need to dissolve the sample and the sample requires a charge for separations. However, CE can be applied to the characterisation of the feed allowing for comparative studies with the membrane and the filtered water

Incorporating different analytical techniques not only provided an analysis of the membrane but showed the capability of these techniques for their respective investigations and how further method development can result in new findings towards functionality. Future research opportunities can be found in relating surface composition to pore sizes through bubble point and water permeability tests.

5.2.1 Developing Relationships between Surface Composition and Pore-size

Pores found within the surface of the membrane, will inherently be affected by the composition of polymers found there. However, industrial means of defining pore-size is limited in developing relationships towards surface composition. Two commonly applied techniques to determine pore-size is through bubble point and water permeability tests.

Table 5-1 Bubble point and water permeability tests.

	Water permeability test (ml/min)	Bubble point test (KPa)
AB membrane	2.3	410
ABC membrane	8.7	370

Preliminary bubble point tests and water permeability tests were conducted for AB and ABC membrane (Table 5-1). Results from both tests can be converted to give a pore-size; however, water permeability tests give an average pore size and bubble point tests give a maximum pore size. While the deductions of pore-size provide a general value, it does not provide an accurate representation on all the pores found on the membrane. To develop relationships to surface composition, liquid-liquid porometry can be applied.

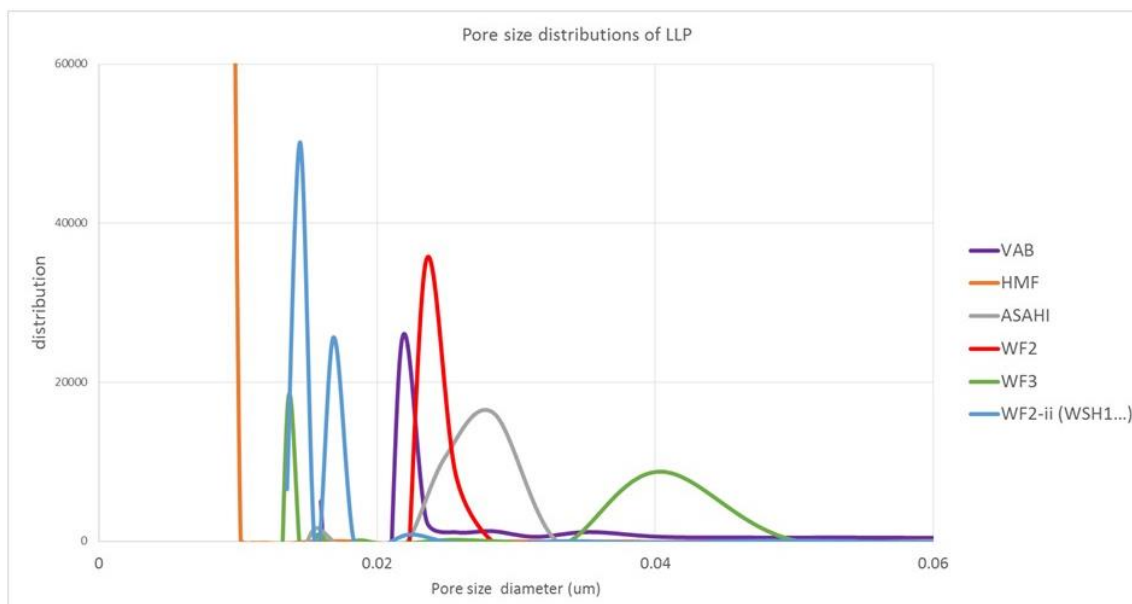


Figure 5-1 Pore-size distributions determined through liquid-liquid porometry of six industrially used membranes.

The pore size distributions of six industrially used membranes were recorded (Figure 5-1). The presence of different populations and difference in line widths allow for more precise determinations on pore-size. Additionally, determining pore-size distributions provides more precise interpretations on the water flux of the membrane; hence the hydrophilicity of the membrane surface.

Utilisation of analytical techniques that complement the findings of other techniques is required. Other analytical techniques that are able to determine different phases in the material can help in understanding the membrane properties.

5.2.2 Identifying Different Phases within the Membranes

While the ABC membrane was determined to be miscible, other influences may affect its lowered functional properties. One aspect that is considered is the different crystalline structures within the material. Different phases provide more complexity to the material as it may affect both physical and chemical properties. Crystalline structures can be identified through X-ray diffraction.

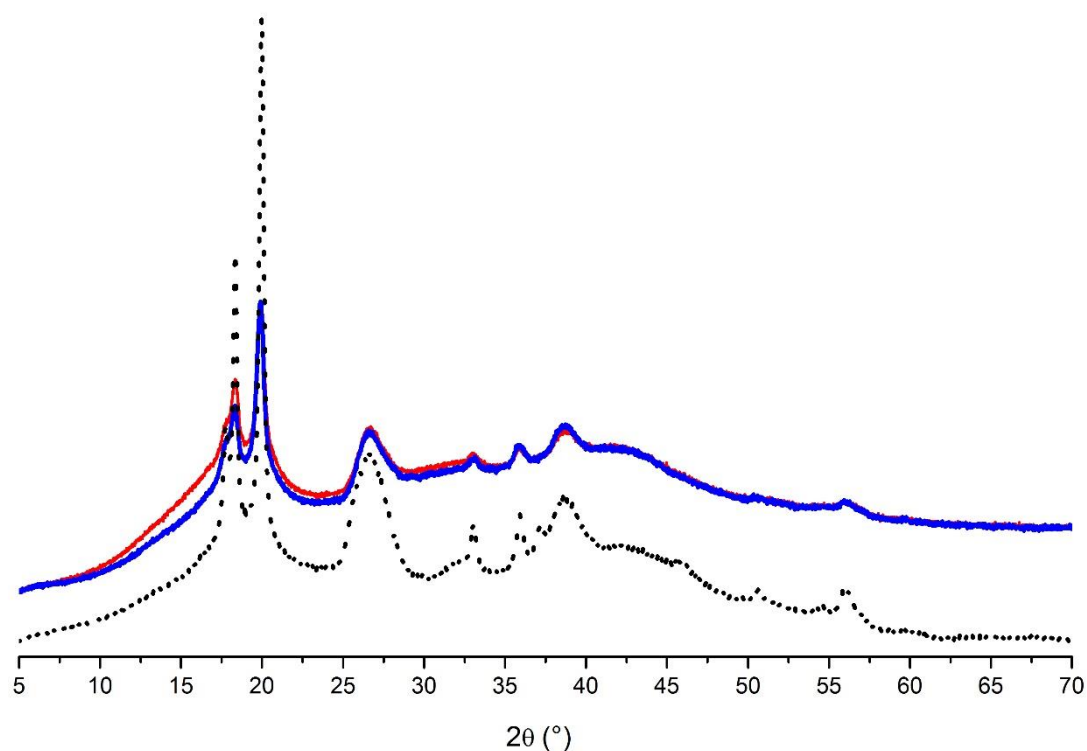


Figure 5-2 Overlays of the diffractograms of AB membrane (blue), ABC membrane (red) and polymer B (black dots).

Comparisons of the AB and ABC membranes show all peaks aligned with peaks from polymer B (Figure 5-2). Interpretations suggest that polymer B primarily contributes to the crystalline structure of the membrane. Identifying the different variations in membranes' composition will contribute to properties affected by crystallinity.

Overall, XRD can help develop connections on how crystallinity can influence the chemical properties of the membrane. Deductions made can help in understanding the overall composition of the membrane and more specifically, the heterogeneity of the material.

5.3 Potential Application of 2D WISE NMR Spectroscopy to Other Complex Systems

The analytical methods applied are not restricted to one system, as the information obtained can be useful in the determination of many materials. Application of 2D WISE NMR was conducted for the first time (according to

literature) on membranes. Characterisation of end groups through CE is novel and the information obtained from both techniques has the potential to investigate the solubility of polyethylene glycol and its nanostructuration in hot-melt adhesives¹¹⁷ and chitosan¹¹⁸. The work applied in this thesis will contribute towards the foundation of a standard technique to understand functionality in various material systems.

6 REFERENCES

1. Shannon, M. A.; Bohn, P. W.; Elimelech, M.; Georgiadis, J. G.; Marinas, B. J.; Mayes, A. M., Science and technology for water purification in the coming decades. *Nature* **2008**, 452, 301-310.
2. van Dijk, A.; Beck, H. E.; Crosbie, R. S.; de Jeu, R. A. M.; Liu, Y. Y.; Podger, G. M.; Timbal, B.; Viney, N. R., The Millennium Drought in southeast Australia (2001-2009): Natural and human causes and implications for water resources, ecosystems, economy, and society. *Water Resources Research* **2013**, 49, 1040-1057.
3. Australian Government Recent rainfall, drought and southern Australia's long-term rainfall decline. Bureau of meteorology Melbourne **2015**, 1.(1), <http://www.bom.gov.au/climate/updates/articles/a010-southern-rainfall-decline.shtml>.
4. Sillanpaa, M.; Ncibi, M. C.; Matilainen, A.; Vepsäläinen, M., Removal of natural organic matter in drinking water treatment by coagulation: A comprehensive review. *Chemosphere* **2018**, 190, 54-71.
5. Healy, M. G.; Rodgers, M.; Mulqueen, J., Treatment of dairy wastewater using constructed wetlands and intermittent sand filters. *Bioresource Technology* **2007**, 98, 2268-2281.
6. Richardson, S. D.; Plewa, M. J.; Wagner, E. D.; Schoeny, R.; DeMarini, D. M., Occurrence, genotoxicity, and carcinogenicity of regulated and emerging disinfection by-products in drinking water: A review and roadmap for research. *Mutation Research-Reviews in Mutation Research* **2007**, 636, 178-242.
7. Fane, A. G.; Wang, R.; Hu, M. X., Synthetic membranes for water purification: Status and future. *Angewandte Chemie -International Edition* **2015**, 54, 3368-3386.
8. Elimelech, M.; Phillip, W. A., The future of seawater desalination: Energy, technology, and the environment. *Science* **2011**, 333, 712-717.
9. Mohammad, A. W.; Teow, Y. H.; Ang, W. L.; Chung, Y. T.; Oatley-Radcliffe, D. L.; Hilal, N., Nanofiltration membranes review: Recent advances and future prospects. *Desalination* **2015**, 356, 226-254.
10. Ulbricht, M., Advanced functional polymer membranes. *Polymer* **2006**, 47, 2217-2262.
11. Kang, I. J.; Yoon, S. H.; Lee, C. H., Comparison of the filtration characteristics of organic and inorganic membranes in a membrane-coupled anaerobic bioreactor. *Water Research* **2002**, 36, 1803-1813.

- 12.Figoli, A.; Marino, T.; Simone, S.; Di Nicolo, E.; Li, X. M.; He, T.; Tornaghi, S.; Drioli, E., Towards non-toxic solvents for membrane preparation: a review. *Green Chemistry* **2014**, 16, 4034-4059.
- 13.Thevarajah, J. J.; Sutton, A. T.; Maniego, A. R.; Whitty, E. G.; Harrisson, S.; Cottet, H.; Castignolles, P.; Gaborieau, M., Quantifying the heterogeneity of chemical structures in complex charged polymers through the dispersity of their distributions of electrophoretic mobilities or of compositions. *Analytical Chemistry* **2016**, 88, 1674-1681.
- 14.Thevarajah, J. J.; Van Leeuwen, M. P.; Du Plessis, M.; Harrisson, S.; Gaborieau, M.; Castignolles, P., Analytical techniques for measurement of polymer dispersity. *Analytica Chimica Acta* **2018**, In preparation.
- 15.Muggli, M. W.; Ward, T. C.; Tchatchoua, C.; Ji, Q.; McGrath, J. E., End-group effect on physical aging and polymer properties for poly(ether sulfones). *Journal of Polymer Science Part B - Polymer Physics* **2003**, 41, 2850-2860.
- 16.Askadskii, A. A., The role of end groups in analysis of the properties of polymers. *Polymer Science U.S.S.R.* **1989**, 31, 2356-2363.
- 17.Johnson, L. M.; Li, Z.; LaBelle, A. J.; Bates, F. S.; Lodge, T. P.; Hillmyer, M. A., Impact of polymer excipient molar mass and end groups on hydrophobic drug solubility enhancement. *Macromolecules* **2017**, 50, 1102-1112.
- 18.Jikei, M.; Kakimoto, M., Hyperbranched polymers: a promising new class of materials. *Progress in Polymer Science* **2001**, 26, 1233-1285.
- 19.Paul, D. R.; Barlow, J. W., Polymer blends (or alloys). *Journal of Macromolecular Science - Reviews in Macromolecular Chemistry and Physics* **1980**, C18, 109-168.
- 20.Kim, Y.; Rana, D.; Matsuura, T.; Chung, W. J., Influence of surface modifying macromolecules on the surface properties of poly(ether sulfone) ultra-filtration membranes. *Journal of Membrane Science* **2009**, 338, 84-91.
- 21.Abdallah, H.; El-Gendi, A.; Khedr, M.; El-Zanati, E., Hydrophobic polyethersulfone porous membranes for membrane distillation. *Frontiers of Chemical Science and Engineering* **2015**, 9, 84-93.
- 22.Muller, M., Miscibility behavior and single chain properties in polymer blends: a bond fluctuation model study. *Macromolecular Theory and Simulations* **1999**, 8, 343-374.
- 23.Fleischer, C. A.; Morales, A. R.; Koberstein, J. T., Interfacial modification through end group complexation in polymer blends. *Macromolecules* **1994**, 27, 379-385.
- 24.He, Y.; Zhu, B.; Inoue, Y., Hydrogen bonds in polymer blends. *Progress in Polymer Science* **2004**, 29, 1021-1051.

- 25.Melnikova, G. B.; Zhavnerko, G. K.; Chizhik, S. A.; Bildyukevich, A. V., Structure and mechanical properties of ultrafiltration membranes modified with Langmuir-Blodgett films. *Petroleum Chemistry* **2016**, 56, 406-412.
- 26.Guillen, G. R.; Pan, Y. J.; Li, M. H.; Hoek, E. M. V., Preparation and characterization of membranes formed by nonsolvent induced phase separation: A review. *Industrial & Engineering Chemistry Research* **2011**, 50, 3798-3817.
- 27.Foret, F.; Krivankova, L.; Bocek, P., *Capillary Zone Electrophoresis*. VCH: Weinheim, Germany, 1993.
- 28.Chamieh, J.; Martin, M.; Cottet, H., Quantitative Analysis in Capillary Electrophoresis: Transformation of Raw Electropherograms into Continuous Distributions. *Analytical Chemistry* **2015**, 87, 1050-1057.
- 29.Thevarajah, J. J.; Gaborieau, M.; Castignolles, P., Separation and characterization of synthetic polyelectrolytes and polysaccharides with capillary electrophoresis. *Advances in Chemistry* **2014**, 2014, 11.
- 30.Cottet, H.; Gareil, P.; Theodoly, O.; Williams, C. E., A semi-empirical approach to the modeling of the electrophoretic mobility in free solution: Application to polystyrenesulfonates of various sulfonation rates. *Electrophoresis* **2000**, 21, 3529-3540.
- 31.Cottet, H.; Gareil, P., From small charged molecules to oligomers: A semiempirical approach to the modeling of actual mobility in free solution. *Electrophoresis* **2000**, 21, 1493-1504.
- 32.Gaborieau, M.; Causon, T. J.; Guillaneuf, Y.; Hilder, E. F.; Castignolles, P., Molecular weight and tacticity of oligoacrylates by capillary electrophoresis - mass spectrometry. *Australian Journal of Chemistry* **2010**, 63, 1219-1226.
- 33.Long, D.; Viovy, J. L.; Ajdari, A., Simultaneous action of electric fields and nonelectric forces on a polyelectrolyte: Motion and deformation. *Physical Review Letters* **1996**, 76, 3858-3861.
- 34.Lau, W. J.; Ismail, A. F.; Goh, P. S.; Hilal, N.; Ooi, B. S., Characterization methods of thin film composite nanofiltration membranes. *Separation and Purification Reviews* **2015**, 44, 135-156.
- 35.Kwak, S. Y.; Ihm, D. W., Use of atomic force microscopy and solid-state NMR spectroscopy to characterize structure-property-performance correlation in high-flux reverse osmosis (RO) membranes. *Journal of Membrane Science* **1999**, 158, 143-153.
- 36.Claridge, T. D. W., High-resolution NMR techniques in organic chemistry. In 2nd ed.; Elsevier Science: Amsterdam, 2009; Chap. 4 pp 99-128.

37. Claridge, T. D. W., Chapter 2: Introducing high-resolution NMR. In *High-Resolution NMR Techniques in Organic Chemistry*, 2nd ed.; Timothy, D. W. C., Ed. Elsevier: 2009; Chap. pp 11-34.
38. Potrzebowski, M. J., What high-resolution solid-state NMR spectroscopy can offer to organic chemists. *European Journal of Organic Chemistry* **2003**, 1367-1376.
39. Brown, S. P.; Spiess, H. W., Advanced solid-state NMR methods for the elucidation of structure and dynamics of molecular, macromolecular, and supramolecular systems. *Chemical Reviews* **2001**, 101, 4125-4155.
40. Gaborieau, M. Solid-state NMR investigation of spatial and dynamic heterogeneity in acrylic pressure sensitive adhesives (PSAs) compared to model poly(n-alkyl acrylates) and poly(n-alkyl methacrylates). PhD thesis, University Louis Pasteur, Strasbourg, France, 2005 http://scd-theses.u-strasbg.fr/956/01/PhD_thesis_Marianne_Gaborieau.pdf, <http://scd-theses.u-strasbg.fr/956/>.
41. Law, R. V.; Sherrington, D. C.; Snape, C. E., Quantitative solid state ^{13}C NMR studies of highly cross-linked poly(divinylbenzene) resins. *Macromolecules* **1997**, 30, 2868-2875.
42. Maroto-Valer, M. M.; Taulbee, D. N.; Andresen, J. M.; Hower, J. C.; Snape, C. E., Quantitative ^{13}C NMR study of structural variations within the vitrinite and inertinite maceral groups for a semifusinite-rich bituminous coal. *Fuel* **1998**, 77, 805-813.
43. Schmidt-Rohr, K.; Clauss, J.; Spiess, H. W., Correlation of structure, mobility and morphological information in heterogeneous polymer materials by 2-Dimensional Wideline-Separation NMR spectroscopy. *Macromolecules* **1992**, 25, 3273-3277.
44. Schmidt-Rohr, K.; Spiess, H. W., *Multidimensional solid-state NMR and polymers*. Academic Press: London, 1994; Vol. 8, p 186-187.
45. Abdullah, S. Z.; Berube, P. R.; Horne, D. J., SEM imaging of membranes: Importance of sample preparation and imaging parameters. *Journal of Membrane Science* **2014**, 463, 113-125.
46. Bujak, T.; Wasilewski, T.; Nizioł-Lukaszewska, Z., Role of macromolecules in the safety of use of body wash cosmetics. *Colloids and Surfaces B - Biointerfaces* **2015**, 135, 497-503.
47. Lee, J., Intrinsic adhesion properties of poly(vinyl pyrrolidone) to pharmaceutical materials: Humidity effect. *Macromolecular Bioscience* **2005**, 5, 1085-1093.
48. Gebru, K. A.; Das, C., Effects of solubility parameter differences among PEG, PVP and CA on the preparation of ultrafiltration membranes: Impacts

of solvents and additives on morphology, permeability and fouling performances. *Chinese Journal of Chemical Engineering* **2017**, 25, 911-923.

49.Su, W.-F., *Principles of polymer design and synthesis*. Springer: Berlin, Heidelberg, 2013; p 306.

50.Orlicki, J. A.; Thompson, J. L.; Markoski, L. J.; Sill, K. N.; Moore, J. S., Synthesis and characterization of end-group modified hyperbranched polyetherimides. *Journal of Polymer Science Part A - Polymer Chemistry* **2002**, 40, 936-946.

51.Zhang, H.; Rankin, A.; Ward, I. M., Determination of the end-group concentration and molecular weight of poly(ethylene naphthalene-2,6-dicarboxylate) using infra-red spectroscopy. *Polymer* **1996**, 37, 1079-1085.

52.Jiang, X. G.; Zhao, B., End group effect on the thermo-sensitive properties of well-defined water-soluble polystyrenics with short pendant oligo(ethylene glycol) groups synthesized by nitroxide-mediated radical polymerization. *Journal of Polymer Science Part A - Polymer Chemistry* **2007**, 45, 3707-3721.

53.Berek, D., Size exclusion chromatography - A blessing and a curse of science and technology of synthetic polymers. *Journal of Separation Science* **2010**, 33, 315-335.

54.Striegel, A. M., Size-exclusion chromatography: smaller, faster, multi-detection, and multi-dimensions. *Analytical and Bioanalytical Chemistry* **2008**, 390, 303-305.

55.Rollet, M.; Pelletier, B.; Altounian, A.; Berek, D.; Maria, S.; Beaudoin, E.; Gigmes, D., Separation of parent homopolymers from polystyrene-*b*-poly(ethylene oxide)-*b*-polystyrene triblock copolymers by means of liquid chromatography: 1. Comparison of different methods. *Analytical Chemistry* **2014**, 86, 2694-2702.

56.Al Samman, M.; Radke, W.; Khalyavina, A.; Lederer, A., Retention behavior of linear, branched, and hyperbranched polyesters in interaction liquid chromatography. *Macromolecules* **2010**, 43, 3215-3220.

57.Favier, A.; Petit, C.; Beaudoin, E.; Bertin, D., Liquid chromatography at the critical adsorption point (LC-CAP) of high molecular weight polystyrene: pushing back the limits of reduced sample recovery. *E-Polymers* **2009**, 1-15.

58.Oliver, J. D.; Sutton, A. T.; Karu, N.; Phillips, M.; Markham, J.; Peiris, P.; Hilder, E. F.; Castignolles, P., Simple and robust monitoring of ethanol fermentations by capillary electrophoresis. *Biotechnology and Applied Biochemistry* **2015**, 62, 329-342.

59.Taylor, D. L.; Ferris, C. J.; Maniego, A. R.; Castignolles, P.; in het Panhuis, M.; Gaborieau, M., Characterization of Gellan Gum by Capillary Electrophoresis. *Australian Journal of Chemistry* **2012**, 65, 1156-1164.

- 60.Thevarajah, J. J.; Van Leeuwen, M. P.; Cottet, H.; Castignolles, P.; Gaborieau, M., Determination of the distributions of degrees of acetylation of chitosan. *International Journal of Biological Macromolecules* **2017**, 95, 40-48.
- 61.Maniego, A. R.; Ang, D.; Guillaneuf, Y.; Lefay, C.; Gigmes, D.; Aldrich-Wright, J. R.; Gaborieau, M.; Castignolles, P., Separation of poly(acrylic acid) salts according to topology using capillary electrophoresis in the critical conditions. *Analytical and Bioanalytical Chemistry* **2013**, 405, 9009-9020.
- 62.Huo, P. F.; Liu, Y.; Na, R. Q.; Zhang, X. R.; Zhang, S. L.; Wang, G. B., Quaternary ammonium functionalized poly(arylene ether sulfone)/poly(vinylpyrrolidone) composite membranes for electrical double layer capacitors with activated carbon electrodes. *Journal of Membrane Science* **2016**, 505, 148-156.
- 63.Haaf, F.; Sanner, A.; Straub, F., Polymers of n-vinylpyrrolidone - Synthesis, characterization and uses. *Polymer Journal* **1985**, 17, 143-152.
- 64.Hoffstetterkuhn, S.; Paulus, A.; Gassmann, E.; Widmer, H. M., Influence of borate complexation on the electrophoretic behavior of carbohydrates in capillary electrophoresis. *Analytical Chemistry* **1991**, 63, 1541-1547.
- 65.Arentoft, A. M.; Michaelsen, S.; Sorensen, H., DETERMINATION OF OLIGOSACCHARIDES BY CAPILLARY ZONE ELECTROPHORESIS. *Journal of Chromatography A* **1993**, 652, 517-524.
- 66.Chamieh, J.; Biron, J. P.; Cipelletti, L.; Cottet, H., Monitoring biopolymer degradation by Taylor Dispersion Analysis. *Biomacromolecules* **2015**, 16, 3945-3951.
- 67.Schmitt-Kopplin, P.; Garmash, A. V.; Kudryavtsev, A. V.; Menzinger, F.; Perminova, I. V.; Hertkorn, N.; Freitag, D.; Petrosyan, V. S.; Kettrup, A., Quantitative and qualitative precision improvements by effective mobility-scale data transformation in capillary electrophoresis analysis. *Electrophoresis* **2001**, 22, 77-87.
- 68.Chamieh, J.; Cottet, H., Comparison of single and double detection points Taylor Dispersion Analysis for monodisperse and polydisperse samples. *Journal of Chromatography A* **2012**, 1241, 123-127.
- 69.Castignolles, P.; Gaborieau, M.; Hilder, E. F.; Sprong, E.; Ferguson, C. J.; Gilbert, R. G., High-resolution separation of oligo(acrylic acid) by capillary zone electrophoresis. *Macromolecular Rapid Communications* **2006**, 27, 42-46.
- 70.Dona, A.; Yuen, C.-W. W.; Peate, J.; Gilbert, R. G.; Castignolles, P.; Gaborieau, M., A new NMR method for directly monitoring and quantifying the dissolution kinetics of starch in DMSO. *Carbohydrate Research* **2007**, 342, 2604-2610.

- 71.Thevarajah, J. J.; Bulanadi, J. C.; Wagner, M.; Gaborieau, M.; Castignolles, P., Towards a less biased dissolution of chitosan. *Analytica Chimica Acta* **2016**, 935, 258-268.
- 72.Schmitz, S.; Dona, A. C.; Castignolles, P.; Gilbert, R. G.; Gaborieau, M., Assessment of the extent of starch dissolution in dimethyl sulfoxide by ^1H NMR Spectroscopy. *Macromolecular Bioscience* **2009**, 9, 506-514.
- 73.Maniego, A. R.; Sutton, A. T.; Gaborieau, M.; Castignolles, P., Assessment of the Branching Quantification in Poly(acrylic acid): Is It as Easy as It Seems? *Macromolecules* **2017**, 50, 9032-9041.
- 74.Guo, X. F.; Guo, X. M.; Wang, H.; Zhang, H. S., One step physically adsorbed coating of silica capillary with excellent stability for the separation of basic proteins by capillary zone electrophoresis. *Talanta* **2015**, 144, 110-114.
- 75.Yu, B.; Shu, X.; Cong, H. L.; Chen, X.; Liu, H. W.; Yuan, H.; Chi, M., Self-assembled covalent capillary coating of diazoresin/carboxyl fullerene for analysis of proteins by capillary electrophoresis and a comparison with diazoresin/graphene oxide coating. *Journal of Chromatography A* **2016**, 1437, 226-233.
- 76.Cherney, L. T.; Krylov, S. N., Slow-equilibration approximation in studying kinetics of protein adsorption on capillary walls. *Analyst* **2015**, 140, 2797-2803.
- 77.de Jong, S.; Krylov, S. N., Pressure-Based Approach for the Analysis of Protein Adsorption in Capillary Electrophoresis. *Analytical Chemistry* **2012**, 84, 453-458.
- 78.Lonsdale, H. K., The growth of membrane technology. *Journal of Membrane Science* **1982**, 10, 81-181.
- 79.Hamza, A.; Pham, V. A.; Matsuura, T.; Santerre, J. P., Development of membranes with low surface energy to reduce the fouling in ultrafiltration applications. *Journal of Membrane Science* **1997**, 131, 217-227.
- 80.Zhao, C. S.; Xue, J. M.; Ran, F.; Sun, S. D., Modification of polyethersulfone membranes - A review of methods. *Progress in Materials Science* **2013**, 58, 76-150.
- 81.Sun, S. D.; Yue, Y. L.; Huang, X. H.; Meng, D. Y., Protein adsorption on blood-contact membranes. *Journal of Membrane Science* **2003**, 222, 3-18.
- 82.Chung, G. C.; Kornfield, J. A.; Smith, S. D., Component dynamics in miscible polymer blends - A 2-dimensional deuterium NMR investigation *Macromolecules* **1994**, 27, 964-973.

- 83.Taguet, A.; Cassagnau, P.; Lopez-Cuesta, J. M., Structuration, selective dispersion and compatibilizing effect of (nano)fillers in polymer blends. *Progress in Polymer Science* **2014**, 39, 1526-1563.
- 84.Jollands, M.; Gupta, R. K., Effect of mixing conditions on mechanical properties of polylactide/montmorillonite clay nanocomposites. *Journal of Applied Polymer Science* **2010**, 118, 1489-1493.
- 85.Mirau, P. A., Solid-state NMR characterization of polymer interfaces. In *Modern Magnetic Resonance*, Webb, G. A., Ed. Springer Netherlands: Dordrecht, 2006; Chap. pp 575-581.
- 86.White, J. L.; Wachowicz, M., Polymer blend miscibility. In *Annual Reports on NMR Spectroscopy*, Webb, G. A., Ed. Elsevier: London, 2008; Chap. pp 189-206.
- 87.Zhang, R. C.; Mroue, K. H.; Ramamoorthy, A., Proton-based ultrafast magic angle spinning solid-state NMR Spectroscopy. *Accounts of Chemical Research* **2017**, 50, 1105-1113.
- 88.Morcombe, C. R.; Zilm, K. W., Chemical shift referencing in MAS solid state NMR. *Journal of Magnetic Resonance* **2003**, 162, 479-486.
- 89.Wilhelm, M.; Neidhofer, M.; Spiegel, S.; Spiess, H. W., A collection of solid-state C-13 CP/MAS NMR spectra of common polymers. *Macromolecular Chemistry and Physics* **1999**, 200, 2205-2207.
- 90.Laupretre, F., Applications of high-resolution solid-state ¹³C NMR to polymers. *Progress in Polymer Science* **1990**, 15, 425-474.
- 91.AE Tonelli; MA Gomesz; H Tanaka; Cozine, M., *Solid state ¹³C NMR studies of the structures, conformations, and dynamics of semi-crystalline polymers*. Plenum Press: New York, 1988; Vol. 4.
- 92.Sharma, M.; Madras, G.; Bose, S., Shear induced crystallization in different polymorphic forms of PVDF induced by surface functionalized MWNTs in PVDF/PMMA blends. *Physical Chemistry Chemical Physics* **2014**, 16, 16492-501.
- 93.Spectral database for organic compounds SDBS. http://www.aist.go.jp/RioDB/SDBS/cgi-bin/cre_index.cgi
- 94.Castignolles, P.; Graf, R.; Parkinson, M.; Wilhelm, M.; Gaborieau, M., Detection and quantification of branching in polyacrylates by size-exclusion chromatography (SEC) and melt-state ¹³C NMR spectroscopy. *Polymer* **2009**, 50, 2373-2383.
- 95.Klimke, K.; Parkinson, M.; Piel, C.; Kaminsky, W.; Spiess, H. W.; Wilhelm, M., Optimisation and application of polyolefin branch quantification by melt-state ¹³C NMR spectroscopy. *Macromolecular Chemistry and Physics* **2006**, 207, 382-395.

- 96.Ladizhansky, V.; Vega, S., Polarization transfer dynamics in Lee-Goldburg cross polarization nuclear magnetic resonance experiments on rotating solids. *Journal of Chemical Physics* **2000**, 112, 7158-7168.
- 97.Wolak, J.; Jia, X.; Gracz, H.; Stejskal, E. O.; White, J. L.; Wachowicz, M.; Jurga, S., Polyolefin miscibility: Solid-state NMR investigation of phase behavior in saturated hydrocarbon blends. *Macromolecules* **2003**, 36, 4844-4850.
- 98.Malaeb, L.; Ayoub, G. M., Reverse osmosis technology for water treatment: State of the art review. *Desalination* **2011**, 267, 1-8.
- 99.Charcosset, C., Membrane processes in biotechnology: An overview. *Biotechnology Advances* **2006**, 24, 482-492.
- 100.Ravanchi, M. T.; Kaghazchi, T.; Kargari, A., Application of membrane separation processes in petrochemical industry: a review. *Desalination* **2009**, 235, 199-244.
- 101.Rana, D.; Matsuura, T.; Narbaitz, R. M.; Feng, C., Development and characterization of novel hydrophilic surface modifying macromolecule for polymeric membranes. *Journal of Membrane Science* **2005**, 249, 103-112.
- 102.Rahimpour, A.; Madaeni, S. S., Polyethersulfone (PES)/cellulose acetate phthalate (CAP) blend ultrafiltration membranes: Preparation, morphology, performance and antifouling properties. *Journal of Membrane Science* **2007**, 305, 299-312.
- 103.Vatanpour, V.; Madaeni, S. S.; Moradian, R.; Zinadini, S.; Astinchap, B., Fabrication and characterization of novel antifouling nanofiltration membrane prepared from oxidized multiwalled carbon nanotube/polyethersulfone nanocomposite. *Journal of Membrane Science* **2011**, 375, 284-294.
- 104.Cohen-Tanugi, D.; Grossman, J. C., Nanoporous graphene as a reverse osmosis membrane: Recent insights from theory and simulation. *Desalination* **2015**, 366, 59-70.
- 105.Ding, M. X.; Ghoufi, A.; Szymczyk, A., Molecular simulations of polyamide reverse osmosis membranes. *Desalination* **2014**, 343, 48-53.
- 106.Wang, K.; Abdalla, A. A.; Khaleel, M. A.; Hilal, N.; Khraisheh, M. K., Mechanical properties of water desalination and wastewater treatment membranes. *Desalination* **2017**, 401, 190-205.
- 107.Cui, Z. L.; Cheng, Y. M.; Xu, K.; Yue, J.; Zhou, Y.; Li, X. G.; Wang, Q.; Sun, S. P.; Wang, Y.; Wang, X. Z.; Wang, Z. H., Wide liquid-liquid phase separation region enhancing tensile strength of poly(vinylidene fluoride) membranes via TIPS method with a new diluent. *Polymer* **2018**, 141, 46-53.

- 108.Washburn, E. W., The dynamics of capillary flow. *Physical Review* **1921**, 17, 273-283.
- 109.Peng, N.; Chung, T. S.; Wang, K. Y., Macrovoid evolution and critical factors to form macrovoid-free hollow fiber membranes. *Journal of Membrane Science* **2008**, 318, 363-372.
- 110.Husain, S.; Koros, W. J., Macrovoids in hybrid organic/inorganic hollow fiber membranes. *Industrial & Engineering Chemistry Research* **2009**, 48, 2372-2379.
- 111.Wang, D. M.; Lin, F. C.; Wu, T. T.; Lai, J. Y., Formation mechanism of the macrovoids induced by surfactant additives. *Journal of Membrane Science* **1998**, 142, 191-204.
- 112.Prencipe, I.; Dellasega, D.; Zani, A.; Rizzo, D.; Passoni, M., Energy dispersive x-ray spectroscopy for nanostructured thin film density evaluation. *Science and Technology of Advanced Materials* **2015**, 16, 9.
- 113.Kostyukevich, Y.; Kononikhin, A.; Popov, I.; Nikolaev, E., Simple atmospheric hydrogen/deuterium exchange method for enumeration of labile hydrogens by electrospray ionization mass spectrometry. *Analytical Chemistry* **2013**, 85, 5330-5334.
- 114.Wan, L. S.; Xu, Z. K.; Wang, Z. G., Leaching of PVP from polyacrylonitrile/PVP blending membranes: A comparative study of asymmetric and dense membranes. *Journal of Polymer Science Part B - Polymer Physics* **2006**, 44, 1490-1498.
- 115.Rosa, M. J.; dePinho, M. N., Membrane surface characterisation by contact angle measurements using the immersed method. *Journal of Membrane Science* **1997**, 131, 167-180.
- 116.Kamat, S. V., Experimental techniques for the measurement of mechanical properties of materials used in microelectromechanical systems. *Defence Science Journal* **2009**, 59, 605-615.
- 117.Bhullar, K.; Thevarajah, J. J.; Rebmann, A.; Cheevers, S.; Wuhner, R.; Castignolles, P.; Gaborieau, M. Characterisation of industrial adhesives with (solid-state) NMR spectroscopy, *255th American Chemical Society (ACS) National Meeting "Nexus of Food, Energy, and Water"*, New Orleans, USA, 2018.
- 118.Mason, M. Generation of human pluripotent stem cell-derived micro-lenses to investigate lens development and lens toxicity. Western Sydney University, Campbelltown, Australia, 2018.

7 APPENDIX

In conditions where the EOF marker comigrates with the analyte, another mobility marker is employed where the formula is expressed in Equation 7.1.

$$\mu_{ep} = \left| \frac{L_d \cdot L_t}{V} \cdot \left(\frac{1}{t_m} - \frac{1}{t_{mm}} \right) \right| - \mu_{ma} \quad 7.1$$

t_{mm} is defined as the migration time of the mobility marker, μ_{ma} is the electrophoretic mobility of the marker. For all other terms, refer to Section 1.7.1.1.

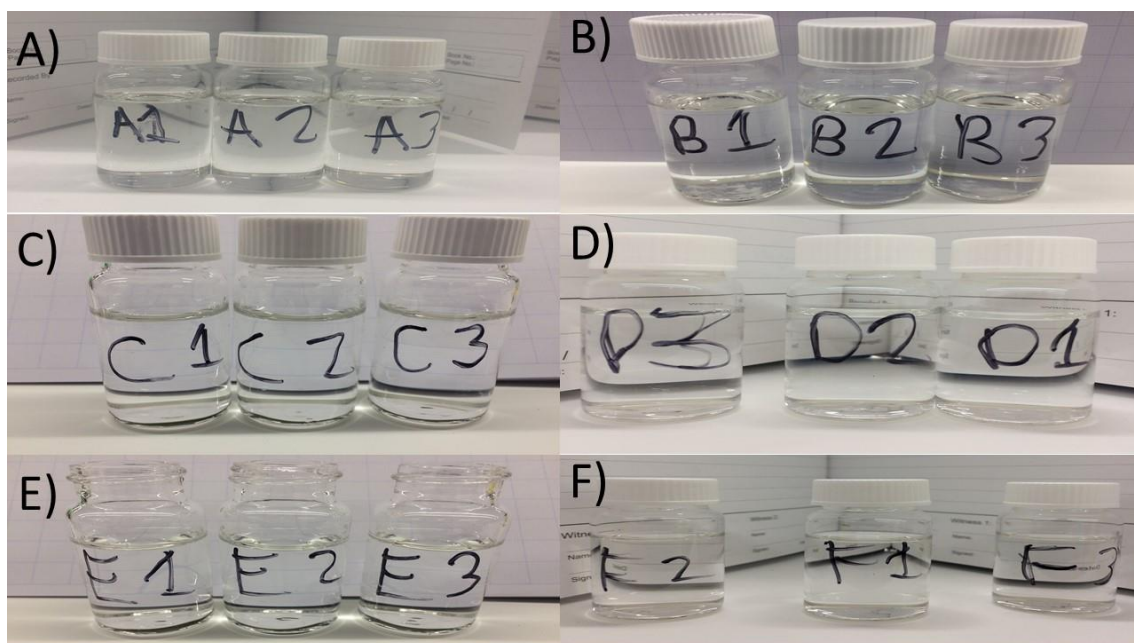


Figure A 1 PVP 1, PVP 2 and PVP 3 dissolved in A) NMP B) THF C) MilliQ water D) Water at pH 4 E) Water at pH 10 F) Ethanol, at 7.5 g·L⁻¹. Images taken at $t_{initial}$.

PVP samples were dissolved in a variety of solvents for empirical determinations on solubility (Figure A 1). Transparent solutions are observed in all solvents except for THF at $t_{initial}$.

Table A 1 Electrophoretic mobilities values of methyl green in NB200 at 25 C (n = 10).
Average mobility and RSD of methyl green was calculated.

Length to window (m)	Total length (m)	Voltage (V)	EOF (DMSO, min)	Migration time (min)	Electrophoretic mobility ($10^{-8} \times m^2 \cdot V^{-1} \cdot s^{-1}$)
1.412	1.497	30000	27.93	21.47	1.26507
1.412	1.497	30000	28.01	21.55	1.25677
1.412	1.497	30000	28.07	21.61	1.25060
1.412	1.497	30000	28.01	21.55	1.25677
1.412	1.497	30000	27.96	21.55	1.24927
1.415	1.500	30000	26.71	20.75	1.26803
1.415	1.500	30000	26.90	20.89	1.26113
1.415	1.500	30000	26.98	20.99	1.24723
1.415	1.500	30000	27.13	21.08	1.24741
1.415	1.500	30000	27.17	21.12	1.24322
Average electrophoretic mobility					1.2550
RSD value					0.63 %

The average electrophoretic mobility was calculated for the CE of methyl green with a RSD of 0.63% (n=10) (Table A 1).

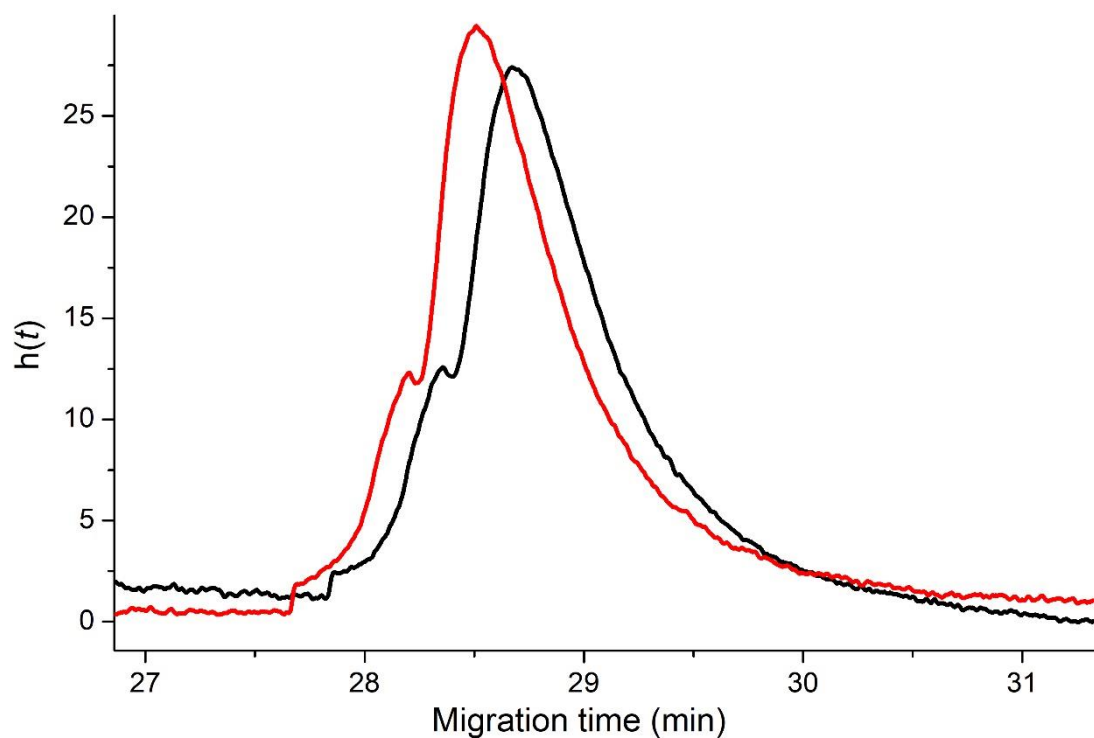


Figure A 2 CE of PVP 1 dissolved in NB200 with MG(black) and without MG (red).

The electropherogram of PVP 1 with and without MG are shown in migration time (Figure A 2). The PVP peak shows no distinct differences in terms of peak shape in both runs indicating little to no interactions with methyl green. The peaks consist of a shift in migration time; however, it can be deduced that instrumental error may have caused for the shift.

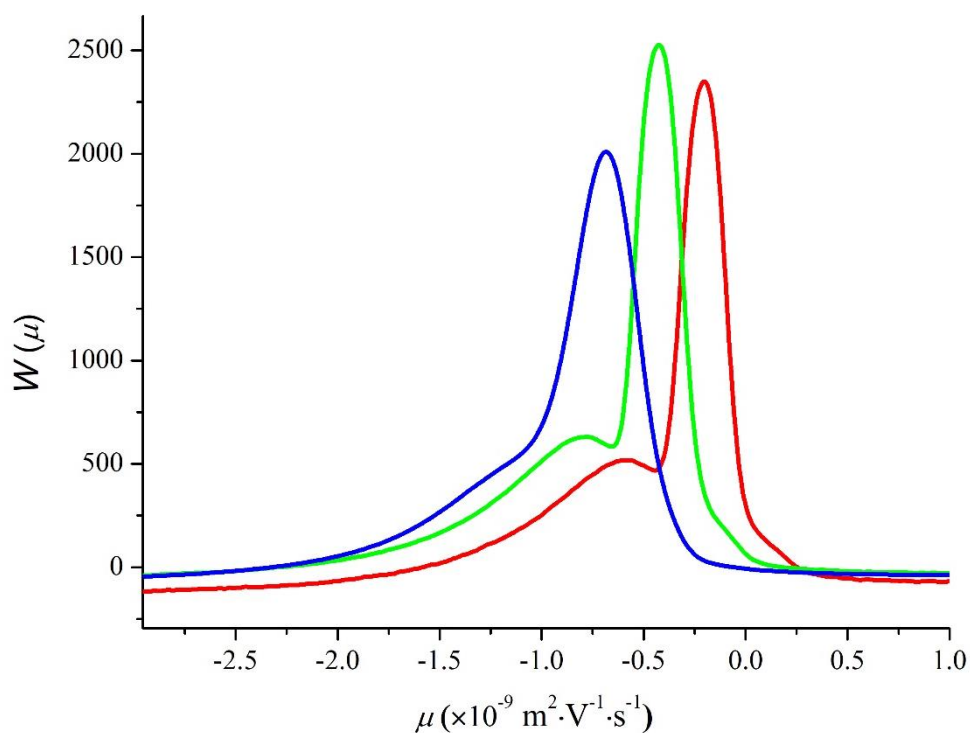


Figure A 3 Normalised peaks of PVP 2 dissolved in NB200 at 1 g·L⁻¹ (blue), 0.5 g·L⁻¹ (green), 0.25 g·L⁻¹(red). MG 0.05 g·L⁻¹ was used as a mobility marker.

CE of PVP 2 at varying concentrations (Figure A 3) exhibits all previously determined populations (Figure 2-3). PVP at 1 gL⁻¹ is observed to be less resolved upon comparison with other concentrations indicating sample overloading.

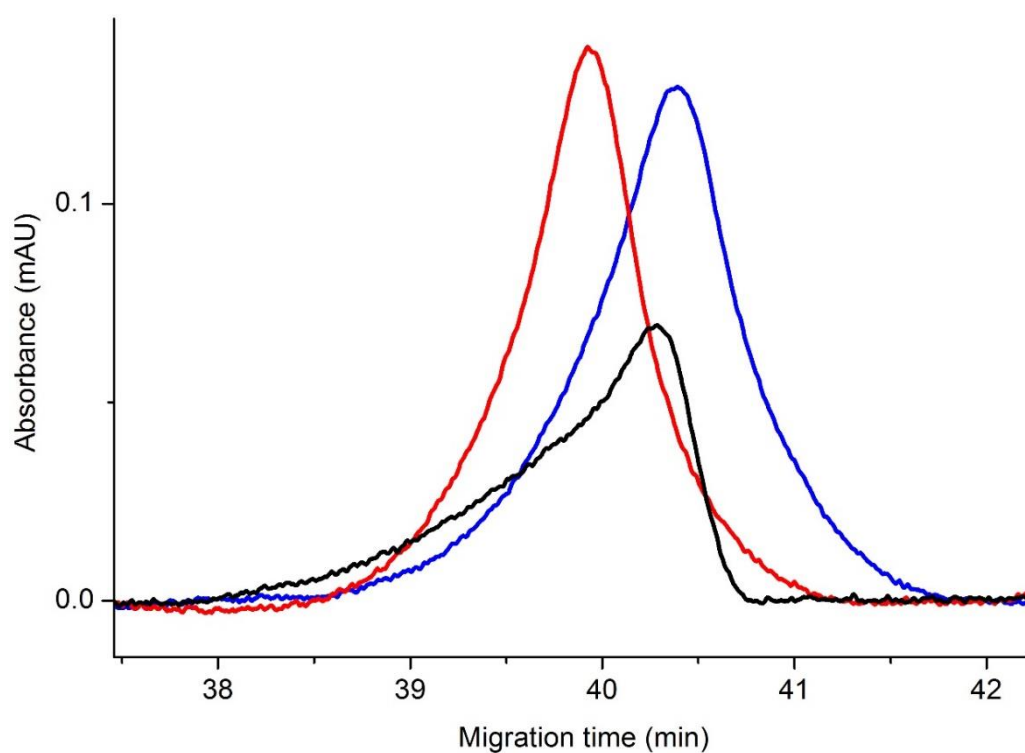


Figure A 4 PM of PVP 1 (Blue), PVP 2 (Red), PVP 3 (black) at $1 \text{ g}\cdot\text{L}^{-1}$ with the capillary at 25°C .

Tailing is observed in both PVP 1 and PVP 2 peaks whereas extensive tailing is present in PVP 3 (Figure A 4).

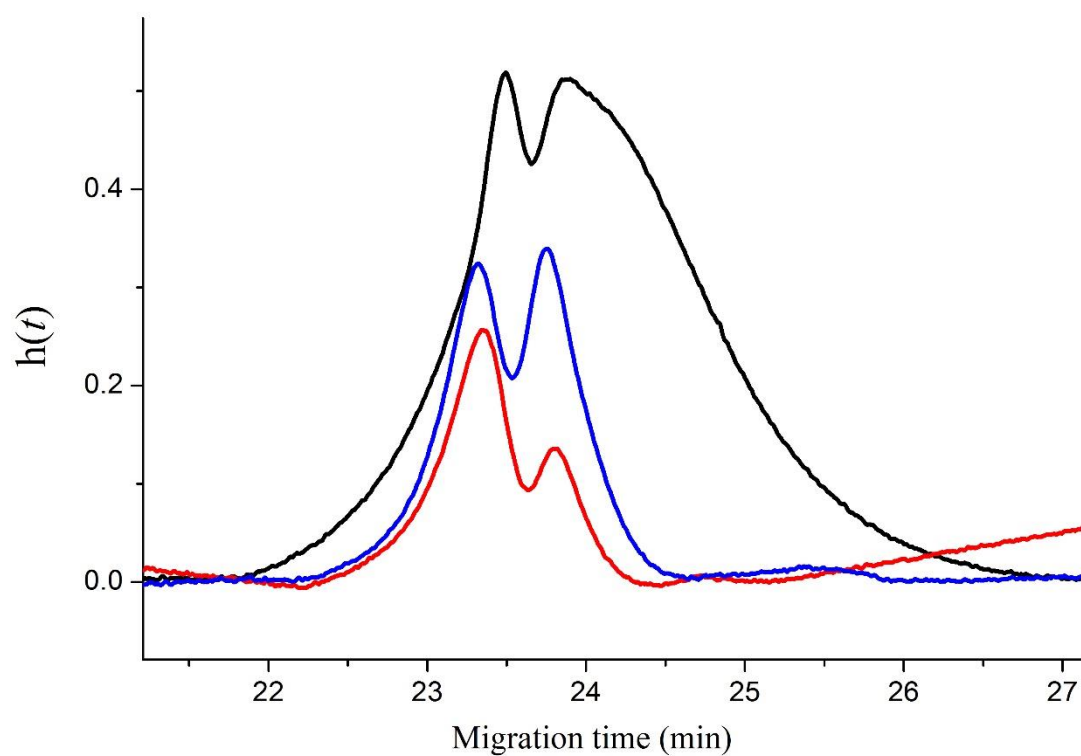


Figure A 5 PM of PVP 1 (blue) PVP 2 (red) and PVP 3 (black) at $1 \text{ g}\cdot\text{L}^{-1}$ with the capillary at 55°C .

Bimodal distributions and tailing are observed in all PVP samples (Figure A 5).

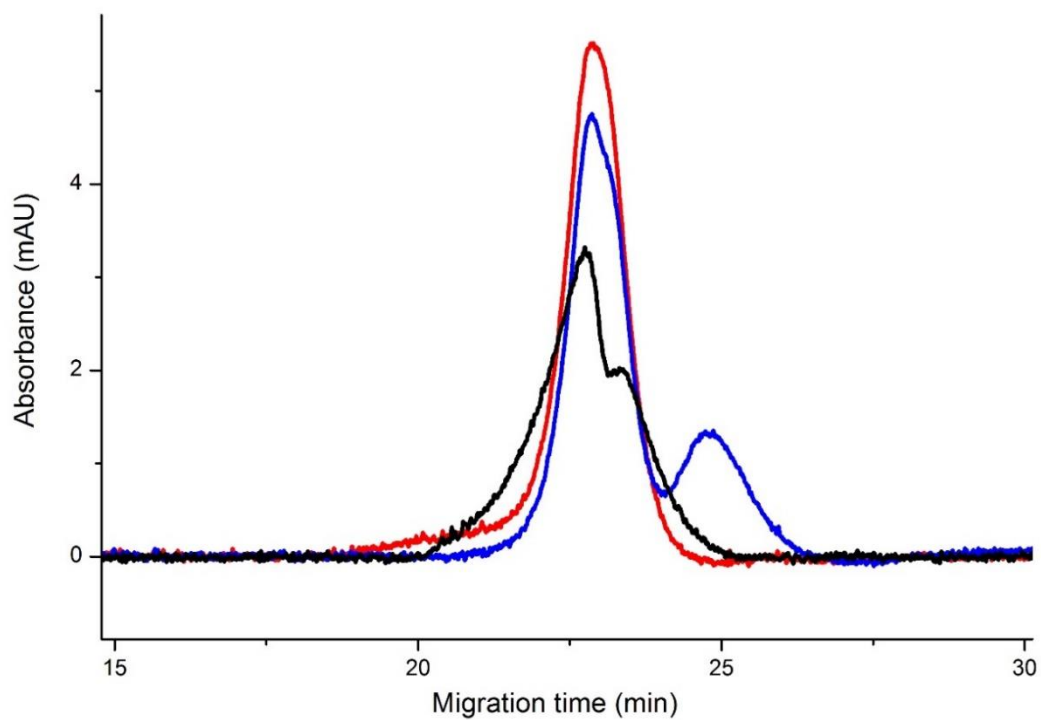


Figure A 6 PM of PVP 1 (blue) PVP 2 (red) PVP 3 (black) at 1 g/L with the capillary at 15 °C.

PVP 1 consist of a bimodal distribution, slight tailing is present in PVP 2 and PVP 3 consist of a shoulder peak (Figure A 6).

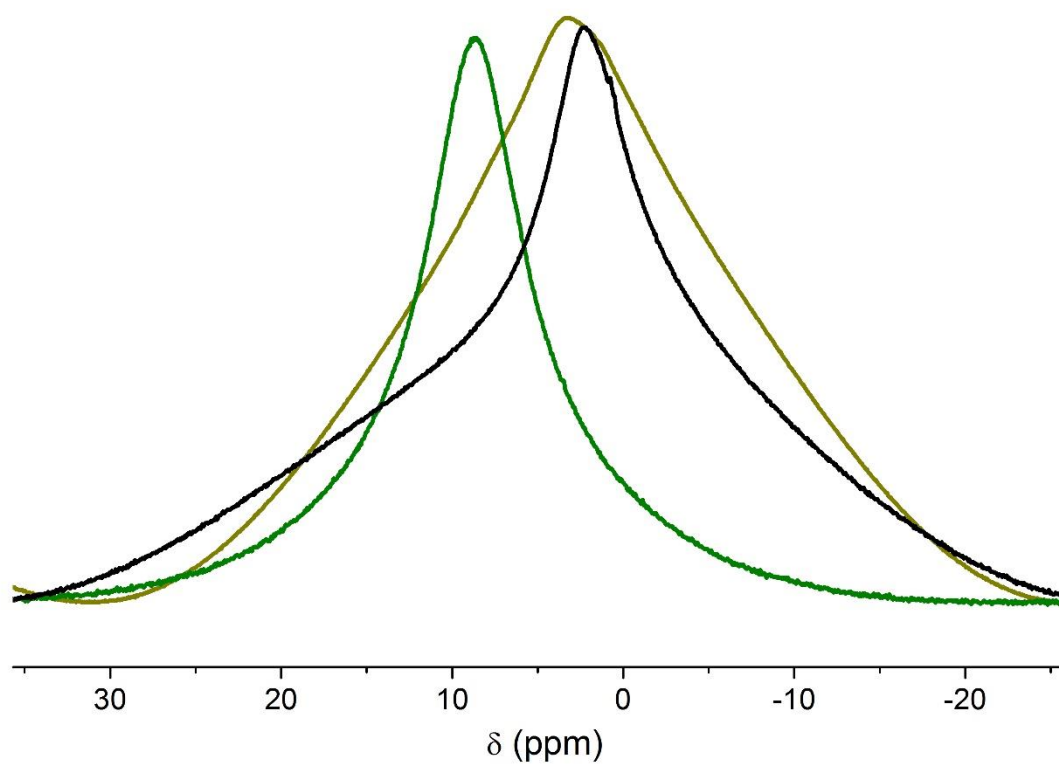


Figure A 7 ^1H SPE of polymer A (green), polymer B (black) and polymer C (gold).

Polymer A and B are observed to have a broad signal superimposed with a narrow signal and Polymer C exhibits a broad signal (Figure A 7).

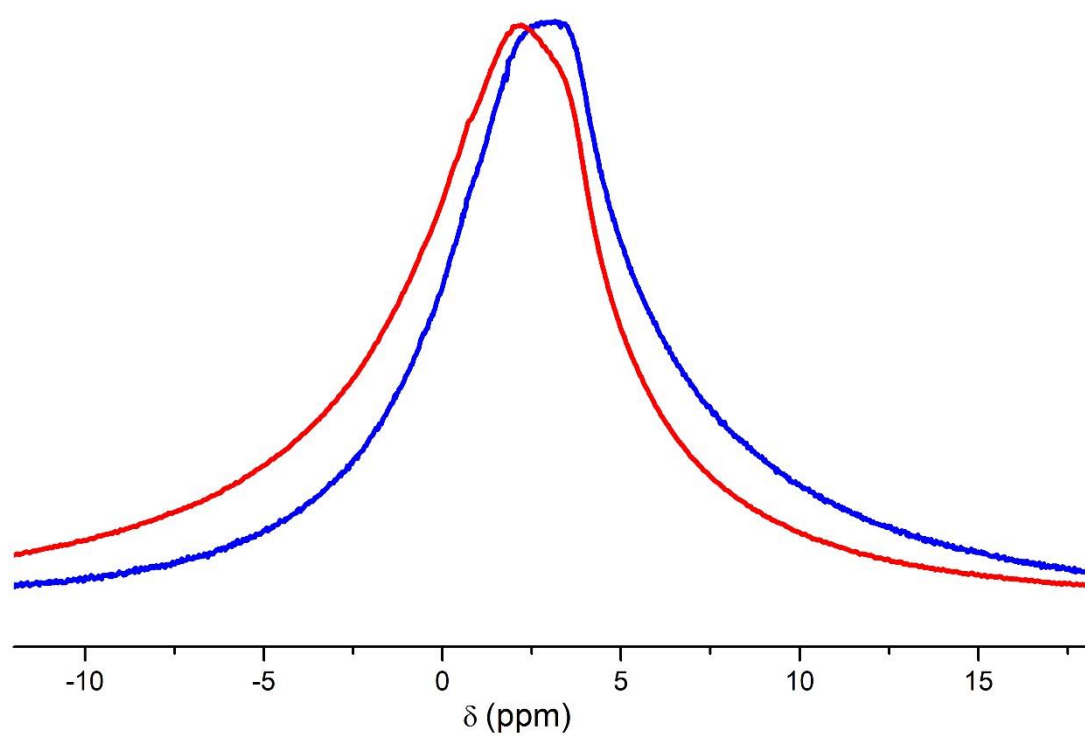


Figure A 8 ^1H SPE of membrane AB (blue) and membrane ABC (red).

A broad signal with a narrow signal superimposed is shown in both membrane AB and membrane ABC (Figure A 8).

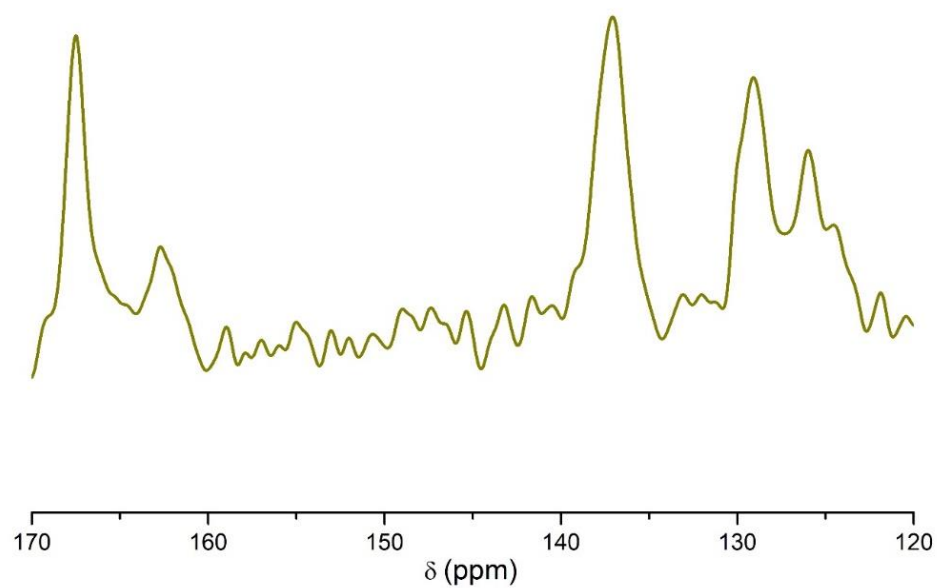


Figure A 9 ^{13}C CP spectrum of polymer C zoomed in between 170 and 120 ppm to show signals attributed to the monomer.

^{13}C CP spectrum of polymer C showing signals attributed to the monomer indicating an impurity within the sample (Figure A 9). Noticeable signals are found at 167 ppm, 137 ppm and 129 ppm.

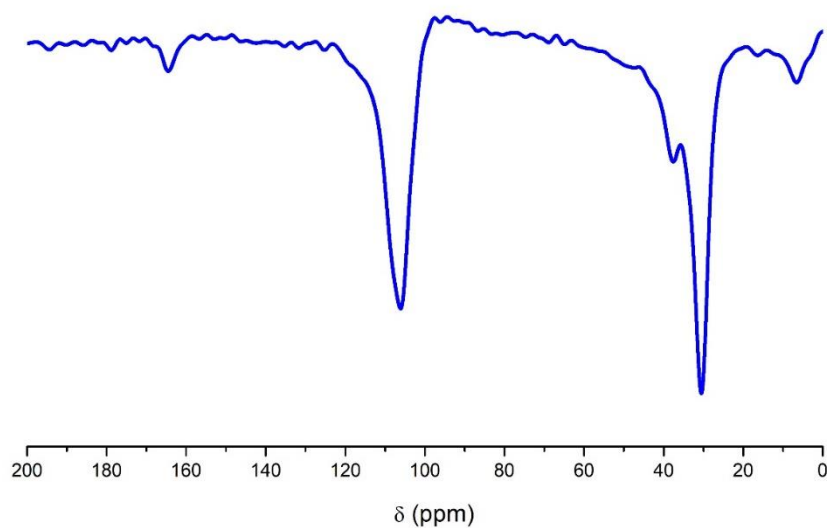


Figure A 10 ^{13}C Inversion recovery of ABC membrane at a τ evolution time of 0.1 sec.

All molecular constituents are observed to have a negative signal at a τ evolution time of 0.1 sec indicating partial relaxation throughout (Figure A 10).

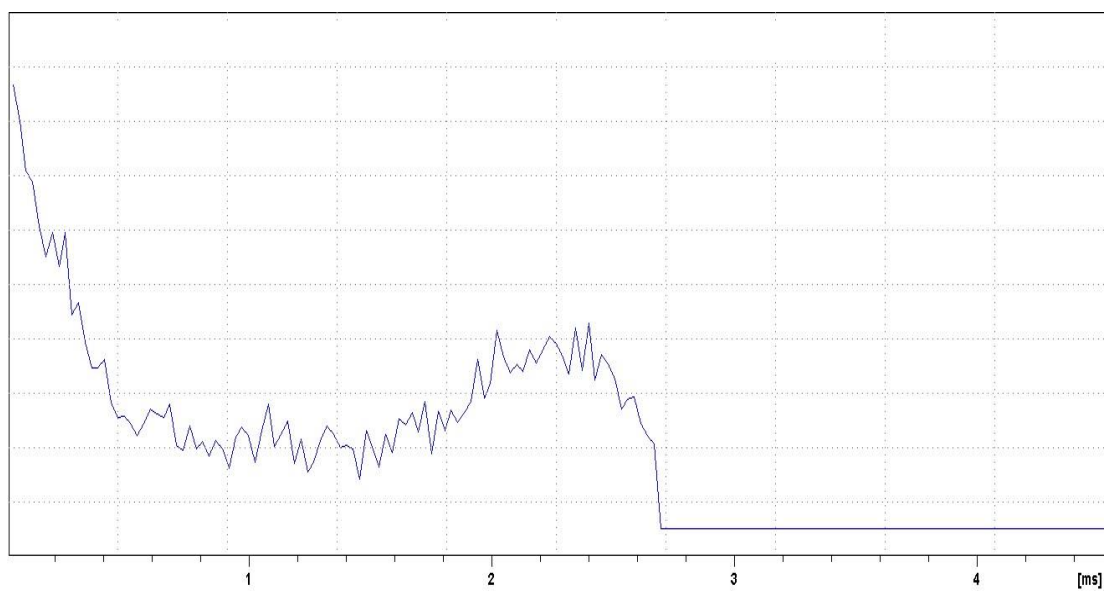


Figure A 11 ^1H FID of the 2D WISE measurement on the ABC membrane.

The FID is observed to have been cut short at an acquisition time of 2.7 ms, hence, the signal is not completely recorded (Figure A 11).

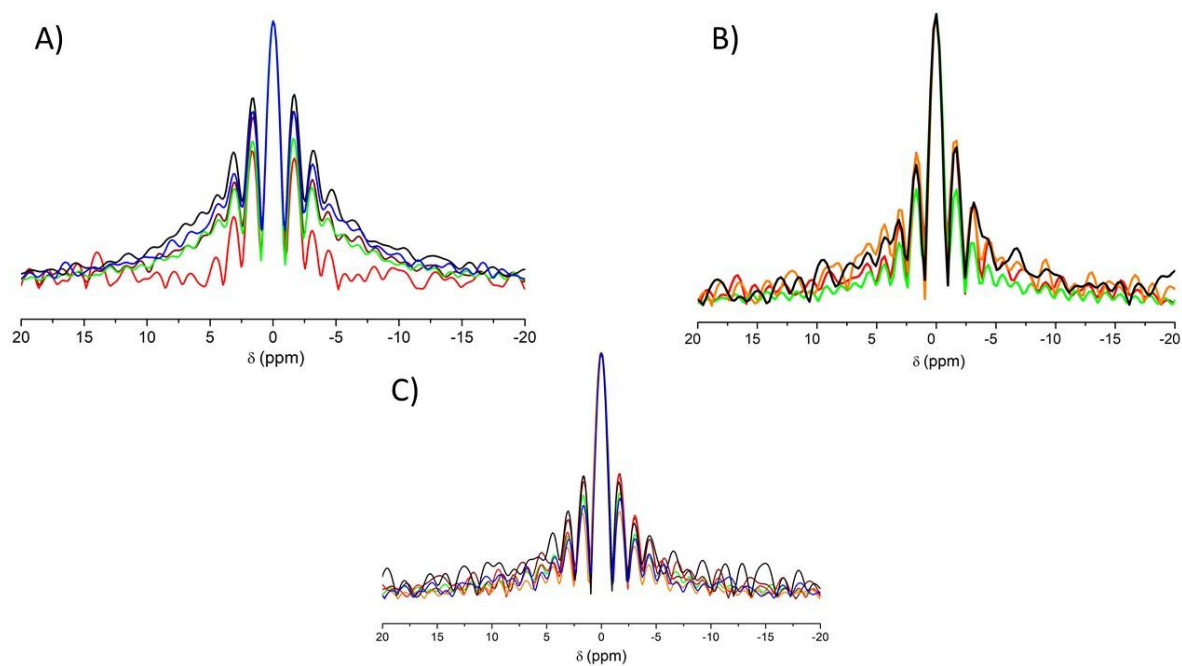


Figure A 12 Normalised ^1H spectra of A) AB powder B) AB membrane and C) ABC membrane.

Strong oscillations are observed in the ^1H slices of the 2D WISE of all samples (Figure A 12).

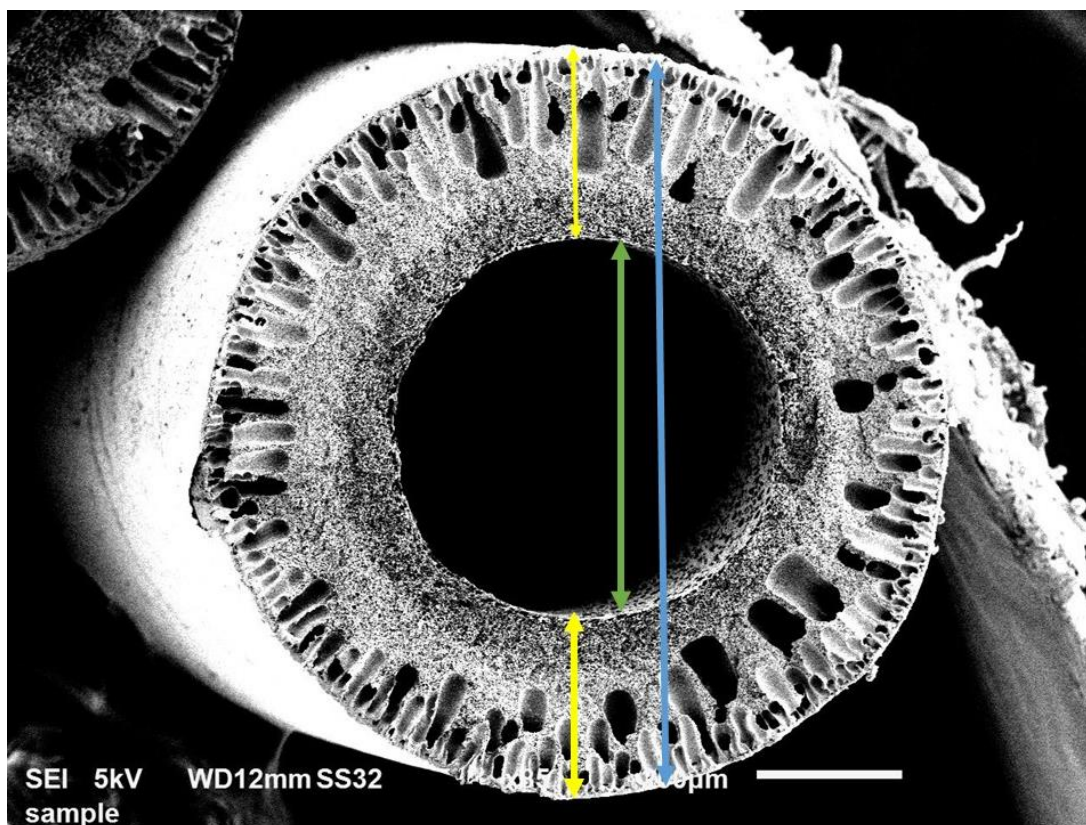


Figure A 13 SEM image of the ABC membrane indicating the general dimensions on length measurements of the inner diameter (green line), membrane wall thickness (yellow line) and outer diameter (blue line)

A SEM image of the ABC membrane was taken with the solid coloured lines detailing the general dimensions of a specific region (Figure A 13).

Table A 2 Length measurements determined through SEM on the regions of interest in both the AB and ABC membrane.

	Outer diameter (mm)	Inner diameter (mm)	Wall thickness (mm)
AB membrane	1.120	0.606	0.258
ABC membrane	1.018	0.526	0.244

Length measurements of the outer diameter, inner diameter and wall thickness were determined in the AB and ABC membrane (Table A 2). General dimensions on the regions of interest are shown in (Figure A 13).

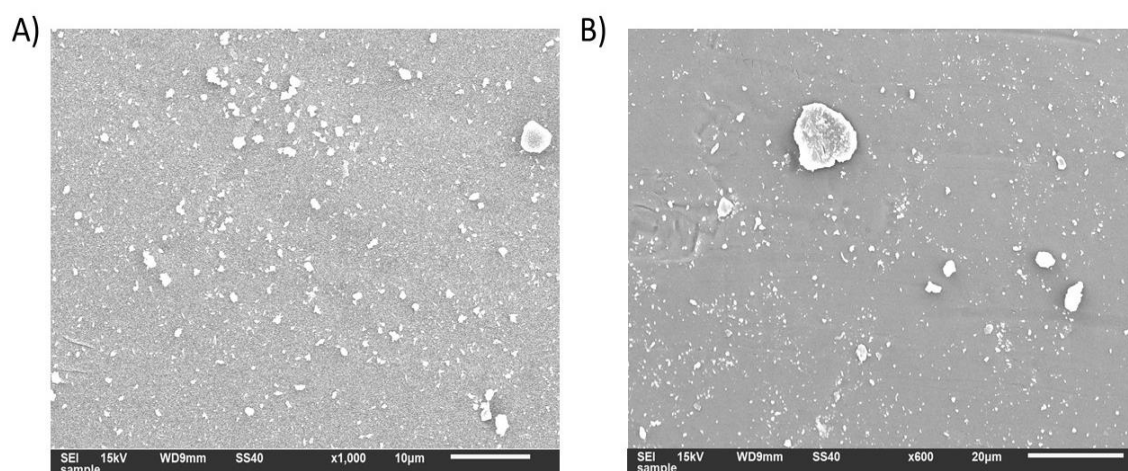


Figure A 14 SEM/EDS images of the surface of the A) AB membrane and B) ABC membrane

Images were taken of the AB and ABC membrane surface for SEM/EDS analysis (Figure A 14).

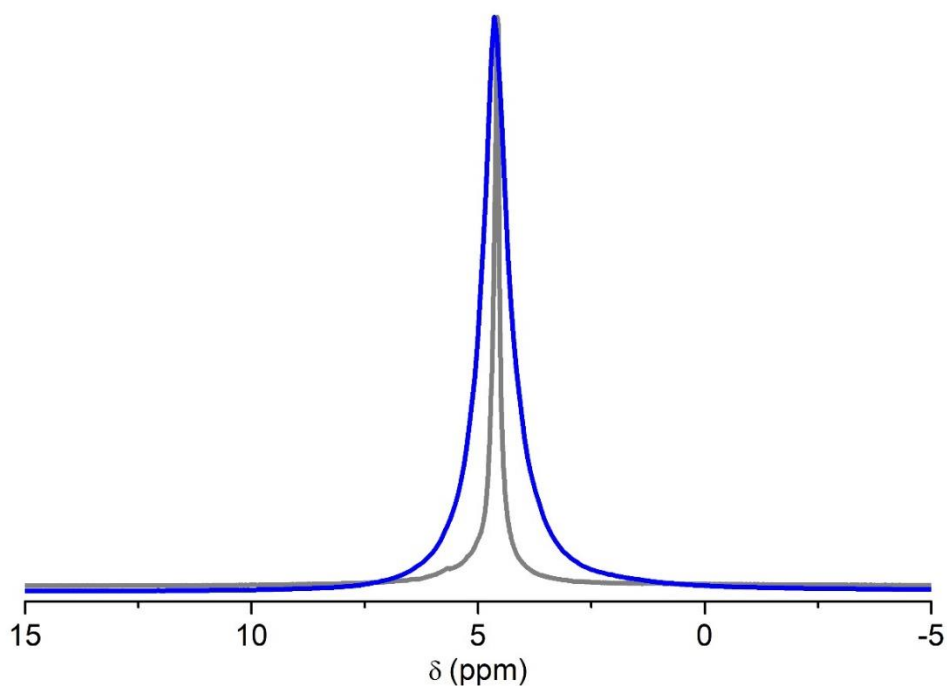


Figure A 15 Normalised ^1H spectra of the ABC membrane in excess D_2O compared to the stock solution of D_2O

^1H SPE spectra of the stock solution of D_2O was compared with the ABC membrane in excess D_2O conditions (Figure A 15). Excess D_2O conditions is defined as the rotor consisting of three fibres of the membrane in a rotor filled completely with D_2O .

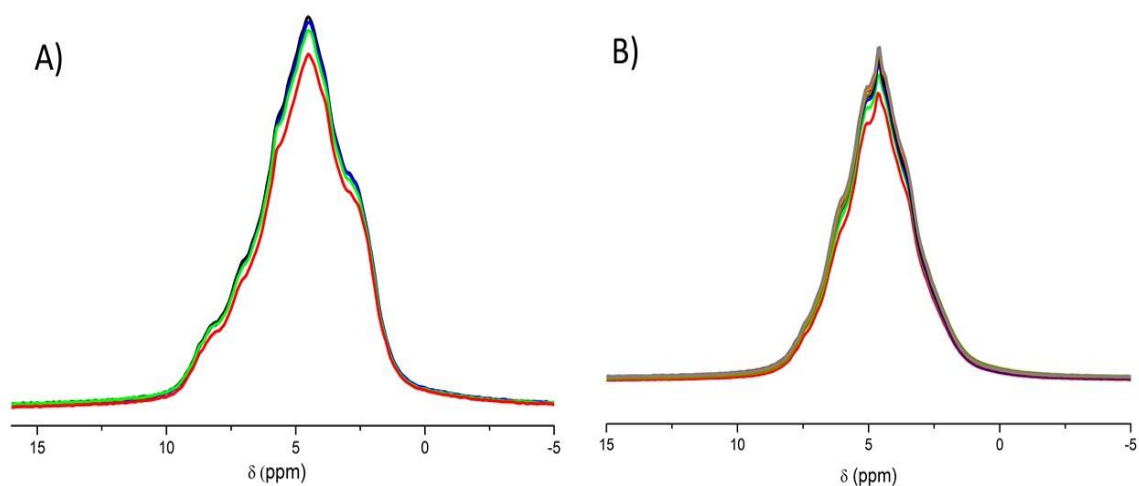


Figure A 16 ^1H SPE spectra A) AB membrane and B) ABC membrane) pre-soaked in D_2O . Respective membranes were left soaking for 15 min (red line) and 30 min (green line), no observable difference in signal was observed past 30 min. AB membrane was recorded for a total of 60 min hour and the AB membrane was recorded for a total of 120 min.

^1H SPE of both membranes pre-soaked in D_2O were recorded at intervals of 15 mins and overlayed for comparative studies (Figure A 16). In both membranes, signal intensity increases for the first 30 min before equilibrating. No differences are observed in line shape between runs.

Table A 3 Tensiometry results on the repeats of both the AB and ABC membrane.

Sample	Repeats	Dry Advancing (°)	Average Wet Advancing (°)
AB membrane	1	84.7	78.7
	2	83.8	78.9
	3	87.4	85.8
ABC membrane	1	98.0	95.3
	2	94.3	90.8
	3	96.9	92.5

Tensiometer tests were conducted on three repeats of the AB and ABC membrane, results were calculated and tabulated (Table A 3). The average wet advancing was conducted twice on each membrane, hence the value given is an average.

Table A 4 Tensile strength results on the repeats of both the AB and ABC membrane

Sample	Repeats	Load at break (N)	Break extension (mm)
AB membrane	1	3.47	272.47
	2	3.39	269.27
	3	3.37	263.20
	4	3.41	271.87
	5	3.42	274.19
ABC membrane	1	2.50	100.71
	2	2.43	96.27
	3	2.55	95.00
	4	2.51	98.72
	5	2.18	100.37

Tensile strength tests were conducted on five repeats of the AB and ABC membrane, results were calculated and tabulated (Table A 4).